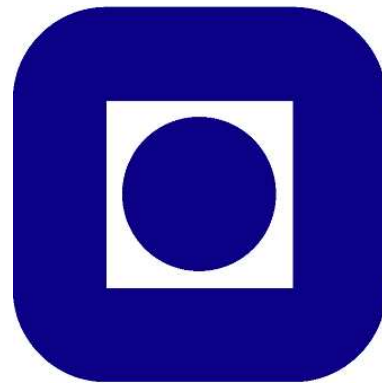


Institut für Automatisierungstechnik  
Fg. Regelungstheorie und Robotik  
Prof. Dr.-Ing. Jürgen Adamy  
Landgraf-Georg-Straße 4  
D-64289 Darmstadt

Dep. of Engineering Cybernetics  
The Norwegian Institute of Technology  
Prof. MSc. Phd. Jan Tommy Gravdahl  
University of Trondheim  
N-7491 Trondheim

Technische Universität Darmstadt

Norges teknisk-naturvitenskapelige universitet



## Diploma Thesis

### Reconfiguration in Formations of Unmanned Aerial Vehicles

Author: Tobias Paul

Supervisors: MSc. Thomas R. Krogstad (NTNU)

Dipl.-Ing. Boris Jasniewicz (TUD)

Date of hand in: 9. April 2007

# Erklärung

Hiermit versichere ich, die vorliegende Diplomarbeit selbstständig und unter ausschließlicher Verwendung der angegebenen Quellen und Hilfsmittel angefertigt zu haben. Diese Arbeit hat in gleicher oder ähnlicher Form noch keiner Prüfungsbehörde vorgelegen.

Darmstadt, den 09. April 2007

---

Tobias Paul

## Abstract

Unmanned aerial vehicles (UAVs) are very interesting for military, industry, and scientific purposes. A group of UAVs could increase the possibilities of a single operating UAV once more. This thesis presents a solution for collision free formation flight of UAVs. For simulation and evaluation purposes, a simplified and a complete model of a real, small-scale helicopter are presented. The complete model is controlled by a nonlinear SDRE controller together with a nonlinear compensator, while the simplified model is controlled by several controllers, including nested saturation, feed forward, and feedback control. The formation flight solution is developed vehicle independently and is implemented and verified, together with the helicopters, in MATLAB<sup>TM</sup>/Simulink<sup>TM</sup>. The formation flight solution is based on a local potential field combined with a virtual leader approach. As necessary for a helicopter, the potential field approach is realized in 3D including obstacle and collision avoidance.

*Keywords:* UAV, helicopter, nonlinear control, model, formation flight, potential field, virtual leader

# Contents

<b>Erklärung</b>	<b>ii</b>
<b>1 Introduction</b>	<b>1</b>
1.1 UAVs	1
1.1.1 Applications	2
1.1.2 Scientific challenge	3
1.2 Literature review	3
1.2.1 UAV modeling and control	3
1.2.2 Formation flying	5
1.3 Thesis outline	5
<b>2 6 DOF equations of motion</b>	<b>7</b>
2.1 Reference frames	7
2.2 Definitions	7
2.2.1 Cross product operator	8
2.2.2 Vector norm	8
2.2.3 Vector definitions	8
2.3 Kinematics	9
2.3.1 Translational kinematics	9
2.3.2 Rotational kinematics	9
<b>3 UAV equations of motion</b>	<b>11</b>
3.1 Helicopter basics	12
3.2 Rigid body dynamics	13
3.3 Forces and moments	14
3.3.1 Gravity	14
3.3.2 Main rotor	15
3.3.3 Thrust	17
3.3.4 Engine, governor and rotor speed model	19
3.3.5 Fuselage forces	19
3.3.6 Tail rotor	20
3.3.7 Horizontal stabilizer forces and moments	22
3.3.8 Vertical fin	22

---

3.4	Model verification . . . . .	23
<b>4</b>	<b>Control of UAV</b>	<b>25</b>
4.1	SDRE theory . . . . .	25
4.2	Reference generation . . . . .	26
4.3	SDRE control of UAV . . . . .	28
4.3.1	SDC form . . . . .	28
4.3.2	Compensator . . . . .	32
4.3.3	Evolutionary algorithm . . . . .	36
<b>5</b>	<b>Model and control of simplified UAV</b>	<b>38</b>
5.1	Simplified model . . . . .	38
5.1.1	Forces and moments . . . . .	39
5.1.2	Engine dynamics . . . . .	41
5.2	Vertical controller . . . . .	41
5.3	Engine controller . . . . .	42
5.4	Lateral and longitudinal controller . . . . .	42
5.4.1	Inner loop . . . . .	43
5.4.2	Outer loop . . . . .	43
5.5	Simulation results . . . . .	44
<b>6</b>	<b>Formation flight</b>	<b>49</b>
6.1	Formation control . . . . .	50
6.1.1	Virtual leader . . . . .	50
6.1.2	Inter vehicle influence . . . . .	51
6.1.3	Collision and obstacle avoidance . . . . .	52
6.1.4	Potential field . . . . .	53
6.2	Formations . . . . .	54
6.2.1	Circular formation . . . . .	56
6.2.2	Triangular formation . . . . .	57
6.2.3	Line formation . . . . .	58
6.3	Simulation results . . . . .	58
6.3.1	Point mass . . . . .	58
6.3.2	Simplified model . . . . .	59
<b>7</b>	<b>Future work</b>	<b>66</b>
	<b>Literature</b>	<b>68</b>
<b>A</b>	<b>Data</b>	<b>71</b>
A.1	UAV model . . . . .	71
A.2	Simplified model and corresponding controller . . . . .	72
A.3	Formation flight . . . . .	73

---

<b>B SDC parameter</b>	<b>75</b>
<b>C Submitted paper to the 2008 American Control Conference</b>	<b>80</b>

# List of Figures

3.1	Helicopter components . . . . .	12
3.2	Moments and forces acting on the helicopter. . . . .	14
3.3	X-Cell model verification. . . . .	24
5.1	Simulation results of simplified helicopter . . . . .	45
5.2	Control input of simplified helicopter . . . . .	46
5.3	Flying a screw . . . . .	47
6.1	Vehicle block diagram . . . . .	50
6.2	Vector definitions for formation flight . . . . .	52
6.3	Ellipsoid using for collision and obstacle avoidance . . . . .	53
6.4	Potential field . . . . .	55
6.5	Circular formation . . . . .	56
6.6	Triangular formation . . . . .	57
6.7	Line formation . . . . .	58
6.8	Point masses changing from circle to triangle formation. . . . .	60
6.9	Scheme of exchanging places . . . . .	61
6.10	Simulation results of exchanging places. . . . .	62
6.11	Formation flight with the simplified model . . . . .	63
6.12	Collision avoidance with the simplified model . . . . .	64
6.13	Obstacle avoidance . . . . .	65

# List of Tables

A.1	Parameter of the helicopter model . . . . .	72
A.2	Parameter of the simplified UAV . . . . .	73
A.3	Parameter of six point mass formation solution . . . . .	73
A.4	Parameter of three helicopter formation solution . . . . .	74

# Symbols

$\mathbf{A}(\mathbf{x})$	SDC system matrix
$A_{\delta_{\text{lon}}}^{\text{nom}}$	longitudinal cyclic to flap gain at nominal rpm
$a$	lift curve slope
$a_{\text{mr/tr}}$	m.r./t.r. blade lift curve slope
$\mathbf{B}(\mathbf{x})$	SDC control matrix
$B_{\delta_{\text{lat}}}^{\text{nom}}$	lateral cyclic to flap gain at nominal rpm
$C_{D_0}^{\text{mr}}, C_{D_0}^{\text{tr}}$	m.r./t.r. blade zero lift drag coefficient
$C_{L\alpha}^{\text{ht}}$	horizontal tail lift curve slope
$C_{L\alpha}^{\text{vf}}$	vertical fin lift curve slope
$C_{\text{RB}}$	coriolis-centripetal matrix
$C_{T_{\text{max}}}^{\text{mr/tr}}$	m.r./t.r. max thrust coefficient
$c_{\text{mr/tr}}$	m.r./t.r. chord
$c_{\text{m}}^{\text{Q,T}}$	constant of simplified model
$F_t$	fin blockage factor
$f(\cdot)$	nonlinear equation
$\mathbf{f}_o^b$	body fixed forces
$f_j$	convergence rate coefficient
$f_q^s$	pitching resonance frequency of suspension system
$f_r^s$	yawing resonance frequency of suspension system
$f_s^p$	rolling resonance frequency of suspension system
$\mathbf{g}$	vector of body forces and moments introduced by gravity
$g$	acceleration due to gravity at sea level
$g_0$	zero function for newton iteration schema
$h_{\text{mr}}$	m.r. hub height above centre of gravity
$h_{\text{tr}}$	t.r. height above centre of gravity
$\mathbf{I}$	unity matrix
$\mathbf{I}_0$	inertia matrix

---

$I_{xx}, I_{yy}, I_{zz}$	moments of inertia
$I_{\beta_{mr}}$	m.r. blade flipping inertia
$K_i$	integral governor gain
$K_p$	proportional governor gain
$K_{TM}$	m.r. constant of simplified model
$K_{TT}$	t.r. constant of simplified model
$K_\beta$	hub torsional stiffness
$K_\lambda$	wake intensity factor
$K_\mu$	scaling of flap response to speed variation
$K_{1/2/3}$	gains of the nested saturated control
$k_{1/2}$	gains of the vertical controller of the simplified model
$k_{3/4}$	gains of the engine controller of the simplified model
$L(\cdot)$	rolling moment; if existent, caused by element ( $\cdot$ )
$l_{ht}$	stabilizer location behind centre of gravity
$l_{tr}$	t.r. hub location behind center of gravity
$M_{RB}$	system inertia matrix
$M(\cdot)$	pitching moment; if existent, caused by element ( $\cdot$ )
$m$	helicopter mass
$\mathbf{m}_o^b$	body fixed moments
$N(\cdot)$	yawing moment; if existent, caused by element ( $\cdot$ )
$n_{es}$	gear ratio of engine shaft to m.r.
$n_{tr}$	gear ratio of t.r. to m.r.
$\mathbf{P}$	solution of discrete time Riccati equation
$P_{eng}^{idle}$	engine idle power
$P_{eng}^{max}$	engine maximum power
$\mathbf{p}^n$	position in north-east-down frame
$p$	pitch rate
$\mathbf{Q}$	positive definite matrix in the SDRE
$\mathbf{q}$	quaternion
$q$	roll rate
$\mathbf{R}$	positive definite matrix in the SDRE
$\mathbf{R}_b^n, \mathbf{R}_n^b$	translation rotation matrix for body and NED frame
$R_{mr/tr}$	m.r./t.r. radius
$r$	yaw rate
$S_{ht}$	horizontal fin area

---

$S_{vf}$	effective vertical fin area
$S_x^{fus}$	frontal fuselage drag area
$S_y^{fus}$	side fuselage drag area
$S_z^{fus}$	vertical fuselage drag area
$T_{mr}^{max}$	maximum rotor thrust
$\mathbf{T}_\Theta$	rotation rotation matrix for body and NED frame
$\mathbf{u}$	vector of control inputs
$u$	body velocity
$V_{imr}, V_{itr}$	m.r./t.r. induced velocity
$V_\infty^{tr}$	axial velocity at tail rotor hub
$\mathbf{v}_o^b$	body fixed velocity
$v_{vf}$	side velocity relative to air at vertical fin
$v$	body verlocity
$w_{tr}$	vertical velocity at tail rotor
$w$	body velocity
$\mathbf{x}$	state vector
$X_{(\cdot)}$	force in $u$ direction; if existent, caused by element $(\cdot)$
$Y_{(\cdot)}$	force in $v$ direction; if existent, caused by element $(\cdot)$
$Z_{(\cdot)}$	force in $w$ direction; if existent, caused by element $(\cdot)$
$z_{1/2}$	Standard normal distributed random number
$\Gamma(\mathbf{x})$	discretization of $\mathbf{B}(\mathbf{x})$
$\gamma_{fb}$	stabilizer bar Lock number
$\delta_{col}$	collective commanded blade pith (rad)
$\delta_{lat}$	lateral commanded blade pith (rad)
$\delta_{lon}$	longitudinal commanded blade pith (rad)
$\delta_r$	collective commanded t.r. blade pith (rad)
$\delta_r^{trim}$	t.r. pitch trim coefficient
$\delta_t$	throttle setting
$\epsilon_{vf}^{tr}$	fraction of vertical fin area exposed to t.r. induced velocity
$\mathbf{v}_j$	function parameter of individual $j$
$\boldsymbol{\eta}$	NED position and attitude vector
$\eta_w$	coefficient of non-ideal wake contraction
$\Theta$	Euler angles
$\theta$	pitch angle
$\theta_0$	commanded collective angle (either $\delta_{col}$ or $\delta_r$ )

---

$\lambda_j^i$	child $j$ of generation $i$
$\lambda_{1/2/3}$	gains of the nested saturated control
$\mu$	advance ratio
$\mu_j^i$	parent $j$ of generation $i$
$\mu_z$	normal airflow component
$\boldsymbol{\nu}$	vector of body velocities
$\rho$	density of air
$\xi^s$	damping ratio of the suspension system material
$\sigma$	solidity ratio
$\varsigma_j$	strategy parameter of individual $j$
$\varsigma_{\min}$	minimum mutation width
$\boldsymbol{\tau}$	vector of body fixed forces and moments
$\tau_e$	rotor time constant for flapping motion
$\Phi(\boldsymbol{x})$	discretization of $\mathbf{A}(\boldsymbol{x})$
$\phi$	roll angle
$\psi$	yaw angle
$\Omega_c$	rotor speed command
$\Omega_{\text{nom}}$	nominal m.r. speed
$\boldsymbol{\omega}_{nb}^b$	body fixed angular velocity

# Chapter 1

## Introduction

The purpose of this thesis is to present a model and control scheme for formation flying unmanned aerial vehicles (UAV). The used aircraft is based on a modified *X-Cell 60 hobby* helicopter used for flight acrobatic tests at the Massachusetts Institute of Technology, Cambridge, USA. The formation flight solution is developed independently of the UAV. The helicopters model and a nonlinear control approach for this model, based on solving the state-dependent Riccati equation, was implemented in MATLAB<sup>TM</sup>/Simulink<sup>TM</sup>. The formation flight solution is based on a local potential field combined with a virtual leader. For verifying the formation flight solution, a simplified model and controller of the X-Cell helicopter was implemented. For an overview of this topic, an literature review is performed in the end of this chapter. The final part is the publication of the results obtained in this thesis in Paul et al. [2007].

### 1.1 UAVs

Unmanned Aerial Vehicles are used since the early beginning of flight, almost exclusive by military (Munn [1849], Sarris [2001], Sullivan [2006]). The term *UAV* includes a wide range of machines. This range straps from unmanned weather balloons to laser guided bombs and full autonomous operating flying robots. Because of that, a lot of different names are used in literature, by companies, and governments. Nevertheless, flying machines had and will have an important roll in flight as shown by Sarris [2001]. The increase of computer power makes UAVs reliable and sufficient. They are able to navigate exactly even in worth sight conditions and can perform long endurance missions. Contrary of on-board human pilots, UAVs can be used for missions with long concentration spans. They can be build in small size, light wight and operating autonomously. They can also be replaced at low cost. These quality makes UAVs very interesting for industry, military, and the scientific community. A lot of research on unmanned vehicles has been done during the last years but just a few full

functioning UAV vehicles have been build. This is because of high prototyping cost and the need of interdisciplinary knowledge. Beside this, building a UAV from scratch takes a long time of research and development. Therefore, it is advisable not to start from scratch but use existing modules or platforms and focus on the individual strengths.

### 1.1.1 Applications

Imagining a small and cheap UAV, with the ability to be equipped with different sensors, a lot of applications are thinkable. The following operations could be performed with UAVs:

- Full autonomous building (e.g., power line) inspection.
- Search and rescue missions using video and infra red sensors. This enables the vehicle to search and localize humans in water, on land, and even through dust.
- Reconnaissance of disaster areas. UAVs are used for fast mapping of hot spots during forest fires as shown by Restas [2006].
- Fishing surveillance using echo-sounding equipment,
- traffic monitoring, or
- communication relay missions are also possible.
- Agricultural and corp (coffee, etc.) monitoring has already be done. Research results are presented by Herwitz et al. [2003].

The wide field of military applications is easy to imagine. A main argument for the use of UAVs in combat, which are than called unmanned combat aerial vehicles (UCAV), is to preserve pilots from high risk or long endurance missions. Applications are

- Surveillance and reconnaissance,
- radio jamming,
- nuclear, biological, and chemical warfare detection,
- mine detection,
- artillery acquisition, and
- target simulation.

Even attack missions are thinkable. UAVs could be the first full autonomous robots in war and this view in the future is raising questions according to morality as suggested by Dawkins [2005] and Gulam and Lee [2006].

UAVs used today are usually controlled by ground personal. Han et al. [2004] analyze the circumstances to operate a UAV cargo system under economic aspects and due to security issues; they also recommend a ground operator.

### 1.1.2 Scientific challenge

A lot of research has been and is still done on UAVs. The research combines all challenges from aircraft and robot development. The research filed concerning UAVs includes, among others,

- mechanical development of an aircraft including vertical take off and landing abilities,
- development of a control strategy for the aircraft, valid in all flight situations including take off and landing, the control needs to be robust due to the fact that uncertainties effect the flight of the UAV (e.g., wind),
- path planning and formation flight including collision and obstacle avoidance,
- decision making algorithms,
- image processing,
- communication strategies, and
- navigation strategies.

The list can easily be expanded due to the additional requirements of individual missions (e.g., requirements on sensors).

## 1.2 Literature review

A lot of work has been done in modeling and control of UAVs and even in formation flight. This section provides a literature review over the thesis related topics.

### 1.2.1 UAV modeling and control

Bogdanov et al. [2004] present a nonlinear state dependent Riccati equation control scheme together with an nonlinear compensator for small scale helicopters. The compensator shall cover these parts of the model which could not

be represented in the state dependent coefficient (SDC) form. The controller was verified by the OGI School of Science and Engineering with a R-MAX and a X-Cell model helicopter during flight tests.

Gavrilets [2003] and Gavrilets et al. [2001] present a complex and sufficient nonlinear model of a small-scale helicopter. Using this model, he was able to develop a linear controller, based on a linearized model. He also included a controller to perform specific acrobatic maneuvers, orientated on the behavior of a real pilot which was verified during flight tests at the Massachusetts Institute of Technology. All necessary parameters are given.

Vélez and Agudelo [2006] present the use of a rapid prototyping software environment, called Colibri, for automatic control and parameter estimation of a small-scale helicopter. The helicopter model is based on the model presented by Gavrilets et al. [2001].

Heffley and Mnich [1988] present one of the first complete helicopter models for simulation purposes.

Isidori et al. [2001] present a nonlinear solution for robust control of a simplified helicopter model using quaternions.

Johnson and Kannan [2002] present a controller for an aerospace system based on neuronal networks. This approach was successfully tested by the Georgia Institute of Technology on a R-MAX model helicopter.

Kondak et al. [2004] presents the model of a LOGO-10 model helicopter. A robust cascade controller, based on a simplified model, is derived and verified during simulations.

Marconi and Naldi [2006] present a robust controller based on simplifications of the model presented by Gavrilets [2003]. The controller is a cascade controller including nested saturation control. All parameters of the simplified model and the controller are given.

Mettler et al. [2000] describes the system identification of a R-50 model helicopter. Models for hover and forward flight are presented.

Munziger [1998] explains helicopter basics and derives a complete model for a R-50 model helicopter. A controller, based on neuronal networks, is also presented schematic.

Padfield [1996] provides complete and very detailed instructions to derive a helicopter model for simulation purposes. Most of the presented papers refer to this book.

Prouty and Jr. [2003] provides an overview about classic helicopter control solutions.

Årdal [2002] explains helicopter basics in detail and derives a model for a small scale helicopter. Several control approaches for autonomous landing on a ship are presented.

### 1.2.2 Formation flying

Borrelli et al. [2006] present solutions for UAV trajectory planning, converting the problem to a non linear program (NLP) and a mixed integer linear program (MILP).

Chen and Wang [2005] present an overview about current formation flight strategies and control issues.

Galzi and Shtessel [2006] present a continuous, robust and collision free leader-follower formation controller based on high order sliding modes. The vehicles must be full feedback linearizable.

Kaminer et al. [2004] presents a solution to launch and recover a swarm of fixed wing UAVs from a ship.

#### Potential field approach

The different potential field approaches are constructed similar. Usually, they calculate a potential field or function for each vehicle in the formation depending on the vehicle's distance to its desired place. Collision and obstacle avoidance is realized by adding a special term depending on the vehicles' distances among each other or to the obstacle.

Do [2006] presents a method to develop a formation controller based on local potential functions. The controller generates the desired velocities to match a given formation. It is a 2-dimensional approach developed for simple marine vehicles. In this approach occur no local minimum in the potential field. Obstacle avoidance is not included.

Elkaim and Kelbley [2006] presents an easy way to calculate a local two dimensional potential field combined with a virtual leader approach. The output is a pseudo force which should direct the single vehicles to its desired positions. Collision avoidance is realized by limiting the maximum force depending on the vehicle's properties.

## 1.3 Thesis outline

**Chapter 2** Introduction to 6 degrees-of-freedom motion; mathematical notations; equations of motion and kinematics

**Chapter 3** Introduction to helicopter basics. Rigid body dynamics and the equations of the forces and moments generated by the actuators and passive parts of a small scale helicopter are presented. Finally, the model is verified through simulations.

**Chapter 4** A nonlinear control approach for the model presented in chapter 2 is derived.

**Chapter 5** A simplified model and nonlinear controller is presented together with corresponding simulation results.

**Chapter 6** The three dimensional formation strategy is derived. Obstacle and collision avoidance is developed and verified through simulation results using groups of point masses and groups of simplified helicopters.

# Chapter 2

## 6 DOF equations of motion

The vehicles used in this thesis are rigid bodies with six degrees-of-freedom (DOF). In Fossen [2002], the equations of motion of marine vehicles in 6 DOF are developed. These are very similar to these of aerial vehicles. Therefore, the equations are easy to adapt.

### 2.1 Reference frames

To describe the motion of a vehicle, it is necessary to define a reference frame. Several frames are used throughout this work, depending on the problem at hand. A common frame, used for all problems, is the body frame with the body fixed axes  $x_b$ ,  $y_b$  and,  $z_b$ . The origin of the body fixed frame is the helicopters center of gravity. The x-axis points from the back through the nose, the z-axis from up to down and the y-axis completes the right-hand coordination system. This frame is used for the calculation of the forces produced by the helicopter. Because of the relative low speed and flight level of the model helicopter, a flat earth assumption is made. For navigation, the North-East-Down (NED) reference frame is used. Here the x-axis points north, the y-axis east, and the z-axis downwards normal to the flat earth surface.

The interested reader is referred to Fossen [2002] for a more detailed explanation of the different reference frames.

### 2.2 Definitions

The definitions of vectors and rotation matrices is taken from Fossen [2002]. This is also the most common way used in the international literature.

### 2.2.1 Cross product operator

The vector cross product is defined by Fossen [2002] as

$$\boldsymbol{\lambda} \times \mathbf{a} := S(\boldsymbol{\lambda})\mathbf{a}, \quad (2.1)$$

where  $\boldsymbol{\lambda}, \mathbf{a} \in \mathbb{R}^3$  and  $S(\cdot)$  is defined as

$$S(\boldsymbol{\lambda}) = -S(\boldsymbol{\lambda})^T = \begin{bmatrix} 0 & -\lambda_3 & \lambda_2 \\ \lambda_3 & 0 & -\lambda_1 \\ -\lambda_2 & \lambda_1 & 0 \end{bmatrix}. \quad (2.2)$$

### 2.2.2 Vector norm

The vector 2-norm  $\|\cdot\|_2$  of a vector  $\mathbf{x} \in \mathbb{R}^n$  is defined as

$$\|\mathbf{x}\|_2 := \sqrt{x_1^2 + x_2^2 + \cdots + x_n^2}. \quad (2.3)$$

In the rest of this work, if not specified, the expression  $\|\cdot\|$  refers to the 2-norm.

### 2.2.3 Vector definitions

In general,  $\boldsymbol{\nu}_o^n$  represents the linear velocity of point O decomposed in frame n.  $\boldsymbol{\omega}_{eb}^n$  represents the angular velocity of frame b with respect to frame e decomposed in frame n.

$$\mathbf{p}^n = \begin{bmatrix} x \\ y \\ z \end{bmatrix} \quad (\text{NED position}) \quad (2.4)$$

$$\mathbf{v}_o^b = \begin{bmatrix} u \\ v \\ w \end{bmatrix} \quad (\text{Body fixed velocity}) \quad (2.5)$$

$$\boldsymbol{\omega}_{nb}^b = \begin{bmatrix} p \\ q \\ r \end{bmatrix} \quad (\text{Body fixed angular velocity}) \quad (2.6)$$

$$\boldsymbol{\Theta} = \begin{bmatrix} \phi \\ \theta \\ \psi \end{bmatrix} \quad (\text{Attitude, Euler angles}) \quad (2.7)$$

$$\mathbf{f}_o^n = \begin{bmatrix} X \\ Y \\ Z \end{bmatrix} \quad (\text{Body fixed forces}) \quad (2.8)$$

$$\mathbf{m}_o^b = \begin{bmatrix} L \\ M \\ N \end{bmatrix} \quad (\text{Body fixed moments}) \quad (2.9)$$

The motion of a 6 DOF vehicle can be described by the following vectors:

$$\boldsymbol{\eta} = \begin{bmatrix} \mathbf{p}^n \\ \boldsymbol{\Theta} \end{bmatrix}, \quad \boldsymbol{\nu} = \begin{bmatrix} \mathbf{v}_o^b \\ \boldsymbol{\omega}_{nb}^b \end{bmatrix}, \quad \text{and} \quad \boldsymbol{\tau} = \begin{bmatrix} \mathbf{f}_o^b \\ \mathbf{m}_o^b \end{bmatrix}. \quad (2.10)$$

### Rotation matrices

Rotation matrices are used to transform vectors between several frames. This leads to a rotation of the axes around the origin. Such a rotation is by (Fossen [2002])

$$\boldsymbol{\nu}^{to} = \mathbf{R}_{from}^{to} \boldsymbol{\nu}^{from}. \quad (2.11)$$

## 2.3 Kinematics

The translational and rotational kinematics are presented in this section.

### 2.3.1 Translational kinematics

With equation (2.11), the relationship between body and NED velocity can be described through the following equation:

$$\dot{\mathbf{p}}^n = \mathbf{R}_b^n(\boldsymbol{\Theta}) \mathbf{v}_o^b \quad (2.12)$$

with

$$\mathbf{R}_b^n(\boldsymbol{\Theta}) = \begin{bmatrix} c\psi c\theta & -s\psi c\phi + c\psi s\theta s\phi & s\psi s\phi + c\psi c\phi s\theta \\ s\psi c\theta & c\psi c\phi + s\phi s\theta s\psi & -c\psi s\phi + s\theta s\psi c\phi \\ -s\theta & c\theta s\phi & c\theta c\phi \end{bmatrix}, \quad (2.13)$$

and  $s \cdot \equiv \sin(\cdot)$  and  $c \cdot \equiv \cos(\cdot)$ . The transformation from NED- to body-frame  $\mathbf{R}_n^b(\boldsymbol{\Theta})$  can be received by transposing  $\mathbf{R}_b^n(\boldsymbol{\Theta})$  (Fossen [2002]):

$$\mathbf{R}_n^b(\boldsymbol{\Theta}) = \mathbf{R}_b^n(\boldsymbol{\Theta})^{-1} = \mathbf{R}_b^n(\boldsymbol{\Theta})^T. \quad (2.14)$$

### 2.3.2 Rotational kinematics

A similar expression to equation (2.12) can be derived for the rotational kinematics (Fossen [2002]):

$$\dot{\boldsymbol{\Theta}} = \mathbf{T}_{\boldsymbol{\Theta}}(\boldsymbol{\Theta}) \boldsymbol{\omega}_{nb}^b \quad \text{or} \quad \boldsymbol{\omega}_{nb}^b = \mathbf{T}_{\boldsymbol{\Theta}}^{-1}(\boldsymbol{\Theta}) \dot{\boldsymbol{\Theta}}, \quad (2.15)$$

where

$$\mathbf{T}_{\boldsymbol{\Theta}}(\boldsymbol{\Theta}) = \begin{bmatrix} 1 & s\phi t\theta & c\phi t\theta \\ 0 & c\phi & -s\phi \\ 0 & s\phi/c\theta & c\phi/c\theta \end{bmatrix}, \quad (2.16)$$

$$\mathbf{T}_{\boldsymbol{\Theta}}^{-1}(\boldsymbol{\Theta}) = \begin{bmatrix} 1 & 0 & -s\theta \\ 0 & c\phi & c\theta s\phi \\ 0 & -s\phi & c\phi c\theta \end{bmatrix}, \quad (2.17)$$

and  $s \cdot \equiv \sin(\cdot)$ ,  $c \cdot \equiv \cos(\cdot)$ , and  $t \cdot \equiv \tan(\cdot)$ . With equation (2.13) and (2.16), the 6 DOF kinematic equation is given by

$$\dot{\boldsymbol{\eta}} = \mathbf{J}(\boldsymbol{\eta})\boldsymbol{\nu} = \begin{bmatrix} \mathbf{R}_b^n(\boldsymbol{\Theta}) & \mathbf{0}_{3 \times 3} \\ \mathbf{0}_{3 \times 3} & \mathbf{T}_{\boldsymbol{\Theta}}(\boldsymbol{\Theta}) \end{bmatrix} \boldsymbol{\nu}. \quad (2.18)$$

The attitude representation with Euler angles is intuitive but can cause singularities, compare equation (2.16). An other way of describing the attitude is to use quaternions, also called *Euler parameters*.

### Quaternions

A quaternion  $\mathbf{q}$  is defined by Fossen [2002, page 29] as follows:

$$\mathbf{q} = \begin{bmatrix} \eta \\ \boldsymbol{\epsilon} \end{bmatrix} \text{ with } \boldsymbol{\epsilon} = \begin{bmatrix} \epsilon_1 \\ \epsilon_2 \\ \epsilon_3 \end{bmatrix}, \quad (2.19)$$

$$\mathbf{q}^T \mathbf{q} = 1. \quad (2.20)$$

$\mathbf{q}$  is defined as a complex number where  $\eta$  represents the real part and  $\boldsymbol{\epsilon}$  three imaginary parts.  $\eta$  and  $\boldsymbol{\epsilon}$  are defined as (Fossen [2002]):

$$\eta = \cos(\beta/2), \quad (2.21)$$

$$\boldsymbol{\epsilon} = \boldsymbol{\lambda} \sin(\beta/2) \text{ with } \boldsymbol{\lambda} = \pm \frac{\boldsymbol{\epsilon}}{\sqrt{\boldsymbol{\epsilon}^T \boldsymbol{\epsilon}}}. \quad (2.22)$$

It is possible to calculate the quaternion representation from Euler angles and vice versa as shown by Fossen [2002]. Using quaternions, the matrices from section 2.3.1 and 2.3.2 change to

$$\dot{\boldsymbol{p}}^n = \mathbf{R}_b^n(\mathbf{q})\boldsymbol{v}_o^b \text{ and} \quad (2.23)$$

$$\dot{\mathbf{q}} = \mathbf{T}_q(\mathbf{q})\boldsymbol{\omega}_{nb}^b \quad (2.24)$$

with

$$\mathbf{R}_b^n(\mathbf{q}) = \begin{bmatrix} 1 - 2(\epsilon_2^2 + \epsilon_3^2) & 2(\epsilon_1\epsilon_2 - \epsilon_3\eta) & 2(\epsilon_1\epsilon_3 + \epsilon_2\eta) \\ 2(\epsilon_1\epsilon_2 + \epsilon_3\eta) & 1 - 2(\epsilon_1^2 + \epsilon_3^2) & 2(\epsilon_2\epsilon_3 - \epsilon_1\eta) \\ 2(\epsilon_1\epsilon_3 - \epsilon_2\eta) & 2(\epsilon_2\epsilon_3 + \epsilon_1\eta) & 1 - 2(\epsilon_1^2 + \epsilon_2^2) \end{bmatrix} \quad (2.25)$$

and

$$\mathbf{T}_q(\mathbf{q}) = \frac{1}{2} \begin{bmatrix} -\epsilon_1 & -\epsilon_2 & -\epsilon_3 \\ \eta & -\epsilon_3 & \epsilon_2 \\ \epsilon_3 & \eta & -\epsilon_1 \\ -\epsilon_2 & \epsilon_1 & \eta \end{bmatrix}. \quad (2.26)$$

Equation (2.14) remains valid. With this, the kinematic equation (2.18) changes to

$$\begin{bmatrix} \dot{\boldsymbol{p}}^n \\ \dot{\mathbf{q}} \end{bmatrix} = \mathbf{J}(\boldsymbol{\eta})\boldsymbol{\nu} = \begin{bmatrix} \mathbf{R}_b^n(\mathbf{q}) & \mathbf{0}_{3 \times 3} \\ \mathbf{0}_{4 \times 3} & \mathbf{T}_q(\mathbf{q}) \end{bmatrix} \boldsymbol{\nu}. \quad (2.27)$$

The quaternion representation is used for the simulations.

## Chapter 3

# UAV equations of motion

The flight of a helicopter is comparable to the flight of a fixed-wing aircraft. The engines of a plane are producing thrust and acceleration. The air flows over the wings and produces lift regarding the flaps setting. Helicopters are classified as rotary-wing aircrafts. Here, the air flows over the *wings*, called blades, because the blades are moving and not the whole aircraft. The main and tail rotor are coupled and should turn with a constant speed. To control the lift and flight direction, it is possible to rotate the blades. One gets a similar effect, using the flaps and ailerons by a fixed-wing aircraft. It is possible to rotate all blades at the same time (collective setting) or induce an angle depending on the position on the blade. Doing this, the blade angle performs a sinusoidal movement (cyclic setting) during one round. The collective setting is used to control the altitude while the cyclic setting controls the attitude and so the flight in a specific direction.

Helicopters have a very wide field of action. They are able to perform vertical take-offs and landings, they can hover, perform low level flight, and fast forward flight. Even acrobatics are possible with helicopters. With these abilities they are able to start and return, for example, to a ship. They can also operate in urban areas. The mathematical model is high nonlinear and the equations of motion are all, more or less, coupled. It is difficult to derive a closed description because of the different fly modes. Nevertheless, with Padfield [1996] and Heffley and Mních [1988] one can find at least two standard models for full scale helicopters. For the usage of helicopters as UAVs, especially small scale helicopter are interesting. They have a very high thrust to weight ratio and can perform extreme maneuvers. For example, usually they are able to perform all movements upside down (Marconi and Naldi [2006]). Furthermore, a scenario is thinkable where a small scale helicopter UAV is used inside a building. Small scale helicopter models have been presented by Munziger [1998], Årdal [2002], Aurstad [2002], Gavrillets et al. [2001], resp. Gavrillets [2003], who derived a complete and very detailed model of a modified X-Cell 60 hobby helicopter.

### 3.1 Helicopter basics

Due to the fact that detailed aircraft models are well treasured secrets, only a few complete models can be found in the literature. Gavrillets [2003] presents a very detailed model of a modified X-Cell 60 hobby helicopter used for flight acrobatic tests at the Massachusetts Institute of Technology, Cambridge, USA. He also provides all necessary data to the model. Because of that, his model was chosen for this thesis. In common, helicopters consists of four main components (Heffley and Mnych [1988]) responsible for the flight characteristics. These are:

1. main rotor (mr),
2. tail rotor (tr),
3. fuselage (fus), and
4. vertical fin (vf).

They may be seen in figure 3.1.

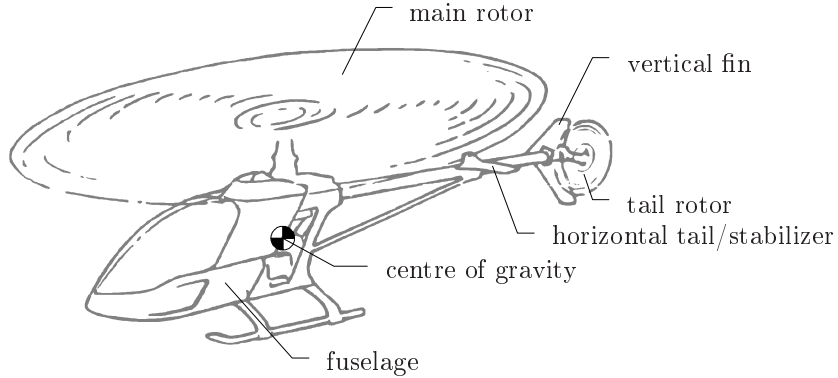


Figure 3.1: Helicopter components

The control inputs of the presented model are equal to those a pilot controls. The control inputs and states of the model are given in equation (3.1) and (3.2) (Vélez and Agudelo [2006]):

$$\mathbf{u} = [ \delta_{col} \quad \delta_{lon} \quad \delta_{lat} \quad \delta_r \quad \delta_t ]^T \text{ and} \quad (3.1)$$

$$\begin{aligned} \mathbf{x} &= [ u \quad v \quad w \quad p \quad q \quad r \quad \phi \quad \theta \quad \psi \quad x \quad y \quad z \quad a_1 \quad b_1 \quad \Omega ]^T \\ &= [ (\mathbf{v}_o^b)^T \quad (\boldsymbol{\omega}_{nb}^n)^T \quad \boldsymbol{\Theta}^T \quad (\mathbf{p}^n)^T \quad a_1 \quad b_1 \quad \Omega ]^T. \end{aligned} \quad (3.2)$$

As explained in chapter 3,  $\delta_{col}$  is the collective control input for the collective pitch of the main rotor blades given in rad as all angular in the thesis.  $\delta_{lon}$  and  $\delta_{lat}$  are the cyclic control inputs giving the explicit pitch in longitudinal ( $u, x$ ) and lateral ( $v, y$ ) direction.  $\delta_r$  is the collective pitch for the tail rotor, where no

cyclic pitch is necessary. Finally  $\delta_t$  is the engine control input to keep the rotor speed constant and varies between 0 and 1.

Three parameters of the state vector are not mentioned yet:  $a_1$ ,  $b_1$  and  $\Omega$ . The denotation of  $a_1$  and  $b_1$  can be seen in figure 3.2, while  $\Omega$  represents the rotor speed. All parameters will be explained in the following sections.

## 3.2 Rigid body dynamics

The equations of motion will be presented following Fossen [2002]. He represents the rigid body dynamics as an vectorial string:

$$\mathbf{M}_{RB}\dot{\boldsymbol{\nu}} + \mathbf{C}_{RB}(\boldsymbol{\nu})\boldsymbol{\nu} = \boldsymbol{\tau}. \quad (3.3)$$

Here,  $\mathbf{M}_{RB}$  is the system inertia matrix,  $\mathbf{C}_{RB}(\boldsymbol{\nu})$  the coriolis-centripetal matrix, and  $\boldsymbol{\tau}$  a vector of forces and moments caused by aerodynamics, gravity, and engines.

$\mathbf{M}_{RB}$  is taken from Fossen [2002] and has a very simple form because the cross-axis moments of inertia can be neglected due to the fact that the origin of the body frame is placed in the helicopter's center of gravity. Doing so,  $\mathbf{M}_{RB}$  is given by:

$$\mathbf{M}_{RB} = \begin{bmatrix} m\mathbf{I}_{3\times 3} & \mathbf{0}_{3\times 3} \\ \mathbf{0}_{3\times 3} & \mathbf{I}_0 \end{bmatrix} \quad (3.4)$$

$$= \begin{bmatrix} m & 0 & 0 & 0 & 0 & 0 \\ 0 & m & 0 & 0 & 0 & 0 \\ 0 & 0 & m & 0 & 0 & 0 \\ 0 & 0 & 0 & I_{xx} & 0 & 0 \\ 0 & 0 & 0 & 0 & I_{yy} & 0 \\ 0 & 0 & 0 & 0 & 0 & I_{zz} \end{bmatrix}. \quad (3.5)$$

$\mathbf{C}_{RB}$  can be realized in different ways. In Fossen [2002], Kirchoff's equations are used to derive an explicit expression.

While

$$\mathbf{M}_{RB} = \mathbf{M}_{RB}^T = \begin{bmatrix} \mathbf{M}_{11} & \mathbf{0}_{3\times 3} \\ \mathbf{0}_{3\times 3} & \mathbf{M}_{22} \end{bmatrix} \quad (3.6)$$

is valid,  $\mathbf{C}_{RB}$  can be build up from the elements of  $\mathbf{M}_{RB}$ :

$$\mathbf{C}_{RB}(\boldsymbol{\nu}) = \begin{bmatrix} \mathbf{0}_{3\times 3} & -S(\mathbf{M}_{11}\boldsymbol{\nu}_1) \\ -S(\mathbf{M}_{11}\boldsymbol{\nu}_1) & -S(\mathbf{M}_{22}\boldsymbol{\nu}_2) \end{bmatrix} \quad (3.7)$$

$$= \begin{bmatrix} 0 & 0 & 0 & 0 & mw & -mv \\ 0 & 0 & 0 & -mw & 0 & mu \\ 0 & 0 & 0 & mv & -mu & 0 \\ 0 & mw & -mv & 0 & I_{zz}r & -I_{yy}q \\ -mw & 0 & mu & -I_{zz}r & 0 & I_{xx}p \\ mv & -mu & 0 & I_{yy}q & -I_{xx}p & 0 \end{bmatrix} \quad (3.8)$$

### 3.3 Forces and moments

From the forces acting on the rigid body, one can separate the forces caused by gravity:

$$\boldsymbol{\tau} = \begin{bmatrix} \mathbf{f}_o^b \\ \mathbf{m}_o^b \end{bmatrix} = \mathbf{T}(\mathbf{x}, \mathbf{u}) + \mathbf{g}(\boldsymbol{\eta}). \quad (3.9)$$

This is done for the needs of the controller presented in chapter 4.  $\mathbf{g}(\boldsymbol{\eta})$  represents the forces caused by gravity and  $\mathbf{T}(\mathbf{x}, \mathbf{u})$  the remaining forces caused by drag and rotor. Gavrillets [2003] modeled 17 forces and moments. These are caused by the different components of the small scale helicopter:

$$\mathbf{T} = \begin{bmatrix} X_{mr} + X_{fus} \\ Y_{mr} + Y_{fus} + Y_{tr} + Y_{vf} \\ Z_{mr} + Z_{fus} + Z_{ht} \\ L_{mr} + L_{vf} + L_{tr} \\ M_{mr} + M_{ht} \\ -Q_e + N_{vf} + N_{tr} \end{bmatrix}. \quad (3.10)$$

Here, the forces and moments acting on the helicopters center of gravity are organized by components:  $(\cdot)_{mr}$  for main rotor,  $(\cdot)_{tr}$  for tail rotor,  $(\cdot)_{fus}$  for fuselage, and  $(\cdot)_{vf}$  for vertical fin. Each of these components and resulting influences will be described briefly below. Figure 3.2 visualizes the forces.

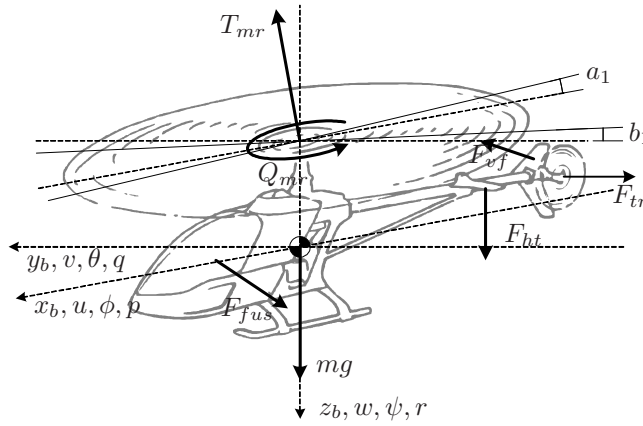


Figure 3.2: Moments and forces acting on the helicopter.

#### 3.3.1 Gravity

The force caused by gravity expressed in the NED frame is:

$$\mathbf{f}_g^n = \begin{bmatrix} 0 \\ 0 \\ mg \end{bmatrix}. \quad (3.11)$$

Transforming this vector to the body frame yields to

$$\mathbf{f}_g^b = \mathbf{R}_b^n(\Theta)^{-1} \mathbf{f}_g^n. \quad (3.12)$$

Finally,  $\mathbf{g}(\boldsymbol{\eta})$  is expressed by

$$\mathbf{g}(\boldsymbol{\eta}) = \begin{bmatrix} \mathbf{f}_g^b \\ 0 \\ 0 \\ 0 \end{bmatrix}. \quad (3.13)$$

With this last equation, the equations of motion in the body frame given by equation (3.3) are written explicitly as:

$$m\dot{u} - mvr + mwq = X_{mr} + X_{fus} - mg \sin \theta \quad (3.14)$$

$$m\dot{v} - mwp + mur = Y_{mr} + Y_{fus} + Y_{tr} + Y_{vf} + mg \sin \phi \cos \theta \quad (3.15)$$

$$m\dot{w} - muq + mvp = Z_{mr} + Z_{fus} + Z_{ht} + mg \cos \phi \cos \theta \quad (3.16)$$

$$I_{xx}\dot{p} + (I_{zz} - I_{yy})qr = L_{mr} + L_{vf} + L_{tr} \quad (3.17)$$

$$I_{yy}\dot{q} + (I_{xx} - I_{zz})pr = M_{mr} + M_{ht} \quad (3.18)$$

$$I_{zz}\dot{r} + (I_{yy} - I_{xx})pq = -Q_e + N_{vf} + N_{tr}. \quad (3.19)$$

### 3.3.2 Main rotor

The main rotor is the primary component of a helicopter. It creates the vertical thrust vector. By rotating the blades, the helicopter is able to move in every direction without rotating the fuselage. The blades are comparable to the wings of an fixed wing aircraft. While rotating, they produce an ascending force, the thrust  $T$ , depending on the angle of attack. One may change the angle of attack by rotating the blades. This is possible in two ways: Either by rotating all blades at the same time, what results in a greater (or less) lift, or by rotating the blades cyclic. Doing so, the blades perform a sine-figure during one rotation. This leads to different lifts on opposite sides of the rotor. The thrust vector pitch and the helicopter moves in this direction. The used main rotor runs with 1600 rpm which is controlled by a governor. The tail rotor is coupled with the main rotor through a gear which is modeled as a simple transition ratio.

#### Main rotor forces and moments

The main rotor forces from equation (3.10) will be described in the following. The main rotor is producing thrust and depending on the cyclic blade settings (cp. figure 3.2). Because of this, the thrust vector has different values in  $u$ ,  $v$  and  $w$  direction:

$$X_{mr} = -T_{mr}a_1, \quad (3.20)$$

$$Y_{mr} = T_{mr}b_1 \text{ and} \quad (3.21)$$

$$Z_{mr} = -T_{mr}. \quad (3.22)$$

$T_{mr}$  is the main rotor thrust and will be presented in section 3.3.3. The angles  $a_1$  and  $b_1$  are based on the blade flapping dynamics described in equation (3.26)-(3.27) and may be seen in figure 3.2. Because of small blade flapping angles (below  $10^\circ$ ), it is possible to use linear approximations (Gavrilets [2003]):

$$\sin \phi \approx \phi \text{ and } \cos \phi \approx 1. \quad (3.23)$$

The total main rotor rolling moment  $L_{mr}$  and the pitching moment  $M_{mr}$  are caused by the distance between the position of the main rotor and the center of gravity and are registered to (Gavrilets [2003])

$$L_{mr} = (K_\beta + T_{mr}h_{mr}) b_1 \text{ and} \quad (3.24)$$

$$M_{mr} = (K_\beta + T_{mr}h_{mr}) a_1. \quad (3.25)$$

Here,  $K_\beta$  is a constant stiffness coefficient of a torsional spring approximating the restrained in the blade attachment to the rotor head, twisted by  $a_1$  resp.  $b_1$ .  $h_{mr}$  stands for the distance between hub height and the center of gravity. The constants can be found in table A.1. The parameters  $a_1$  and  $b_1$  are coming from the main rotor flapping dynamics.

### Blade flapping dynamics

According to Gavrilets [2003], a lot of work has been done on modeling a small scale rotor-craft with Bell-Hiller stabilizer bars. Taking this work into account, the blade flapping dynamics can be represented by the blade tip-path plane lateral ( $b_1$ ) and longitudinal ( $a_1$ ) flapping dynamics presented by Gavrilets [2003]:

$$\dot{b}_1 = -p - \frac{b_1}{\tau_e} - \frac{1}{\tau_e} \frac{\partial b_1}{\partial \mu_v} \frac{v_a}{\Omega R} + \frac{B_{\delta_{lat}}}{\tau_e} \delta_{lat} \text{ and} \quad (3.26)$$

$$\dot{a}_1 = -q - \frac{a_1}{\tau_e} - \frac{1}{\tau_e} \left( \frac{\partial a_1}{\partial \mu} \frac{u_a}{\Omega R} + \frac{\partial a_1}{\partial \mu_z} \frac{w_a}{\Omega R} \right) + \frac{A_{\delta_{lon}}}{\tau_e} \delta_{lon}. \quad (3.27)$$

The  $(\cdot)_a$  components in the equations (3.26) and (3.27) are wind dependent components along the corresponding axes:

$$x_a = x - x_w. \quad (3.28)$$

Here,  $x$  represents a body velocity ( $u$ ,  $v$ , or  $w$ ) and  $x_w$  the wind component along the corresponding axis. In the following,  $(\cdot)_a$  will be used to represent the difference between body velocities and wind.

$B_{\delta_{lat}}$  and  $A_{\delta_{lon}}$  represent the rotor speed dependent cyclic control input to flap gain and can be calculated via equations (3.29) and (3.30):

$$B_{\delta_{lat}} = B_{\delta_{lat}}^{\text{nom}} \left( \frac{\Omega}{\Omega_{\text{nom}}} \right)^2 \text{ and} \quad (3.29)$$

$$A_{\delta_{lon}} = A_{\delta_{lon}}^{\text{nom}} \left( \frac{\Omega}{\Omega_{\text{nom}}} \right)^2. \quad (3.30)$$

$\Omega$  is the current motor speed, compare equation (3.50).  $\tau_e$ ,  $\Omega_{\text{nom}}$ ,  $B_{\delta_{\text{lat}}}^{\text{nom}}$ , and  $A_{\delta_{\text{lon}}}^{\text{nom}}$  can be found in table A.1. The derivatives in equations (3.26) and (3.27) can be expressed through the following set of equations:

$$\frac{\partial a_1}{\partial \mu} = 2K_\mu \left( \frac{4\delta_{\text{col}}}{3} - \lambda_0 \right), \quad (3.31)$$

$$\frac{\partial b_1}{\partial \mu_z} = -\frac{\partial a_1}{\partial \mu}, \text{ and} \quad (3.32)$$

$$\frac{\partial a_1}{\partial \mu_z} = K_\mu \frac{16\mu^2}{(1 - \mu^2/2)(8|\mu| + a\sigma)} \text{sign}(\mu) \approx K_\mu \frac{16\mu^2}{8|\mu| + a\sigma} \text{sign}(\mu). \quad (3.33)$$

$K_\mu$  can be found in table A.1.  $\delta_{\text{lat}}$ ,  $\delta_{\text{lon}}$ , and  $\delta_{\text{col}}$  are control inputs for lateral, longitudinal or collective blade pitch. The calculation of  $\lambda_0$  is explained in equation (3.39)-(3.42) while  $\mu$  is calculated in equation (3.44).

### 3.3.3 Thrust

The basic force generated by an engine is the thrust  $T$ . It is assumed that the rotor inflow is steady and uniform. Gavrillets [2003] shows that the cyclic control authority is dominated by the hub torsional stiffness what makes the modeling of the rotor inflow less critical. Furthermore the inflow is treated to be steady and uniform. Because of this, the induced velocity  $V_{i_{mr}}$  is set to be constant:

$$V_{i_{mr}} = \sqrt{\frac{T_{mr}}{2\rho\Omega_{\text{nom}}R_{mr}}}. \quad (3.34)$$

With  $T_{mr} = mg$  and assuming constant air density with  $\rho = 1.2kg/m^3$ ,  $V_{i_{mr}}$  is set to 4.2 m/s. In general, the thrust  $T$  can be calculated via the thrust coefficient  $C_T$ :

$$T = C_T \rho (\Omega R)^2 \pi R^2. \quad (3.35)$$

The dynamics for  $\Omega$  are described in equation (3.50) and  $R$  represents the rotor radius. The values for main and tail rotor can be found in table A.1. The thrust coefficient  $C_T$  is depending on the inflow ratio  $\lambda_0$  and the commanded collective blade angle  $\theta_0$  which is  $\delta_{\text{col}}$  for the main and  $\delta_r$  for the tail rotor:

$$C_T^{\text{ideal}} = \frac{a\sigma}{2} \left( \theta_0 \left( \frac{1}{3} + \frac{\mu^2}{2} \right) + \frac{\mu_z - \lambda_0}{2} \right). \quad (3.36)$$

Unfortunately the inflow ratio is depending on the thrust coefficient:

$$\lambda_0 = \frac{C_T}{2\eta_w \sqrt{\mu^2 + (\lambda_0 - \mu_z)^2}}. \quad (3.37)$$

Therefore, this set of equations needs to be solved iteratively (Gavrilets [2003], Padfield [1996]). To ensure that the thrust holds the engines limitations, equation (3.38) is applied on the thrust coefficient:

$$C_T = \begin{cases} C_{T_{max}} & \text{if } C_T^{ideal} < -C_{T_{max}} \\ C_{T_{max}} & \text{if } C_T^{ideal} > C_{T_{max}} \\ C_T^{ideal} & \text{otherwise} \end{cases} \quad \text{with} \quad (3.38)$$

$$C_{T_{max}} = \frac{T^{max}}{\rho(\Omega R)^2 \pi R^2}.$$

The following iteration scheme needs to be applied to calculate  $\lambda_0$  and  $C_T$  (Gavrilets [2003], Padfield [1996]):

$$\lambda_{0_{j+1}} = \lambda_{0_j} + f_j h_j(\lambda_{0_j}), \quad (3.39)$$

$$h_j = - \left( \frac{g_0}{dg_0/d\lambda_0} \right)_{\lambda_0=\lambda_{0_j}}, \quad (3.40)$$

$$g_0 = \lambda_0 - \frac{C_T^{ideal}}{2\eta_w \Lambda^{1/2}}, \quad \text{and} \quad (3.41)$$

$$\Lambda = \mu^2 + (\lambda_0 - \mu_z)^2. \quad (3.42)$$

With this, an explicit expression for  $h_j$  can be seen in equation (3.43):

$$h_j = - \frac{(2\eta_w \lambda_{0_j} \Lambda^{1/2} - C_T^{ideal}) \Lambda}{2\eta_w \Lambda^{3/2} + \frac{\sigma}{4} \Lambda - C_T^{ideal} (\mu_z - \lambda_{0_j})}. \quad (3.43)$$

It follows the remaining variables and functions:

$$\mu = \frac{\sqrt{u_a^2 + v_a^2}}{\Omega R}, \quad (3.44)$$

$$\mu_z = \frac{w_a}{\Omega R}, \quad \text{and} \quad (3.45)$$

$$\sigma = \frac{2c}{\pi R}. \quad (3.46)$$

$a$  is the lift curve slope.  $T^{max}$  and  $\eta_w$  can be found in table A.1. Notice that the  $(\cdot)_{mr}$  or  $(\cdot)_{tr}$  index needs to be applied to the above equations to find the corresponding values in table A.1.

Just a few ( $< 10$ ) iteration steps are necessary for converging (Gavrilets [2003]). During hover the denominator of equation (3.37) could become zero when the vertical velocity is equal to inflow velocity (vortex ring conditions). Therefore, it needs to be separated from zero numerically. This is because the presented calculation of the thrust is based on momentum theory and momentum theory can not model the helicopter dynamics during vortex ring conditions.

### 3.3.4 Engine, governor and rotor speed model

The torque  $Q_e$ , produced by the engine (positive clockwise), can be assumed to be proportional to the throttle setting  $0 < \delta_t < 1$  (Gavrilets [2003]):

$$Q_e = \frac{P_e}{\Omega_{mr}} = \frac{P_e^{\max} \delta_t}{\Omega_{mr}}. \quad (3.47)$$

The throttle setting  $\delta_t$  is controlled by the governor, which is modeled as a proportional-integral feedback controller (Gavrilets [2003]) and can be expressed through equation (3.48):

$$\delta_t = K_p(\Omega_c - \Omega_{mr}) + K_i \omega_i \quad \text{with} \quad (3.48)$$

$$\dot{\omega}_i = \Omega_c - \Omega_{mr}, \quad (3.49)$$

where  $\Omega_c$  is the rotor speed command and  $K_i$  and  $K_p$  are feedback gains of the governor and were determined for the modeled helicopter by Gavrilets [2003]. The values can be found in table A.1.

The rotor speed dynamics are represented by (Gavrilets [2003]):

$$\dot{\Omega} = \dot{r} + \frac{1}{I_{\text{rot}}} (Q_e - Q_{mr} - n_{\text{tr}} Q_{tr}), \quad (3.50)$$

where  $n_{\text{tr}}$  can be found in table A.1. Approximating the main rotor as a flat solid plate with equal distributed weight one get for  $I_{\text{rot}}$ :

$$I_{\text{rot}} = \frac{1}{4} m_{\text{blades}} R_{\text{mr}}^2. \quad (3.51)$$

The total weight of blades and stabilizer bars is estimated to be 0.4 kg based on proposals of several blade distributors.

The torque  $Q_{mr}$  (positive counter clockwise) can be expressed through the torque coefficient  $C_Q$ :

$$Q_{mr} = C_Q \rho (\Omega R)^2 \pi R^3 \quad \text{with} \quad (3.52)$$

$$C_Q = C_T (\lambda_0 - \mu_z) + \frac{C_{D_0} \sigma}{8} \left( 1 + \frac{7}{3} \mu^2 \right). \quad (3.53)$$

### 3.3.5 Fuselage forces

Forces, caused by the rotor down wash hitting the fuselage can be approximated by following equations Gavrilets [2003]:

$$X_{fus} = -0.5 \rho S_x^{\text{fus}} u_a V_\infty, \quad (3.54)$$

$$Y_{fus} = -0.5 \rho S_y^{\text{fus}} v_a V_\infty, \quad (3.55)$$

$$Z_{fus} = -0.5 \rho S_z^{\text{fus}} (w_a + V_{\text{imr}}) V_\infty \quad \text{with} \quad (3.56)$$

$$V_\infty = \sqrt{u_a^2 + v_a^2 + (w_a + V_{\text{imr}})^2}. \quad (3.57)$$

The  $S_{(\cdot)}^{\text{fus}}$  components represent the effective drag areas of the fuselage. The values for  $S_x^{\text{fus}}$ ,  $S_y^{\text{fus}}$ ,  $S_z^{\text{fus}}$ , and  $V_{\text{imr}}$  can be found in table A.1.

### 3.3.6 Tail rotor

The tail rotor is responsible for rotating the helicopter around its vertical axis and controls the yaw dynamics. Therefore, it needs to compensate the yawing moment introduced by the main rotor (cp. equation (3.52)).

The tail rotor is used in a lot of different flow circumstances. It can be fully or partial in the down wash of the main rotor (e.g. during forward flight) or it can operate in it's own wake at low in-plane airspeed (Gavrilets [2003]). The presented iteration scheme from equation (3.39)-(3.43) would fail. Therefore, the nominal force  $Y_{tr}$  needs to be calculated in an other way than  $Z_{mr}$ . The side force from equation (3.58), the resulting yawing moment from equation (3.59), and a rolling moment from equation (3.60) will be calculated in the following:

$$Y_{tr} = mY_{\delta_r}^{tr} \delta_r + mY_v^{tr} \mu_z^{tr} \Omega_{tr} R_{tr}, \quad (3.58)$$

$$N_{tr} = -Y_{tr} l_{tr}, \text{ and} \quad (3.59)$$

$$L_{tr} = Y_{tr} h_{tr}. \quad (3.60)$$

In equation (3.58), the thrust inflow iteration is linearized around the trim conditions ( $\dot{\boldsymbol{\nu}} = 0$ )

$$\mathbf{C}_{RB}(\boldsymbol{\nu})\boldsymbol{\nu} = \mathbf{T}(\mathbf{x}, \mathbf{u}_{trim}) + \mathbf{g}(\boldsymbol{\eta}). \quad (3.61)$$

This results in the corresponding dimensional stability derivatives  $Y_v^{tr}$  and  $Y_{\delta_r}^{tr}$ :

$$Y_v^{tr} = -C_{T_{\mu_z^{tr}}}^{tr} \frac{f_t \rho \Omega_{tr} R_{tr} \pi R_{tr}^2}{m} \text{ and} \quad (3.62)$$

$$Y_{\delta_r}^{tr} = -C_{T_{\delta_r}}^{tr} \frac{f_t \rho (\Omega_{tr} R_{tr})^2 \pi R_{tr}^2}{m}. \quad (3.63)$$

Where  $C_{T_{\mu_z^{tr}}}^{tr}$  and  $C_{T_{\delta_r}}^{tr}$  are partial, non dimensional derivatives of the thrust coefficient:

$$C_{T_{\mu_z^{tr}}}^{tr} = \frac{\partial C_T^{tr}}{\partial \mu_z^{tr}} (|\mu_{tr}|, \mu_z^{tr} = 0, \delta_r^{trim}), \text{ and} \quad (3.64)$$

$$C_{T_{\delta_r}}^{tr} = \frac{\partial C_T^{tr}}{\partial \delta_r} (|\mu_{tr}|, \mu_z^{tr} = 0, \delta_r^{trim}). \quad (3.65)$$

In Gavrilets [2003] those derivatives were calculated numerically, while  $C_T^{tr}$  is calculated like the main rotor thrust coefficient using tail rotor values. In this thesis, the derivatives are realized by implementing a solution given in Padfield [1996], page 219 and 229. Padfield found for each derivative two approximations, one for forward flight:

$$\frac{\partial C_T}{\partial \mu_z} \approx \frac{2a\sigma\mu}{8\mu + a\sigma}, \quad (3.66)$$

$$\frac{\partial C_T}{\partial \theta_0} \approx \frac{4}{3} \left[ \frac{a\sigma\mu(1 + 1.5\mu^2)}{8\mu + a\sigma} \right], \quad (3.67)$$

and one for hover:

$$\frac{\partial C_T}{\partial \mu_z} \approx \frac{2a\sigma\lambda_0}{16\lambda_0 + a\sigma}, \quad (3.68)$$

$$\frac{\partial C_T}{\partial \theta_0} \approx \frac{8}{3} \left[ \frac{a\sigma\lambda_0}{16\lambda_0 + a\sigma} \right]. \quad (3.69)$$

The transition is realized by a linear adaption:

$$\frac{\partial C_T}{\partial \mu_z} = x \frac{\partial C_T}{\partial \mu_z}_{hover} + (1-x) \frac{\partial C_T}{\partial \mu_z}_{forward\ flight} \quad \text{with} \quad (3.70)$$

$$x = \begin{cases} 0 & \|\mathbf{v}_b^0\| > \mathbf{v}_{b\,ff}^0 \\ \frac{\|\mathbf{v}_b^0\|}{\mathbf{v}_{b\,ff}^0} & \text{otherwise} \end{cases}. \quad (3.71)$$

Furthermore, it is necessary to calculate the tail rotor inflow components  $\mu_z^{tr}$  and  $\mu_{tr}$  which are given by

$$\mu_{tr} = \frac{\sqrt{u_a^2 + w_{tr}^2}}{\Omega_{tr} R_{tr}} \quad \text{and} \quad (3.72)$$

$$\mu_{z\,tr} = \frac{v_{tr}}{\Omega_{tr} R_{tr}}. \quad (3.73)$$

The corresponding tail rotor body velocities  $w_{tr}$  and  $v_{tr}$  are given by Gavrilets [2003]:

$$\begin{aligned} v_{tr} &= v_a - l_{tr}r + h_{tr}p \quad \text{and} \\ w_{tr} &= w_a + l_{tr}q - K_\lambda V_{i\,mr}. \end{aligned} \quad (3.74)$$

$K_\lambda$  approximates the very complex relationship between main rotor wake affects and tail rotor thrust. Depending on helicopter speed and main rotor induced velocity, the backward components tail rotor, horizontal stabilizer bar, and vertical fin are complete, partial, or not in the wake or down wash of the main rotor (Gavrilets [2003]):

$$K_\lambda = \begin{cases} 0 & V_{i\,mr} \leq w_a & \text{not in wake} \\ 0 & \frac{u_a}{V_{i\,mr} - w_a} \leq g_i & \text{not in wake} \\ 1.5 & \frac{u_a}{V_{i\,mr} - w_a} \geq g_f & \text{full in wake} \\ 1.5 \frac{\frac{u_a}{V_{i\,mr} - w_a} - g_i}{g_f - g_i} & \text{else} & \text{partial in wake} \end{cases}, \quad \text{with} \quad (3.75)$$

$$g_i = \frac{l_{tr} - R_{mr} - R_{tr}}{h_{tr}} \quad \text{and} \quad (3.76)$$

$$g_f = \frac{l_{tr} - R_{mr} + R_{tr}}{h_{tr}}. \quad (3.77)$$

Two parameter are missing to complete equation (3.58):

$$f_t = 1.0 - \frac{3}{4} \frac{S_{vf}}{\pi R_{tr}^2} \text{ and} \quad (3.78)$$

$$\Omega_{tr} = n_{tr} \Omega_{mr}. \quad (3.79)$$

$f_t$  is the fin blockage factor (Gavrilets [2003], Padfield [1996]) and can be found together with the tail rotor gear ratio  $n_{tr}$  in table A.1.

### 3.3.7 Horizontal stabilizer forces and moments

The horizontal tail produces primary lift (cp. equation (3.80)). Furthermore it stabilizes the, by main rotor blade flapping disturbed, pitching motion during vertical flight (cp. equation (3.81)). Therefore, it is assumed that the horizontal tail is located in the flow field of the main rotor Gavrilets [2003], Heffley and Mnich [1988]. The corresponding horizontal stabilizer force and moment are calculated by

$$Z_{ht} = 0.5 \rho S_{ht} [C_{L\alpha}^{ht} |u_a| w_{ht} + |w_{ht}| w_{ht}] \text{ and} \quad (3.80)$$

$$M_{ht} = Z_{ht} l_{ht} \text{ with} \quad (3.81)$$

$$w_{ht} = w_a + l_{ht} q - K_\lambda V_{imr}. \quad (3.82)$$

The same  $K_\lambda$  is used as presented in the tail rotor section (cp. equation(3.75)). The lift force is limited in respect to stall:

$$|Z_{ht}| \leq 0.5 \rho S_{ht} [u_a^2 + w_{ht}^2]. \quad (3.83)$$

### 3.3.8 Vertical fin

The side force caused by the verticla fin can be approximated through

$$Y_{vf} = -0.5 \rho S_{vf} (C_{L\alpha}^{vf} V_\infty^{tr} + |v_{vf}|) v_{vf}, \quad (3.84)$$

where

$$V_\infty^{tr} = \sqrt{u_a^2 + w_{tr}^2}, \text{ and} \quad (3.85)$$

$$v_{vf} = v_a - \epsilon_{vf}^{tr} V_{itr} - l_{tr} r. \quad (3.86)$$

The tail rotor induced velocity  $V_{itr}$  can be calculated by Padfield [1996, page 116]:

$$V_{itr} = \lambda_0 \Omega R. \quad (3.87)$$

$\lambda_0$  and the tail rotor thrust coefficient  $C_T$  can be calculated with the iteration scheme given for the main rotor, using the tail rotor parameters.  $Q_{tr}$  could be

calculated the same way using equation (3.52) as basis.

$w_{tr}$  is calculated in equation (3.74). Notice that there is an absolute value for  $Y_{vf}$ . This is to take stall into account:

$$|Y_{vf}| \leq 0.5\rho S_{vf} \left[ (V_{\infty}^{tr})^2 + V_{vf}^2 \right]. \quad (3.88)$$

The side force generated by the vertical fin in equation (3.84) causes the two moments  $N_{vf}$  and  $L_{vf}$ :

$$N_{vf} = -Y_{vf}l_{tr} \text{ and} \quad (3.89)$$

$$L_{vf} = Y_{vf}h_{tr} \quad (3.90)$$

### 3.4 Model verification

The model has been implemented in MATLAB<sup>TM</sup>/Simulink<sup>TM</sup>. Therefore, the quaternion representation, respectively equation (2.27), was used. Figure 3.3 shows a simulation, controlling the altitude and the yaw angle of the presented X-Cell model with simple PD controllers. The model behaves as suggested. A pitch angle  $\theta$  result in a movement in negative  $x$  direction and a roll angle  $\psi$  in a movement in  $y$  direction. The angles are introduced because of tail rotor moments and blade flapping.

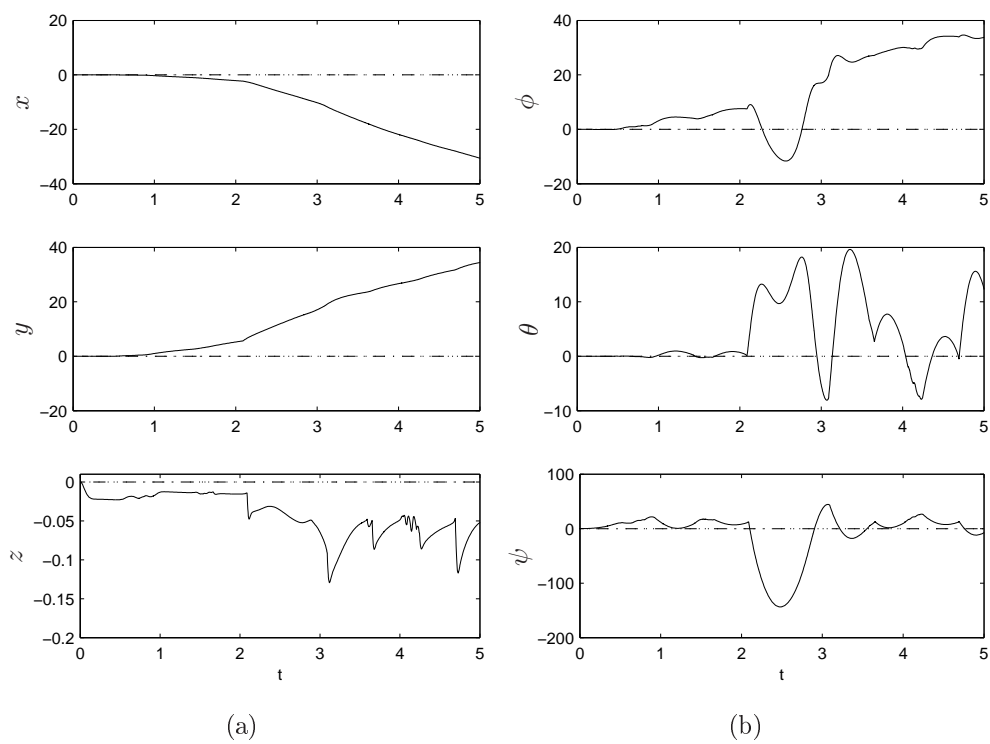


Figure 3.3: X-Cell model verification.  
Subfigure 3.3(a) shows the position and 3.3(b) the attitude in degree.

# Chapter 4

## Control of UAV

During flight the states of a helicopter show a large variation. In addition, a helicopter has fewer independent control actuators than degrees of freedom to be controlled. As shown by Gonzalez et al. [2004], linear control laws can be applied for hovering but result in instability during flight. Therefore, it is necessary to use nonlinear control techniques.

There are several approaches for nonlinear control of Gavrillets helicopter model. At first Marconi and Naldi [2006] was implemented. This controller is based on decoupling of the control inputs and a nested saturation control, compare Angeli et al. [2003]. This controller seems to be very robust and works very well for a simplified model. Unfortunately these simplifications make a lot of problems if the controller runs on the complete model. Because of that, an other approach was chosen. In Bogdanov et al. [2004] a controller, based on a state-dependent Riccati equation (SDRE), is presented. This controller was verified in simulations and during real flights with a X-Cell and R-Max model helicopter. The controller will be presented in the following. An other approach which seems to be very successful is based on neuronal networks and presented by Johnson and Kannan [2002].

### 4.1 SDRE theory

The state-dependent Riccati equation control is a nonlinear discrete time approach. Unfortunately, there are no proofs for global asymptotic stability and robustness of SDRE systems as shown by Erdem [2001]. But Erdem wrote also:

In other words, via SDRE, the design flexibility of LQR formulation is directly translated to control of nonlinear systems.

And Bogdanov et al. [2004] wrote:

The SDRE control generally exhibits greater stability and better performance than linear control laws (e.g. LQR), and empirical

experience often shows that in many cases the domain of attraction is as large as the domain of interest.

As a major disadvantage, the discrete-time Riccati equation has to be solved at each time step:

$$\mathbf{P}_k = \Phi^T [\mathbf{P}_{k+1} - \mathbf{P}_{k+1} \Gamma (\mathbf{R} + \Gamma \mathbf{P}_{k+1} \Gamma)^{-1} \Gamma^T \mathbf{P}_{k+1}] \Phi + \mathbf{Q}. \quad (4.1)$$

Hereby,  $\Phi(\mathbf{x})$  and  $\Gamma(\mathbf{x})$  are approximated discretizations of the state-dependent matrices  $\mathbf{A}(\mathbf{x})$  and  $\mathbf{B}(\mathbf{x})$  in the state-dependent coefficient (SDC) system

$$\dot{\mathbf{x}} = \mathbf{A}(\mathbf{x})\mathbf{x} + \mathbf{B}(\mathbf{x})\mathbf{u}. \quad (4.2)$$

With

$$\mathbf{0} = \mathbf{A}(\mathbf{x}_0)\mathbf{x}_0 + \mathbf{B}(\mathbf{x}_0)\mathbf{u}|_{\mathbf{x}_0=\mathbf{0}}. \quad (4.3)$$

$\mathbf{A}(\mathbf{x})$  and  $\mathbf{B}(\mathbf{x})$  need to be point wise controllable (Bogdanov et al. [2004]). The discretization could be performed by applying

$$\Phi(\mathbf{x}_a) \approx e^{\mathbf{A}(\mathbf{x}_a)\Delta t} \text{ and} \quad (4.4)$$

$$\Gamma(\mathbf{x}_a) \approx \mathbf{B}(\mathbf{x}_a)\Delta t. \quad (4.5)$$

This leads to the control law

$$\mathbf{u}_k = -\mathbf{R}^{-1}\Gamma(\mathbf{x}_k)^T \mathbf{P}(\mathbf{x}_k) (\mathbf{x}_k - \mathbf{x}_k^{ref}) \equiv -\mathbf{K}(\mathbf{x}_k)\mathbf{e}_k. \quad (4.6)$$

## 4.2 Reference generation

As a trajectory  $x_r$ ,  $y_r$ ,  $z_r$ , and  $\psi_r$  have to be given.  $\psi_r$  can be chosen in different ways. Either it can be set explicitly or it can be chosen to cause forward flight. This could be realized by using the helicopters position  $\mathbf{p}^n$  and the reference position  $\mathbf{p}_r^n$ :

$$\mathbf{e}^n = \mathbf{p}^n - \mathbf{p}_r^n = [e_x \ e_y \ e_z]^T. \quad (4.7)$$

Depending on the direction of flight, which should be toward the reference trajectory,  $\psi_r$  can be calculated via the arctan:

$$\tilde{\psi}_r = -\arctan\left(\frac{e_y}{e_x}\right). \quad (4.8)$$

One should be aware that the z axis is going from up to down and therefore  $\psi$  rotates clockwise if the helicopter is seen from above. One should also keep in mind that  $\arctan(e_y/e_x)$  returns the same result for the first and third and for the second and fourth quadrant. Because of that, a determination is necessary:

$$\psi_r = \begin{cases} \tilde{\psi}_r & e_x \geq 0 \\ -\tilde{\psi}_r - \pi/2 \text{ sign}(e_y) & e_x < 0 \end{cases}. \quad (4.9)$$

The case  $e_x = e_y = 0$  needs to be covered separately. Depending on the controller used for the vehicle it can be possible that a continuous trajectory is needed. Therefor  $\psi_r$  can be filtered by a simple PT<sub>2</sub>:

$$G(s) = \frac{K}{\frac{1}{\omega_0^2}s^2 + \frac{2D}{\omega_0}s + 1}. \quad (4.10)$$

It is advisable to avoid overshooting. Therefor the damping factor  $D$  should be  $\geq 1$ . Due to several tests

$$G(s) = \frac{1}{\frac{1}{25}s^2 + \frac{2.6}{5}s + 1} \quad (4.11)$$

could be validated.

A positive change in  $\psi_r$  is done by a positive rotation and a negative change by a negative. If  $\psi_r$  changes from  $\pi - \epsilon$  to  $\pi + \epsilon$  with  $\epsilon > 0$  it is possible that an almost  $2\pi$  rotation is performed. If this change is caused by an overshoot the yawing movement can become unstable. To solve this problem, it is either necessary to avoid these changes by declaring  $-\pi + \epsilon < \psi_r < \pi - \epsilon$  choosing  $\epsilon > 0$  or implement some kind of hysteresis to cause the controller to rotate the helicopter over the short interval.

The remaining states are calculated via the following equations which are presented by Marconi and Naldi [2006]:

$$\phi_r = \text{atan2}(-c\theta_r s\phi_r n_x + c\theta_r c\psi_r n_y, -n_z) \text{ and} \quad (4.12)$$

$$\theta_r = \text{atan2}(-s\psi_r n_y + c\psi_r n_x, n_z) \quad (4.13)$$

with  $s \equiv \sin(\cdot)$  and  $c \equiv \cos(\cdot)$ . here,  $\mathbf{n}$  represents the normalized vector:

$$\mathbf{n} = \begin{bmatrix} n_x \\ n_y \\ n_z \end{bmatrix} = \begin{bmatrix} \ddot{x}_r/a_r \\ \ddot{y}_r/a_r \\ (\ddot{z}_r - \mathbf{g})/a_r \end{bmatrix}, \quad (4.14)$$

$$a_r = \sqrt{\ddot{x}_r^2 + \ddot{y}_r^2 + (\ddot{z}_r - \mathbf{g})^2}. \quad (4.15)$$

As one can see, a singularity appears for  $\ddot{x}_r = \ddot{y}_r = 0$  and  $\ddot{z}_r = \mathbf{g}$ . If the used simulation program is able to divide by zero, the arctan handles the  $\infty$  value. If the program is not able to deal with dividing by zero a numerical separation is necessary.

$\omega_{nb}^b$  can be calculated using equation (2.15).

### 4.3 SDRE control of UAV

The controller presented by Bogdanov et al. [2004] observes 12 states. These are:

$$\left. \begin{array}{l} u \\ v \\ w \\ p \\ q \\ r \end{array} \right\} \left. \begin{array}{l} \mathbf{v}_b^0 \\ \\ \boldsymbol{\omega}_{nb}^n \end{array} \right\} \boldsymbol{\nu}$$

$$\left. \begin{array}{l} x \\ y \\ z \\ \phi \\ \theta \\ \psi \end{array} \right\} \left. \begin{array}{l} \mathbf{p}^n \\ \\ \boldsymbol{\Theta} \end{array} \right\} \boldsymbol{\eta}$$

The controller calculates the control variables known from equation (3.1) except for  $\delta_t$  which is given by the governor:

$$\mathbf{u} = [ \delta_{col} \quad \delta_{lon} \quad \delta_{lat} \quad \delta_r ]^T. \quad (4.16)$$

Unfortunately, the helicopter model can not be represented by equation (4.2) completely. Because of this, a mismatch term  $\Delta f(\mathbf{x})$  is added to (4.2) to represent the remaining parts of the model:

$$\dot{\mathbf{x}} = f(\mathbf{x}, \mathbf{u}) = \mathbf{A}(\mathbf{x})\mathbf{x} + \mathbf{B}(\mathbf{x})\mathbf{u} + \Delta f(\mathbf{x}, \mathbf{u}). \quad (4.17)$$

Therefore, a compensator is developed from Bogdanov et al. [2004] to cancel this mismatch:

$$f(\mathbf{x}, \mathbf{u}^{sd} + \mathbf{u}^c) \approx \mathbf{A}(\mathbf{x})\mathbf{x} + \mathbf{B}(\mathbf{x})\mathbf{u}. \quad (4.18)$$

Here, the SDRE control  $\mathbf{u}^{sd}$  is supplemented with a static nonlinear compensator  $\mathbf{u}^c$ . The calculation of both parts will be presented in the following.

#### 4.3.1 SDC form

Regarding that the helicopters equation of motion are build up due to gravity and external forces one can write

$$\dot{\mathbf{x}} = f_{rb}(\mathbf{x}) + \mathbf{T}(\mathbf{x}, \mathbf{u}) \quad (4.19)$$

with the rigid body dynamics  $f_{rb}(\mathbf{x})$  and the external forces  $\mathbf{T}(\mathbf{x}, \mathbf{u})$ . These parts can now be split up in one part which can be represent in SDC form and an other part which can not:

$$\begin{aligned} f_{rb}(\mathbf{x}) + \mathbf{T}(\mathbf{x}, \mathbf{u}) &= \mathbf{A}_{rb}(\mathbf{x})\mathbf{x} + \Delta f_{rb}(\mathbf{x}) + \\ &\quad \mathbf{A}_T(\mathbf{x})\mathbf{x} + \mathbf{B}_T(\mathbf{x})\mathbf{u} + \Delta \mathbf{T}(\mathbf{x}, \mathbf{u}). \end{aligned} \quad (4.20)$$

Another description for the nonlinear model is

$$\dot{\mathbf{x}} = f_{rb}(\mathbf{x}) + \mathbf{T}_d(\mathbf{x}, \mathbf{u}) + \mathbf{T}_u(\mathbf{x}, \mathbf{u}). \quad (4.21)$$

$f_{rb}(\mathbf{x})$  represents the rigid body dynamics while  $\mathbf{T}_d(\mathbf{x}, \mathbf{u})$  and  $\mathbf{T}_u(\mathbf{x}, \mathbf{u})$  represents the external drag ( $\mathbf{T}_d(\mathbf{x}, \mathbf{u})$ ) and rotor ( $\mathbf{T}_u(\mathbf{x}, \mathbf{u})$ ) dependent forces.

The split up will be performed for the external forces in the following.

### External Forces

To derive a control law, the flapping  $a_1$  and  $b_1$  are approximated as steady state. Following Bogdanov et al. [2004] and Marconi and Naldi [2006], the influence of the cyclic control input is neglected. As shown in section 3.3, the forces acting on the helicopter are:

$$\mathbf{T} = \begin{bmatrix} X \\ Y \\ Z \\ L \\ M \\ N \end{bmatrix} = \begin{bmatrix} X_{mr} + X_{fus} \\ Y_{mr} + Y_{fus} + Y_{tr} + Y_{vf} \\ Z_{mr} + Z_{fus} + Z_{ht} \\ L_{mr} + L_{vf} + L_{tr} \\ M_{mr} + M_{ht} \\ -Q_e + N_{vt} + N_{tr} \end{bmatrix}. \quad (4.22)$$

For the split up, the thrust is linearized around a specific control input  $\delta_{col}^0$  and the current state:

$$T_{mr} = T_{mr}(\mathbf{x}, \mathbf{x}_w, \delta_{col}^0) + \frac{\partial T_{mr}(\mathbf{x}, \mathbf{x}_w, \delta_{col}^0)}{\partial \delta_{col}} (\delta_{col} - \delta_{col}^0) + O^2. \quad (4.23)$$

For a better accuracy,  $\delta_{col}^0$  can be chosen as the  $\delta_{col}$  value from the last time step.  $\partial T_{mr}(\mathbf{x}, \mathbf{x}_w, \delta_{col}^0) / \partial \delta_{col}$  is given in Bogdanov et al. [2004] as

$$\begin{aligned} \frac{\partial T_{mr}}{\partial \delta_{col}} &= \frac{a_{mr}\sigma}{4} \left( \frac{2}{3} + \mu^2 - \frac{C_T a_{mr} \sigma \lambda_0 (2/3 + \mu^2)}{4C_t^2 + C_T a_{mr} \sigma \lambda_0 - 16\lambda_0^3 \eta_w^2 (\mu_z - \lambda_0)} \right) \rho \\ &\quad \cdot V_{tip}^2 S_{mr}. \end{aligned} \quad (4.24)$$

Because of a shorter notation,  $\Delta T_{mr}(\mathbf{x}, \mathbf{x}_w, \delta_{col}^0)$  is introduced and defined as follows:

$$\Delta T_{mr}(\mathbf{x}, \mathbf{x}_w, \delta_{col}^0) = T_{mr}(\mathbf{x}, \mathbf{x}_w, \delta_{col}^0) - \frac{\partial T_{mr}(\mathbf{x}, \mathbf{x}_w, \delta_{col}^0)}{\partial \delta_{col}} \delta_{col}^0. \quad (4.25)$$

**$X_{mr}$ -force** The split up will be done in detail for the  $X_{mr}$  force. The results for the remaining forces can be found in appendix B. The  $X_{mr}$  force is given by equation (3.20) as follows:

$$X_{mr} = -T_{mr}a_1(\mathbf{x}, \mathbf{x}_w, \delta_{lon}) \quad (4.26)$$

$$= -T_{mr} [a_1(\mathbf{x}, 0, 0) + a_1(0, \mathbf{x}_w, 0) + a_1(0, 0, \delta_{lon})]. \quad (4.27)$$

Applying the thrust linearization leads to

$$\begin{aligned} X_{mr} = & - \left( T_{mr}(\mathbf{x}, \mathbf{x}_w, \delta_{col}^0) + \frac{\partial T_{mr}(\mathbf{x}, \mathbf{x}_w, \delta_{col}^0)}{\partial \delta_{col}} (\delta_{col} - \delta_{col}^0) + O^2 \right) \\ & \cdot \left( -\tau_e q + \frac{\partial a_1}{\partial \mu} \frac{u - u_w}{\Omega_{mr} R_{mr}} + \frac{\partial a_1}{\partial \mu_z} \frac{w - w_w}{\Omega_{mr} R_{mr}} + A_{\delta_{lon}}^{\text{nom}} \delta_{lon} \right). \end{aligned} \quad (4.28)$$

This equation can be separated in parts regarding the different states and control inputs with respect to equation (4.20). The state depending parts will go into  $\mathbf{A}_T(\mathbf{x})$  while the control input depending parts enter  $\mathbf{B}_T(\mathbf{x})$ :

$$X_{mr}^q = \left( T_{mr}(\mathbf{x}, \mathbf{x}_w, \delta_{col}^0) - \frac{\partial T_{mr}(\mathbf{x}, \mathbf{x}_w, \delta_{col}^0)}{\partial \delta_{col}} \delta_{col}^0 \right) \tau_e \quad (4.29)$$

$$= \Delta T_{mr}(\mathbf{x}, \mathbf{x}_w, \delta_{col}^0) \tau_e, \quad (4.30)$$

$$X_{mr}^u = -\Delta T_{mr}(\mathbf{x}, \mathbf{x}_w, \delta_{col}^0) \frac{\partial a_1}{\partial \mu} \frac{1}{\Omega_{mr} R_{mr}}, \quad (4.31)$$

$$X_{mr}^w = -\Delta T_{mr}(\mathbf{x}, \mathbf{x}_w, \delta_{col}^0) \frac{\partial a_1}{\partial \mu_z} \frac{1}{\Omega_{mr} R_{mr}}, \quad (4.32)$$

$$X_{mr}^{\delta_{col}} = -\frac{\partial T_{mr}(\mathbf{x}, \mathbf{x}_w, \delta_{col}^0)}{\partial \delta_{col}} a_1(\mathbf{x}, \mathbf{x}_w, 0), \text{ and} \quad (4.33)$$

$$X_{mr}^{\delta_{lon}} = -\Delta T_{mr}(\mathbf{x}, \mathbf{x}_w, \delta_{col}^0) A_{\delta_{lon}}^{\text{nom}}. \quad (4.34)$$

The remaining part can not be used in the SDC form and needs to be covered by the compensator:

$$\begin{aligned} \Delta X_{mr} = & \left( \Delta T_{mr}(\mathbf{x}, \mathbf{x}_w, \delta_{col}^0) + \frac{\partial T_{mr}(\mathbf{x}, \mathbf{x}_w, \delta_{col}^0)}{\partial \delta_{col}} \delta_{col} + O^2 \right) \\ & \cdot \frac{\partial a_1}{\partial \mu} \frac{u_w}{\Omega_{mr} R_{mr}} - \left( \frac{\partial T_{mr}(\mathbf{x}, \mathbf{x}_w, \delta_{col}^0)}{\partial \delta_{col}} \delta_{col} + O^2 \right) A_{\delta_{lon}}^{\text{nom}} \delta_{lon}. \end{aligned} \quad (4.35)$$

**Matrix  $\mathbf{A}(\mathbf{x})$** 

With

$$\mathbf{A}(\mathbf{x}) = \mathbf{A}_{rb}(\mathbf{x}) + \mathbf{A}_T(\mathbf{x}), \quad (4.36)$$

matrix  $\mathbf{A}$  is given by

$$\mathbf{A} = \begin{bmatrix} \mathbf{A}_{11} & \mathbf{A}_{12} & \mathbf{0}_{3 \times 3} & \mathbf{A}_{14} \\ \mathbf{A}_{21} & \mathbf{A}_{22} & \mathbf{0}_{3 \times 3} & \mathbf{0}_{3 \times 3} \\ \mathbf{0}_{3 \times 3} & \Psi(\phi, \theta, \psi) & \mathbf{0}_{3 \times 3} & \mathbf{0}_{3 \times 3} \\ \mathbf{R}(\phi, \theta, \psi) & \mathbf{0}_{3 \times 3} & \mathbf{0}_{3 \times 3} & \mathbf{0}_{3 \times 3} \end{bmatrix}. \quad (4.37)$$

Here,  $\mathbf{A}_{11}$  describes the influence of the body velocity to the body accelerations:

$$\mathbf{A}_{11} = \begin{bmatrix} \frac{X_{mr}^u + X_{fus}^u}{m} & r & -q + \frac{X_{mr}^w}{m} \\ -r & \frac{Y_{mr}^v + Y_{fus}^v + Y_{vf}^v}{m} & p \\ q & -p & \frac{Z_{fus}^w + Z_{ht}^w}{m} \end{bmatrix}. \quad (4.38)$$

$\mathbf{A}_{12}$  describes the influence of the body angular velocity to the body accelerations:

$$\mathbf{A}_{12} = \begin{bmatrix} 0 & X_{mr}^q & 0 \\ Y_{mr}^p & 0 & Y_{fv}^r \\ 0 & Z_{ht}^q & 0 \end{bmatrix}. \quad (4.39)$$

$\mathbf{A}_{14}$  describes the influence of gravity to the body accelerations:

$$\mathbf{A}_{14} = \begin{bmatrix} 0 & -g \frac{\sin \theta}{\theta} & 0 \\ g \frac{\sin \phi}{\phi} \cos \theta & 0 & 0 \\ 0 & 0 & 0 \end{bmatrix}. \quad (4.40)$$

Notice that  $\sin x/x = 1$  for  $x = 0$ . Because of this,  $\mathbf{A}_{14}$  is nonsingular. This probably has to be covered in the simulation manually. The last row of  $\mathbf{A}_{14}$  is zero because the gravity influence on  $\dot{w}$  does not full fill the requirement from equation (4.3). For a complete presentation the forces, caused by gravity, are given by:

$$f(\mathbf{x})_{rb} = \mathbf{A}_{rb}(\mathbf{x})\mathbf{x} + \Delta \mathbf{f}_{rb}(\mathbf{x}), \quad (4.41)$$

$$\mathbf{A}_{rb}(\mathbf{x}) = \begin{bmatrix} \mathbf{A}_{14} \\ \mathbf{0}_{9 \times 1} \end{bmatrix}, \text{ and} \quad (4.42)$$

$$\Delta \mathbf{f}_{rb} = \begin{bmatrix} \mathbf{0}_{2 \times 1} \\ g \cos \theta \cos \phi \\ \mathbf{0}_{9 \times 1} \end{bmatrix}. \quad (4.43)$$

$\mathbf{A}_{21}$  describes the influence of the body velocity to the body angular accelerations:

$$\mathbf{A}_{21} = \begin{bmatrix} 0 & L_{mr}^v + L_{vf}^v & 0 \\ M_{mr}^u & 0 & M_{mr}^w + M_{ht}^w \\ 0 & N_{vf}^v & 0 \end{bmatrix}. \quad (4.44)$$

$\mathbf{A}_{22}$  describes the influence of the body angular velocity to the body angular accelerations:

$$\mathbf{A}_{22} = \begin{bmatrix} L_{mr}^p/I_{xx} & \frac{I_{yy}-I_{zz}}{2I_{xx}}r & \frac{I_{yy}-I_{zz}}{2I_{xx}}q + L_{vf}^r/I_{xx} \\ \frac{I_{zz}-I_{xx}}{2I_{yy}}r & (M_{mr}^q + M_{ht}^q)/I_{yy} & \frac{I_{zz}-I_{xx}}{2I_{yy}}p \\ \frac{I_{xx}-I_{yy}}{2I_{zz}}q & \frac{I_{xx}-I_{yy}}{2I_{zz}}p & N_{vf}^r/I_{zz} \end{bmatrix}. \quad (4.45)$$

### Matrix $\mathbf{B}(\mathbf{x})$

Matrix  $\mathbf{B}_T$  from equation (4.20) will be named just  $\mathbf{B}$  in the former. Similar to matrix  $\mathbf{A}$ ,  $\mathbf{B}$  is build up from several sub-matrices:

$$\mathbf{B} = \begin{bmatrix} \mathbf{B}_1 \\ \mathbf{B}_2 \\ \mathbf{0}_{6 \times 4} \end{bmatrix}. \quad (4.46)$$

Matrix  $\mathbf{B}_1$  describes the influence of the four control values, calculated by the controller, on the body velocity:

$$\mathbf{B}_1 = \begin{bmatrix} X_{mr}^{\delta_{col}} & X_{mr}^{\delta_{lon}} & 0 & 0 \\ Y_{mr}^{\delta_{col}} & 0 & Y_{mr}^{\delta_{lat}} & Y_{tr}^{\delta_r} \\ Z_{mr}^{\delta_{col}} & 0 & 0 & 0 \end{bmatrix}. \quad (4.47)$$

Matrix  $\mathbf{B}_2$  describes the influence of the four control values on the body angular velocity:

$$\mathbf{B}_2 = \begin{bmatrix} L_{mr}^{\delta_{col}} & 0 & L_{mr}^{\delta_{lat}} & L_{tr}^{\delta_r} \\ M_{mr}^{\delta_{col}} & M_{mr}^{\delta_{lon}} & 0 & 0 \\ 0 & 0 & 0 & N_{tr}^{\delta_r} \end{bmatrix}. \quad (4.48)$$

### 4.3.2 Compensator

A compensator is designed to eliminate the mismatch between the SDC model and the real model. The idea is to add an additional control input based on the current state and  $\mathbf{u}^{sd}$ , following Bogdanov et al. [2004]:

$$f(\mathbf{x})_{rb} + \mathbf{T}(\mathbf{x}, \mathbf{x}_w, \mathbf{u}^{sd}) \equiv \mathbf{A}(\mathbf{x})\mathbf{x} + \mathbf{B}(\mathbf{x})\mathbf{u}^{sd} + \Delta f(\mathbf{x}, \mathbf{u}^{sd}), \quad (4.49)$$

$$f(\mathbf{x})_{rb} + \mathbf{T}(\mathbf{x}, \mathbf{x}_w, \mathbf{u}^{sd} + \mathbf{u}^c) \approx \mathbf{A}(\mathbf{x})\mathbf{x} + \mathbf{B}(\mathbf{x})\mathbf{u}^{sd}, \quad (4.50)$$

$$f(\mathbf{x})_{rb} + \mathbf{T}_d(\mathbf{x}, \mathbf{x}_w) + \mathbf{T}_u(\mathbf{x}, \mathbf{x}_w, \mathbf{u}^{sd} + \mathbf{u}^c) \approx \mathbf{A}(\mathbf{x})\mathbf{x} + \mathbf{B}(\mathbf{x})\mathbf{u}^{sd}. \quad (4.51)$$

Beside this, the compensator is able to handle disturbances (e.g. wind) in a better way (Bogdanov and Wan [2003]). While only matrix  $\mathbf{T}_u(\mathbf{x}, \mathbf{x}_w, \mathbf{u}^{sd} + \mathbf{u}^c)$  is affected by an additional control input this input has to cover the mismatch including the influence of wind:

$$\mathbf{T}_u(\mathbf{x}, \mathbf{x}_w, \mathbf{u}^{sd} + \mathbf{u}^c) \approx -f(\mathbf{x})_{rb} - \mathbf{T}_d(\mathbf{x}, \mathbf{x}_w) + \mathbf{A}(\mathbf{x})\mathbf{x} + \mathbf{B}(\mathbf{x})\mathbf{u}^{sd}. \quad (4.52)$$

The right side of equation (4.52) can be calculated due to the current state and the SDRE control input. Finally, one derives the compensator control input  $\mathbf{u}^c$  by solving the system of equations given by (4.52). Therefore, a vector  $\mathbf{D}(\mathbf{x}, \mathbf{x}_w, \mathbf{u}^{sd})$  is defined:

$$\mathbf{D}(\mathbf{x}, \mathbf{x}_w, \mathbf{u}^{sd}) \equiv -f(\mathbf{x})_{rb} - \mathbf{T}_d(\mathbf{x}, \mathbf{x}_w) + \mathbf{A}(\mathbf{x})\mathbf{x} + \mathbf{B}(\mathbf{x})\mathbf{u}^{sd} \quad (4.53)$$

and equation (4.52) will be solved for  $\mathbf{u}^c$ :

$$\mathbf{u}^c \approx \mathbf{T}_u^{-1}(\mathbf{x}, \mathbf{x}_w, \mathbf{D}(\mathbf{x}, \mathbf{x}_w, \mathbf{u}^{sd})). \quad (4.54)$$

The above expression covers the mismatch.

The rotor induced forces  $\mathbf{T}_u(\mathbf{x}, \mathbf{x}_w, \mathbf{u})$  with  $\mathbf{u} = \mathbf{u}^{sd} + \mathbf{u}^c$  are given explicitly by

$$\mathbf{T}_u(\mathbf{x}, \mathbf{x}_w, \mathbf{u}) = \begin{bmatrix} X_{mr}(\delta_{col}, \delta_{lon})/m \\ [Y_{mr}(\delta_{col}, \delta_{lat}) + Y_{tr}(\delta_r)]/m \\ Z_{mr}(\delta_{col})/m \\ [L_{mr}(\delta_{col}, \delta_{lat}) + L_{tr}(\delta_r)]/I_{xx} \\ M_{mr}(\delta_{col}, \delta_{lon})/I_{yy} \\ [-Q_e(\delta_t) + N_{tr}(\delta_r)]/I_{zz} \\ 0 \\ \vdots \\ 0 \end{bmatrix}_{12 \times 1}. \quad (4.55)$$

Problematic is the mapping of the four control inputs in  $\mathbb{R}^6$ . Hence, the first two elements of  $\mathbf{T}_u$  are neglected due to the fact that the helicopter movement in the XY-plane is dominated by the vehicle attitude. The remaining vector is given by:

$$\mathbf{T}_u^*(\mathbf{x}, \mathbf{x}_w, \mathbf{u}) = \begin{bmatrix} Z_{mr}(\delta_{col})/m \\ [L_{mr}(\delta_{col}, \delta_{lat}) + L_{tr}(\delta_r)]/I_{xx} \\ M_{mr}(\delta_{col}, \delta_{lon})/I_{yy} \\ [-Q_e(\delta_t) + N_{tr}(\delta_r)]/I_{zz} \end{bmatrix}. \quad (4.56)$$

Notice that  $\mathbf{D}(\mathbf{x}, \mathbf{x}_w, \mathbf{u}^{sd})$  is only depending on  $\mathbf{u}^{sd}$ . The vector  $\mathbf{D}(\mathbf{x}, \mathbf{x}_w, \mathbf{u}^{sd})$ , respectively the reduced  $\mathbf{D}^*(\mathbf{x}, \mathbf{x}_w, \mathbf{u}^{sd})$ , is explicitly given by

$$\mathbf{D}(\mathbf{x}, \mathbf{x}_w, \mathbf{u}^{sd}) \equiv -f(\mathbf{x})_{rb} - \mathbf{T}_d(\mathbf{x}, \mathbf{x}_w) + \mathbf{A}(\mathbf{x})\mathbf{x} + \mathbf{B}(\mathbf{x})\mathbf{u}^{sd}, \quad (4.57)$$

$$f(\mathbf{x})_{rb} = \mathbf{A}_{rb}(\mathbf{x})\mathbf{x} + \Delta\mathbf{f}_{rb}(\mathbf{x}) \quad (4.58)$$

$$\mathbf{A}_{rb}(\mathbf{x}) = \begin{bmatrix} \mathbf{A}_{14} \\ \mathbf{0}_{9 \times 1} \end{bmatrix}, \quad (4.59)$$

$$\Delta\mathbf{f}_{rb} = \begin{bmatrix} \mathbf{0}_{2 \times 1} \\ g \cos \theta \cos \phi \\ \mathbf{0}_{9 \times 1} \end{bmatrix}, \text{ and} \quad (4.60)$$

$$\mathbf{T}_d(\mathbf{x}, \mathbf{x}_w) = \begin{bmatrix} X_{fus}/m \\ [Y_{fus} + Y_{vf}]/m \\ [Z_{fus} + Z_{ht}]/m \\ L_{vf}/m \\ M_{ht}/m \\ N_{vt}/m \\ 0 \\ \vdots \\ 0 \end{bmatrix}_{12 \times 1}. \quad (4.61)$$

And the reduced vector by

$$\mathbf{T}_d^*(\mathbf{x}, \mathbf{x}_w) = \begin{bmatrix} [Z_{fus} + Z_{ht}]/m \\ L_{vf}/m \\ M_{ht}/m \\ N_{vf}/m \end{bmatrix}. \quad (4.62)$$

The reduced Matrix  $\mathbf{D}^*(\mathbf{x}, \mathbf{x}_w, \mathbf{u}^{sd}) = [D_3 \ D_4 \ D_5 \ D_6]^T$  is given by:

$$D_3 = -g \cos \theta \cos \phi - \frac{Z_{fus} + Z_{ht}}{m} + qu - pv + \frac{Z_{fus}^w + Z_{ht}^w}{m}w + Z_{ht}^q q + Z_{mr}^{\delta_{col}} \delta_{col}^{sd}, \quad (4.63)$$

$$D_4 = -L_{vf}/m + (L_{mr}^v + L_{vf}^v)v + L_{mr}^p p / I_{xx} + \frac{I_{yy} - I_{zz}}{2I_{xx}} r q + \left( \frac{I_{yy} - I_{zz}}{2I_{xx}} q + L_{vf}^r / I_{xx} \right) r + L_{mr}^{\delta_{col}} \delta_{col}^{sd} + L_{mr}^{\delta_{lat}} \delta_{lat}^{sd} + L_{tr}^{\delta_r} \delta_r^{sd}, \quad (4.64)$$

$$D_5 = -M_{ht}/m + M_{mr}^u u + (M_{mr}^w + M_{ht}^w)w + \frac{I_{zz} - I_{xx}}{2I_{yy}} r p + (M_{mr}^q + M_{ht}^q)q / I_{yy} + \frac{I_{zz} - I_{xx}}{2I_{yy}} p r \quad (4.65)$$

$$+ M_{mr}^{\delta_{col}} \delta_{col}^{sd} + M_{mr}^{\delta_{lon}} \delta_{lon}^{sd}, \text{ and} \quad (4.66)$$

$$\begin{aligned}
D_6 = & -N_{vt}/m + N_{vf}^v v + \frac{I_{xx} - I_{yy}}{2I_{zz}} qp + \frac{I_{xx} - I_{yy}}{2I_{zz}} pq \\
& + N_{vf}^r r / I_{zz} + N_{tr}^{\delta_r} \delta_r^{sd}.
\end{aligned} \tag{4.67}$$

Expression (4.52) yields to

$$-T_{mr}(\delta_{col}) \approx mD_3(\delta_{col}^{sd}) \tag{4.68}$$

what leads to  $\delta_{col}^c$ . With

$$(K_\beta + T_{mr}(\delta_{col})h_{mr})b_1(\mathbf{x}, \mathbf{x}_w, \delta_{lat}) + L_{tr}(\delta_r) \approx I_{xx}D_4(\delta_{col}^{sd}, \delta_{lat}^{sd}, \delta_r^{sd}) \tag{4.69}$$

one can calculate  $\delta_{lat}^c$ .

$$(K_\beta + T_{mr}(\delta_{col})h_{mr})a_1(\mathbf{x}, \mathbf{x}_w, \delta_{lon}) \approx I_{yy}D_5(\delta_{col}^{sd}, \delta_{lon}^{sd}) \tag{4.70}$$

leads to  $\delta_{lon}^c$  and

$$-Q_e(\delta_t) - (mY_{\delta_r}^{tr} \delta_r + mY_v^{tr} \mu_z^{tr} \Omega_{tr} R_{tr}) l_{tr} \approx I_{zz}D_6(\delta_r^{sd}) \tag{4.71}$$

to  $\delta_r^c$ . Where  $\delta = \delta^{sd} + \delta^c$  is. Finally, one receive:

$$\delta_{col}^c \approx T_{mr}^{-1}(-mD_3) - \delta_{col}^{sd}, \tag{4.72}$$

$$\delta_r^c \approx -\frac{\frac{I_{zz}D_6 + Q_e(\delta_t)}{l_{tr}} + mY_v^{tr} \mu_z^{tr} \Omega_{tr} R_{tr}}{mY_{\delta_r}^{tr}} + \delta_r^{sd}, \tag{4.73}$$

$$\delta_{lat}^c \approx \frac{\frac{I_{xx}D_4 - L_{tr}(\delta_r)}{K_\beta + T_{mr}(\delta_{col})h_{mr}} + \tau_e p - \frac{\partial b_1}{\partial \mu_v} \frac{v_a}{\Omega_{mr} R_{mr}}}{B_{\delta_{lat}}^{nom}} - \delta_{lat}^{sd}, \text{ and} \tag{4.74}$$

$$\delta_{lon}^c \approx \frac{\frac{I_{yy}D_5}{K_\beta + T_{mr}(\delta_{col})h_{mr}} + \tau_e q - \frac{\partial a_1}{\partial \mu} \frac{u_a}{\Omega_{mr} R_{mr}} - \frac{\partial a_1}{\partial \mu_z} \frac{w_a}{\Omega_{mr} R_{mr}}}{A_{\delta_{lon}}^{nom}} - \delta_{lon}^{sd}. \tag{4.75}$$

The calculation of  $T_{mr}^{-1}$  is similar to the calculation of  $T_{mr}$  in section 3.3.3 itself:

1. calculation of  $-mD_3$ ,
2. calculation of  $C_T = \frac{T}{\rho(\Omega R)^2 \pi R^2} = \frac{-mD_3}{\rho(\Omega R)^2 \pi R^2}$ ,
3. calculation of  $\lambda_0$  via the iteration scheme  $\lambda_{0_{j+1}} = \lambda_{0_j} + f_j h_j(\lambda_{0_j})$ , and
4. calculation of  $\delta_{col} = \delta_{col}^{sd} + \delta_{col}^c = 3 \frac{4C_T - \mu_z + \lambda_0}{2 + 3\mu^2}$ .

One should remember the simplification made in (3.23). Applying the controller on the real helicopter makes it necessary to cover this simplification also, what leads to

$$\delta_{lon}^c \approx \frac{\arcsin\left(\frac{I_{yy}D_5}{K_\beta + T_{mr}(\delta_{col})h_{mr}}\right) + \tau_e q - \frac{\partial a_1}{\partial \mu} \frac{u_a}{\Omega_{mr}R_{mr}} - \frac{\partial a_1}{\partial \mu_z} \frac{w_a}{\Omega_{mr}R_{mr}}}{A_{\delta_{lon}}^{\text{nom}}} - \delta_{lon}^{sd} \quad (4.76)$$

and

$$\delta_{lat}^c \approx \frac{\arcsin\left(\frac{I_{xx}D_4 - L_{tr}(\delta_r)}{K_\beta + T_{mr}(\delta_{col})h_{mr}}\right) + \tau_e p - \frac{\partial b_1}{\partial \mu_v} \frac{v_a}{\Omega_{mr}R_{mr}}}{B_{\delta_{lat}}^{\text{nom}}} - \delta_{lat}^{sd}. \quad (4.77)$$

### 4.3.3 Evolutionary algorithm

For the solution of equation (4.1) and the calculation of equation (4.6) it is necessary to determine the matrices  $\mathbf{R}_{12 \times 12}$  and  $\mathbf{Q}_{4 \times 4}$ . As in linear-quadratic regulator (LQR) design,  $\mathbf{Q}$  has to be positive semidefinite ( $\geq 0$ ) and  $\mathbf{R}$  has to be positive definite ( $> 0$ ) (Erdem [2001]). Because  $\mathbf{Q}$  and  $\mathbf{R}$  are at least positive definite it is possible to do a Cholesky factorization. Reverted, it means that these matrices can be build up out of triangular matrices:

$$\mathbf{Q} = \tilde{\mathbf{Q}}^T \tilde{\mathbf{Q}} \text{ with } \tilde{\mathbf{Q}} = \begin{bmatrix} \tilde{q}_{11} & \tilde{q}_{12} & \cdots & \tilde{q}_{1n} \\ 0 & \tilde{q}_{22} & \cdots & \tilde{q}_{2n} \\ \vdots & \vdots & \ddots & \vdots \\ 0 & 0 & 0 & \tilde{q}_{nn} \end{bmatrix}. \quad (4.78)$$

The same holds for  $\mathbf{R}$ . The representation through the triangular matrices leads to 78 values for  $\mathbf{Q}$  respectively  $\tilde{\mathbf{Q}}$  and ten values for  $\mathbf{R}$  respectively  $\tilde{\mathbf{R}}$  which need to be tuned. Therefore an  $(\mu + \lambda)$  evolution strategy was used.

#### $(\mu + \lambda)$ evolution strategy

Evolution strategies follow the evolution theory. The process starts with a set of individuals which are represented by a set of parameters. Offspring (children) are inherited by combining the parameters of two individuals (parents) and by doing slightly changes to the result (mutation). Calculating a fitness-value for all existing individuals (parents and children) makes it possible to select these individuals with the best parameters in the sense of the used fitness function. The remaining individuals will be discard (Adamy [2005]).

In this thesis, ten parents ( $\mu$ ) are used for each generation and these generate  $5\mu = 50$  offspring. The individuals are build as a vector containing function parameter ( $\varsigma$ ) which shall be optimized (the elements of  $\tilde{\mathbf{Q}}$  and  $\tilde{\mathbf{R}}$ ) and as many

strategy parameters ( $\mathbf{v}$ ) which are used for the mutation. Equation (4.79) is representing an individual  $j$  of generation  $i$ .

$$\boldsymbol{\mu}_j^i = \begin{bmatrix} \boldsymbol{\varsigma}_j^i \\ \mathbf{v}_j^i \end{bmatrix} \text{ with} \quad (4.79)$$

$$\boldsymbol{\varsigma}_j^i = [\tilde{q}_1^i \ \cdots \ \tilde{q}_{78}^i \ \tilde{r}_1^i \ \cdots \ \tilde{r}_{10}^i]^T, \quad (4.80)$$

$$\mathbf{v}_j^i = [\sigma_1^i \ \cdots \ \sigma_{88}^i]^T. \quad (4.81)$$

### Reproduction and recombination

The function parameter of child  $\boldsymbol{\lambda}_j^i$  are inherited by the parents function parameters  $\boldsymbol{\varsigma}_k^i$  and  $\boldsymbol{\varsigma}_l^i$  by calculating the mean values. While for each strategy parameter one of the two parents is chosen by random to inherit the accordingly strategy parameter directly to the child.

### Mutation

The mutation of the strategy parameter is done by

$$\mathbf{v}^{i+1} = \max\{\mathbf{v}^i \cdot \exp(0.2 \cdot z_1), \mathbf{v}_{min}\} \quad (4.82)$$

and the mutation of the function parameter by

$$\boldsymbol{\varsigma}^{i+1} = \boldsymbol{\varsigma}^i + z_2 \cdot \mathbf{v}^i. \quad (4.83)$$

Here,  $z_1$  and  $z_2$  are standard normal distributed random numbers and  $\mathbf{v}_{min}$  is the minimum mutation width.

### Selection

The  $\mu$  individuals with the lowest fitness values are taken as parents for the next generation. For the calculation of the fitness value the controller behavior, using the individuals values, is analyzed. The reference position is set to  $x_r = y_r = z_r = \psi_r = 0$  while for the helicopter position a sinusoidal signal is used in the first step. The goal is to find a individual which returns valid control output under this deflections. The fitness value is than given as

$$f(\boldsymbol{\varsigma}^i) = \int_0^t \delta_{col}^2 dt + \int_0^t \delta_{lon}^2 dt + \int_0^t \delta_{lat}^2 dt + \int_0^t \delta_r^2 dt. \quad (4.84)$$

The so found individual should be used as a basis for an evolutionary algorithm which uses the full helicopter together with the controller. This split up would significantly increase the calculation time. Unfortunately the success of the algorithm is coupled with the computational power. Today the simulation just of the controller, which is needed for the calculation of  $f(\boldsymbol{\varsigma}^i)$ , is very slow. Only 624 generations are performed during 38 hours and no useful result was found during the time of this thesis. In addition, it looks like the algorithm runs in a local minimum.

# Chapter 5

## Model and control of simplified UAV

Due to the fact that the simulation of the complete model takes a long time and the control is very difficult, a simplified model is used. This enables an early work on the formation flight controller. The simplified model is based on Marconi and Naldi [2006]. They also developed a control law for this simplified model. It is a robust nonlinear control, based on a vertical controller and a cascade controller which controls the horizontal and attitude dynamics.

### 5.1 Simplified model

The following assumptions are made in compare to the full model:

- The flapping angles  $a_1$  and  $b_1$  are assumed to be equal to the control inputs  $\delta_{lon}$  and  $\delta_{lat}$ . Besides that  $\sin \delta_{lat,lon} \approx \delta_{lat,lon}$  and  $\cos \delta_{lat,lon} \approx 1$ .
- $Y_{tr}$  is assumed to be canceled out by the main rotor force  $Y_{mr}$ .
- The only main rotor force is  $Z_{mr}$ .  $X_{mr}$  is neglected in  $\mathbf{f}_o^b$  and is only taken into account in  $\mathbf{m}_0^b$ .
- The thrust and rotor speed calculations are strictly simplified.
- The influences of vertical fin and horizontal stabilizer bar are neglected.

Doing so, the forces  $\mathbf{f}_o^b$  and moments  $\mathbf{m}_o^b$  in equation (3.3) respectively (3.9) change to

$$\mathbf{f}_o^b = \begin{bmatrix} 0 \\ 0 \\ Z_{mr} \end{bmatrix} + \mathbf{R}_o^n(\Theta)^T \begin{bmatrix} 0 \\ 0 \\ mg \end{bmatrix}, \text{ and} \quad (5.1)$$

$$\mathbf{m}_o^b = \begin{bmatrix} L_{mr} \\ M_{mr} \\ N_{mr} \end{bmatrix} + \begin{bmatrix} Y_{mr}h_{mr} + Y_{tr}h_{mr} \\ -X_{mr}h_{mr} \\ -Y_{tr}l_{tr} \end{bmatrix}. \quad (5.2)$$

The following states are observed by the controller:

$$\left. \begin{array}{l} x \\ y \\ z \\ \phi \\ \theta \\ \psi \\ p \\ q \\ r \\ \Omega_{mr} \end{array} \right\} \left. \begin{array}{l} \mathbf{p}^n \\ \Theta \\ \boldsymbol{\omega}_{nb}^b \end{array} \right\} \boldsymbol{\eta}$$

The reference can be generated as presented in section 4.2.

### 5.1.1 Forces and moments

In this section the modeling of forces and moments will be presented.

#### Forces

The forces from equation (5.1) are expressed by Marconi and Naldi [2006] as follows:

$$X_{mr} = -T_{mr}\delta_{lon}, \quad (5.3)$$

$$Y_{mr} = -T_{mr}\delta_{lat}, \quad (5.4)$$

$$Z_{mr} = -T_{mr}, \text{ and} \quad (5.5)$$

$$Y_{tr} = -T_{tr}. \quad (5.6)$$

Marconi and Naldi [2006] does not uses the iteration scheme calculating the thrust. They modeled it as

$$T_{mr} = K_{TM}\Omega_{mr}^2\delta_{col} \text{ and} \quad (5.7)$$

$$T_{tr} = K_{TT}\Omega_{mr}^2\delta_r. \quad (5.8)$$

$K_{TM}$  and  $K_{TT}$  are constants. Their values can be found in table A.2.

## Moments

The moments from equation (5.2) are expressed by Marconi and Naldi [2006] as follows:

$$L_{mr} = c_M^{Q,T} \delta_{lat} - \frac{P_{max} \delta_t}{\Omega_{mr}} \delta_{lon}, \quad (5.9)$$

$$M_{mr} = c_M^{Q,T} \delta_{lon} + \frac{P_{max} \delta_t}{\Omega_{mr}} \delta_{lat}, \text{ and} \quad (5.10)$$

$$N_{mr} = -\frac{P_{max} \delta_t}{\Omega_{mr}}. \quad (5.11)$$

Equation (5.2) can also be expressed by

$$\mathbf{m}_o^b = \mathbf{A}(\delta_{col}, \delta_t, \Omega_{mr}) \begin{bmatrix} \delta_{lon} \\ \delta_{lat} \\ \delta_r \end{bmatrix} + \mathbf{B}(\delta_{col}, \delta_t, \Omega_{mr}). \quad (5.12)$$

The matrices  $\mathbf{A}(\delta_{col}, \delta_t, \Omega_{mr})$  and  $\mathbf{B}(\delta_{col}, \delta_t, \Omega_{mr})$  are used for the lateral and longitudinal controller later. They are explicitly given by

$$\mathbf{A} = [ \mathbf{A}_1 \quad \mathbf{A}_2 \quad \mathbf{A}_3 ], \text{ with} \quad (5.13)$$

$$\mathbf{A}_1 = \begin{bmatrix} -\frac{P_{max} \delta_t}{\Omega_{mr}} \\ c_{Q,T}^M + K_{T_M} \Omega_{mr}^2 h_{mr} \delta_{col} \\ 0 \end{bmatrix}, \quad (5.14)$$

$$\mathbf{A}_2 = \begin{bmatrix} c_{Q,T}^M - K_{T_M} \Omega_{mr}^2 h_{mr} \delta_{col} \\ \frac{P_{max} \delta_t}{\Omega_{mr}} \\ 0 \end{bmatrix}, \quad (5.15)$$

$$\mathbf{A}_3 = \begin{bmatrix} -K_{T_T} \Omega_{mr}^2 h_{tr} \\ 0 \\ K_{T_T} \Omega_{mr}^2 l_{tr} \end{bmatrix}, \text{ and} \quad (5.16)$$

$$\mathbf{B} = \begin{bmatrix} 0 \\ 0 \\ -\frac{P_{max} \delta_t}{\Omega_{mr}} \end{bmatrix}. \quad (5.17)$$

The values of the used constants can be found in table A.2.

### 5.1.2 Engine dynamics

The engine dynamic is simplified to

$$\dot{\Omega}_{mr} = \frac{1}{I_{rot}} (Q_e - Q_{mr}). \quad (5.18)$$

The engine torque  $Q_e$  is modeled as for the complete model in equation (3.47). The torque  $Q_{mr}$ , caused by the aerodynamic resistance of the rotor, is modeled as

$$Q_{mr} = (c + d\delta_{col}^2) \Omega_{mr}^2. \quad (5.19)$$

The values of  $c$  and  $d$  can be found in table A.2.

## 5.2 Vertical controller

The vertical dynamics are described by the third line of equation (3.3) regarding the changes made in (5.1). Explicitly the vertical dynamics of the simplified helicopter are given by

$$m\dot{w} + m(-vp + uq) = -T_M + \cos \phi \cos \theta mg. \quad (5.20)$$

Transforming them to the NED frame leads to

$$m\ddot{z} + m\tilde{n} = -\cos \phi \cos \theta K_{TM} \delta_{col} \Omega_{mr}^2 + mg. \quad (5.21)$$

While  $\tilde{n}$  represents the third line of  $\mathbf{R}_b^n(\Theta)\mathbf{C}_{RB}(\boldsymbol{\nu})\boldsymbol{\nu}$ . Marconi and Naldi [2006] introduce a preliminary control law of the form

$$\delta_{col} = \frac{-\delta'_{col} + mg - m\ddot{z}_r}{K_{TM0} \Omega_{mr_s}^2 \cos \phi_s \cos \theta_s}. \quad (5.22)$$

Here, the influence of the vertical dynamics ( $\tilde{n}$ ) are decoupled from the attitude and engine dynamics by the auxiliary control input  $\delta'_{col}$ .  $\Omega_{mr_s}$ ,  $\cos \phi_s$ , and  $\cos \theta_s$  are constructs to avoid singularities, e.g. the values could be separated numerically from zero.  $K_{TM0}$  is introduced to respect a mismatch between the model and the real helicopter.

Solving equation (5.21) for  $\delta_{col}$  and equate it with equation (5.22) leads to

$$m\ddot{z} = \frac{\cos \phi \cos \theta K_{TM} \Omega_{mr}^2}{\cos \phi_s \cos \theta_s K_{TM0} \Omega_{mr_s}^2} \left( \delta'_{col} - mg + m\ddot{z}_r \right) + mg - m\tilde{n}. \quad (5.23)$$

Marconi and Naldi [2006] prove, taking the design of the remaining controller into account that  $\cos \phi \cos \theta \Omega_{mr}^2 = \cos \phi_s \cos \theta_s \Omega_{mr_s}^2$  after a finite time. Subtracting  $m\ddot{z}_r$  from equation (5.23) leads with the vertical error  $e_z = z - z_r$  to

the vertical error dynamics:

$$\begin{aligned} m\ddot{e}_z &= \frac{K_{TM}}{K_{TM0}} \left( \delta'_{col} - mg + m\ddot{z}_r \right) + mg - m\tilde{n} - m\ddot{z}_r \\ &= \frac{K_{TM}}{K_{TM0}} \delta'_{col} + m \left( 1 - \frac{K_{TM}}{K_{TM0}} \right) (g + \ddot{z}_r) - m\tilde{n}. \end{aligned} \quad (5.24)$$

Finally,  $\delta'_{col}$  is designed as a PID controller with respect to equation (5.24):

$$\delta'_{col} = \xi - k_2 \dot{e}_z - k_2 k_1 e_z \quad \text{with} \quad (5.25)$$

$$\dot{\xi} = -k_2 \dot{e}_z - k_2 k_1 e_z + m \dot{e}_z. \quad (5.26)$$

$k_1$  and  $k_2$  are design parameters. The values of the constants can be found in table A.2.

### 5.3 Engine controller

Based on equation (5.18) a preliminary feedback is chosen by Marconi and Naldi [2006] to compensate  $Q_{mr}$ :

$$\delta_t = \frac{\Omega_{mr}^3}{P_{\max}} \left( \delta'_t + c + d\delta_{col}^2 \right). \quad (5.27)$$

While  $\delta'_t$  is designed as a nonlinear PI controller:

$$\delta'_t = -k_3 (\Omega_{mr} - \Omega_{nom}) - k_4 \xi \quad \text{with} \quad (5.28)$$

$$\dot{\xi} = k_3 \Omega_{mr}^2 (\Omega_{mr} - \Omega_{nom}). \quad (5.29)$$

### 5.4 Lateral and longitudinal controller

The helicopters attitude has a huge influence on the lateral and longitudinal movement. This is caused by the dependence of the rotation matrix  $\mathbf{R}_b^n$  of  $\Theta$  as one can see in equation (2.13) and by the fact that the transformation of the body velocities leads to NED accelerations, referred to equation (2.12) and (2.15). Because of that, a cascade control structure is chosen by Marconi and Naldi [2006]. The inner loop controls the attitude and the outer loop the lateral and longitudinal dynamics. This split up is common in helicopter control (e.g., Kondak et al. [2004], Johnson and Kannan [2002]). As presented in section 4.2 a lateral or longitudinal deflection from the lateral and longitudinal reference trajectory causes also a deflection of the attitude reference and leads to a rotation in the appropriate direction.

As a preliminary feedback control,

$$\begin{bmatrix} \delta_{lon} \\ \delta_{lat} \\ \delta_r \end{bmatrix} = \mathbf{A}^{-1} (\tilde{\mathbf{v}} - \mathbf{B}) \quad (5.30)$$

is chosen with respect to equation (5.12),  $\mathbf{A}$  given in equation (5.13), and  $\mathbf{B}$  in (5.17).  $\tilde{\mathbf{v}}$  represents the cascade structure mentioned above.

### 5.4.1 Inner loop

In Marconi and Naldi [2006], the inner loop is based on feedforward and high-gain-feedback control, processing the attitude and the outer loop output  $\Theta_{out}$ , which is designed using a nested saturation control law. The inner loop is given by

$$\tilde{\mathbf{v}} = \tilde{\mathbf{v}}_1 + \tilde{\mathbf{v}}_2 + \tilde{\mathbf{v}}_3 \text{ with} \quad (5.31)$$

$$\tilde{\mathbf{v}}_1 = -K_P K_D (\boldsymbol{\omega}_{nb}^b - \boldsymbol{\omega}_{nb,r}^b) - K_P \begin{bmatrix} t\phi - t\phi_r \\ t\theta - t\theta_r \\ \psi + K_\psi \eta_\psi - \psi_r \end{bmatrix}, \quad (5.32)$$

$$\tilde{\mathbf{v}}_2 = K_P \begin{bmatrix} \begin{bmatrix} -c\psi & s\psi c\theta/c\phi \\ s\psi/c\theta & c\psi/c\phi \end{bmatrix} \Theta_{out} \\ 0 \end{bmatrix}. \text{ and} \quad (5.33)$$

$$\tilde{\mathbf{v}}_3 = \mathbf{I}_0 \dot{\boldsymbol{\omega}}_{nb,r}^b + \mathbf{S}(\boldsymbol{\omega}_{nb,r}^b) \mathbf{I}_0 \boldsymbol{\omega}_{nb,r}^b. \quad (5.34)$$

Where  $s \cdot \equiv \sin(\cdot)$ ,  $c \cdot \equiv \cos(\cdot)$  and  $t \cdot \equiv \tan(\cdot)$ .

As one can see in equation (2.15),  $\boldsymbol{\omega}_{nb,r}^b$  can be derived by a transformation of  $\dot{\Theta}$ :

$$\boldsymbol{\omega}_{nb,r}^b = \mathbf{T}_{\Theta}^{-1}(\Theta_r) \dot{\Theta}_r. \quad (5.35)$$

With  $\mathbf{T}_{\Theta}^{-1}(\Theta_r)$  given in equation (2.16) and  $\mathbf{I}_0$  in (3.5).  $\eta_\psi$  is given by

$$\dot{\eta}_\psi = \psi - \psi_r. \quad (5.36)$$

The values of the remaining constants can be found in table A.2.

### 5.4.2 Outer loop

The outer loop can be defined as *slow* while the inner loop is *fast*. It provides the decoupling between the attitude and the lateral and longitudinal dynamics. As already mentioned, a nested saturation control law is used:

$$\Theta_{out} = \lambda_3 \sigma \left( \frac{K_3}{\lambda_3} \xi_3 \right). \quad (5.37)$$

Be aware that  $\sigma(\cdot)$  is a saturation function defined in Marconi and Naldi [2006] as

$$\left| \frac{d\sigma(s)}{ds} \right| \leq 2 \quad \forall s, \quad (5.38)$$

$$s\sigma(s) > 0 \quad \forall s \neq 0, \quad \sigma(0) = 0, \quad (5.39)$$

$$\sigma(s) = \text{sign}(s) \quad \text{for } |s| \geq 1, \quad \text{and} \quad (5.40)$$

$$|s| < |\sigma(2)| < 1 \quad \text{for } |s| < 1. \quad (5.41)$$

$\xi_3$  is calculated as follows:

$$\xi_3 = \begin{bmatrix} \ddot{\eta}_y \\ \ddot{\eta}_x \end{bmatrix} + \lambda_2 \sigma \left( \frac{K_2}{\lambda_2} \xi_2 \right), \quad (5.42)$$

$$\xi_2 = \begin{bmatrix} \dot{\eta}_y \\ \dot{\eta}_x \end{bmatrix} + \lambda_1 \sigma \left( \frac{K_1}{\lambda_1} \xi_1 \right), \quad (5.43)$$

$$\xi_1 = \begin{bmatrix} \eta_y \\ \eta_x \end{bmatrix}, \quad (5.44)$$

$$\dot{\eta}_y = y - y_r, \quad \text{and} \quad (5.45)$$

$$\dot{\eta}_x = x - x_r. \quad (5.46)$$

As mentioned in section 5.2, Marconi and Naldi [2006] prove the validity of the presented controller by the tuning of the gains and the combined working of the three controllers. They show that perfect asymptotic tracking is achieved for perfect knowledge of the helicopter. In case of existing uncertainties, the tracking error can be rendered arbitrarily small by increasing  $K_P$  used in equation (5.31). The values of the remaining constants can be found in table A.2.

## 5.5 Simulation results

The presented controller works very well with the simplified model. The several derivatives used in the controller can be the reason for problems during the simulation which are caused by the numerical solution of calculating those derivatives. To prevent those problems, fixed time steps can be used. In addition, critical derivatives can be approximated by the differences of two following time steps. Figure 5.1 shows the simulation result from the controller working with the simplified model. Figure 5.2 shows the generated control input during the flight. The trajectory is performing a sinusoidal movement in each direction in addition to a linear movement in  $x$  direction. A step in each direction is included at  $t = 15$ . The controller handles both, the tracking and the converge

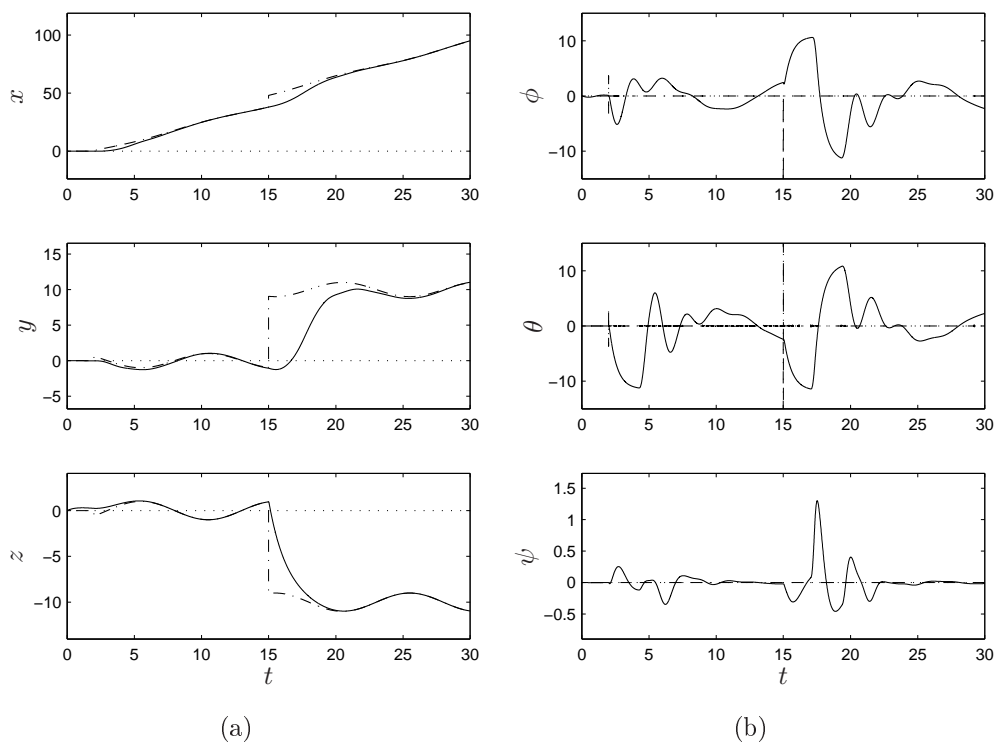


Figure 5.1: Simulation results of simplified helicopter  
The figures show the reference (dash-dotted) and the simulated (solid) trajectory of the helicopter. Subfigure (a) shows the position, while subfigure (b) shows attitude in degree.

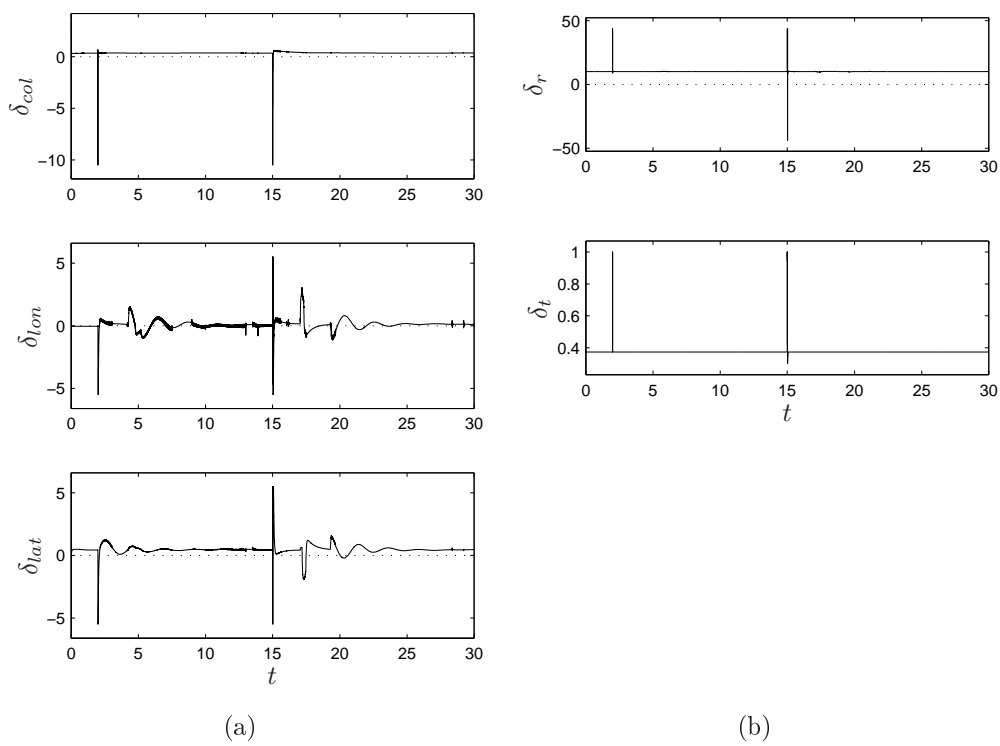


Figure 5.2: Control input of simplified helicopter  
The figures shows the generated control input during the flight, which is presented in figure 5.1. All control values are presented in degree except  $\delta_t$ .

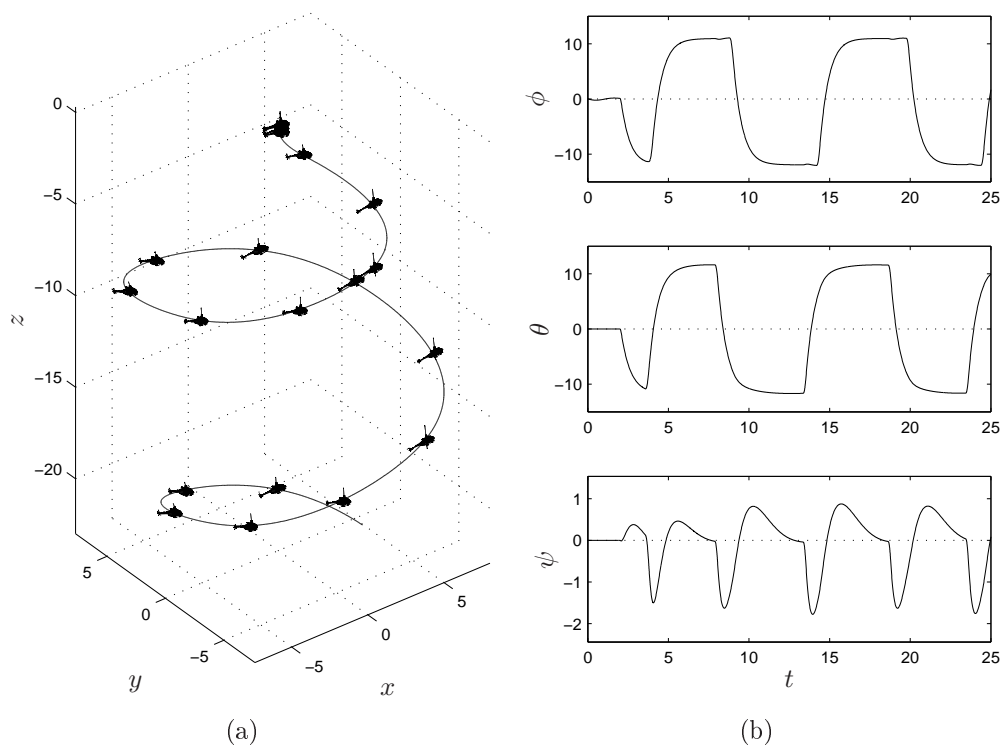


Figure 5.3: Flying a screw  
Figure (a) shows the position while figure (b) shows the attitude in degree.

after the step without overshooting. This is a very important fact for formation flight, when overshooting could cause collisions.

Figure 5.3 shows an other flight where the helicopter is ordered to move screwing downwards.

# Chapter 6

## Formation flight

Formations of autonomous vehicles offer a huge increase of performance and robustness compared to a single operating vehicle. A single small autonomous vehicle can carry only few equipment, while formations can distribute the equipment, necessary for a specific mission, to all vehicles in the swarm (e.g., one vehicle responsible for navigation, one for video analysis, etc.). Applications for autonomous vehicle formations can be accounted for all kind of robots, underwater, on land, in air, and in space (Do [2006]).

Different types of autonomous vehicle formation solutions can be found in the literature (Chen and Wang [2005], Borrelli et al. [2006]). The two main approaches are potential field and leader-follower approach. In leader-follower approach one or several vehicles act as a leader while the rest is following, tracking transformed states of their neighbors. The advantage of this approach is that it is easy to understand and also easy to realize. The disadvantage is the missing feedback from the followers to the leader (Do [2006]). The potential field approach is more complex and needs more computational power but offers a very effective way of building formations with respect to collision and obstacle avoidance (Do [2006], Elkaim and Kelbley [2006]). Combinations of these two approaches are often used to build and move formations because they are very effective, robust and easy to handle. This thesis presents a local potential field in combination with a virtual leader formation approach that addresses the helicopter's autopilot presented in chapter 4 based on Elkaim and Kelbley [2006] and Do [2006].

Most of formation flight control literature is about spacecrafts or ground vehicles. The literature engaging on aircrafts deals mostly with fixed wing aircrafts. Nevertheless, formations of helicopters are very interesting because of their ability to hover and to perform vertical flight.

## 6.1 Formation control

The approach presented in the following is not a controller in the usual sense. The algorithm is generating trajectories depending on the interaction of the swarm, the desired position and formation. Figure 6.1 shows the formation flight solution in interaction with the helicopter systems. It is a combination of virtual leader and potential field approach. At least one vehicle in the swarm is responsible for the swarm navigation. It provides the absolute virtual leader position and the relative position to the virtual leader for each vehicle. Doing this, a continuous calculation and update of the formation for each vehicle is not necessary. In addition, depending on the vehicles memory and computing power, calculation of the current distance between the vehicles is either provided by the swarm navigation vehicle or by the individual vehicles itself. If possible, the vehicles should be able to measure the distance to their neighbors and to obstacles itself. This would increase the robustness of collision and obstacle avoidance.

A movement of the virtual leader results in a deflection from the provided distance and causes the affected vehicle to correct its position. To control the movement of the single vehicles a potential field is used. Taking the distributed positions and distances into account one can derive a place dependent potential field for each vehicle which is finally used for obstacle and collision avoidance. A specific position can be assigned to a specific vehicle in the formation .

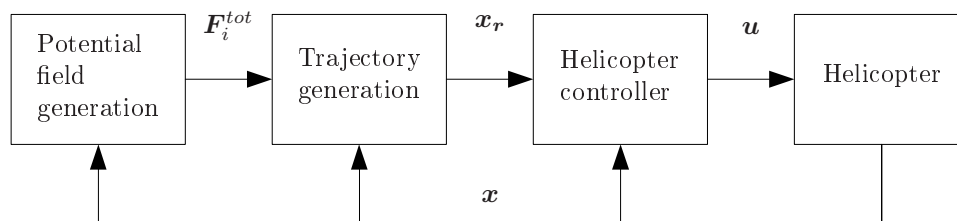


Figure 6.1: Vehicle block diagram

The advantage of this approach in compare to other published approaches is the application of a potential field formation control in three dimensions. In addition, a continuous field and thus a continuous trajectory for the single vehicles is guaranteed while providing obstacle and collision avoidance. Finally, the algorithm provides maximum vehicle speed.

### 6.1.1 Virtual leader

The virtual leader is the anchor of each formation and causes the formation moving. Its trajectory need not be continuous and can either be calculated previously or dynamically during flight. Both ends in a set of way points and

event points where, e.g the formation changes. If a continuous presentation of the virtual leader movement is necessary a morph between the steps could be used. A linguistic description of the track could look like the following:

1. Adopt circle position at initial position  $\mathbf{p}_{ini}^n$ .
2. Move (virtual leader) to  $\mathbf{p}_{vl}^n = [ 15 \ 0 \ 15 ]^T$ .
3. Adopt line formation.
4. Adopt triangle formation while moving (virtual leader) to  $\mathbf{p}_{vl}^n = [ 100 \ 0 \ 20 ]^T$ .

As said above, the virtual leader is the reference or anchor point for the formations. A well initial point for the virtual leader is that's why the center of mass of the swarm, assuming that in the first step all vehicles are distributed in the area. This ends in short ways while adopting the first formation and so in less power usage. The center of mass of  $N$  vehicles with absolute positions  $\mathbf{p}_i^n$  can be calculated by:

$$\mathbf{p}_{cm}^n = \frac{1}{N} \sum_{i=1}^N \mathbf{p}_i^n. \quad (6.1)$$

The virtual leader's component to the local time dependent potential field is

$$\mathbf{F}_{vl} = K_{vl} (\mathbf{p}_{vl}^n - \mathbf{p}_i^n - [\mathbf{p}_{vl}^n - \mathbf{p}_{i0}^n]) \quad (6.2)$$

$$= K_{vl} (\mathbf{d}_i - \mathbf{d}_{i0}). \quad (6.3)$$

$K_{vl}$  is the virtual leader gain which needs to be tuned. The meaning of the variables is explained by figure 6.2. It is advisable to limit the virtual leader influence. Due to the fact, that a way point can be far away from the actual position, equation (6.2) respectively (6.3) can become large because of a large  $\mathbf{d}_i$ . This would result in a domination of the virtual leader component in the potential field and could constrict an effective collision or obstacle avoidance.

### 6.1.2 Inter vehicle influence

The influence of the other vehicles to the potential field is expressed by:

$$\mathbf{F}_{ij} = K_{ij} (\mathbf{p}_j^n - \mathbf{p}_i^n - [\mathbf{p}_{j0}^n - \mathbf{p}_{i0}^n]) \quad (6.4)$$

$$= K_{ij} (\mathbf{d}_{ij} - \mathbf{d}_{ij0}). \quad (6.5)$$

Similar to equations (6.2) and (6.3)  $\mathbf{p}_j^n$  is the position vector for vehicle  $j$  and  $\mathbf{p}_{j0}^n$  is the position vector pointing to vehicle  $j$ 's place in the formation.  $K_{ij}$  is the inter vehicle gain which needs to be tuned. Equation (6.4), respectively

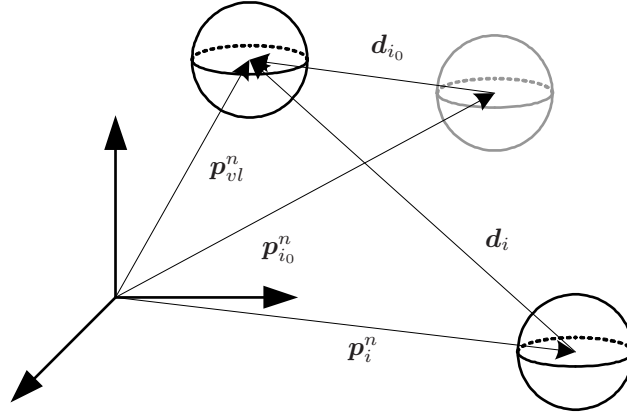


Figure 6.2: Vector definitions for formation flight  
 $\mathbf{p}_{vl}^n$ : position vector of virtual leader;  $\mathbf{p}_i^n$ : current position vector of vehicle  $i$ ;  $\mathbf{p}_{i0}^n$ : position vector of vehicle  $i$ 's place in the formation

(6.5), is calculated for each vehicle. This leads for vehicle  $i$  to the total amount of

$$\mathbf{F}_{ij}^{tot} = \sum_{j=1}^N \mathbf{F}_{ij}(i, j) \text{ for } j \neq i \quad (6.6)$$

$$= K_{ij} \left( \sum_{j=1}^N \mathbf{p}_j^n - N\mathbf{p}_i^n - \left[ \sum_{j=1}^N \mathbf{p}_{j0}^n - N\mathbf{p}_{i0}^n \right] \right) \text{ for } j \neq i. \quad (6.7)$$

The ratio of  $K_{vl}$  and  $K_{ij}$  decides if the vehicles fly primary to the next way point or adopt primary their new formation.

### 6.1.3 Collision and obstacle avoidance

To avoid collision between the vehicles or obstacles a safety space around each vehicle is defined. This space is also used to build up formations. Because of simplicity this area is defined as a sphere with positive radius  $r_{sav}$ . Other forms like ellipsoids or even more complex are also thinkable to cover the form of the vehicle in a better way if necessary. Tests have been performed, using an ellipsoid space. By adding a small pitch angle to the ellipsoid, the vehicle should be supported in going up or down while avoiding a collision. This should be realized by using the surface of the sphere as a reflection surface comparable to a mirror. Figure 6.3 clarifies the idea.

Nevertheless, it turned out that the advantage in compare to the sphere do not justify the additional calculation costs. If something enters the sphere an

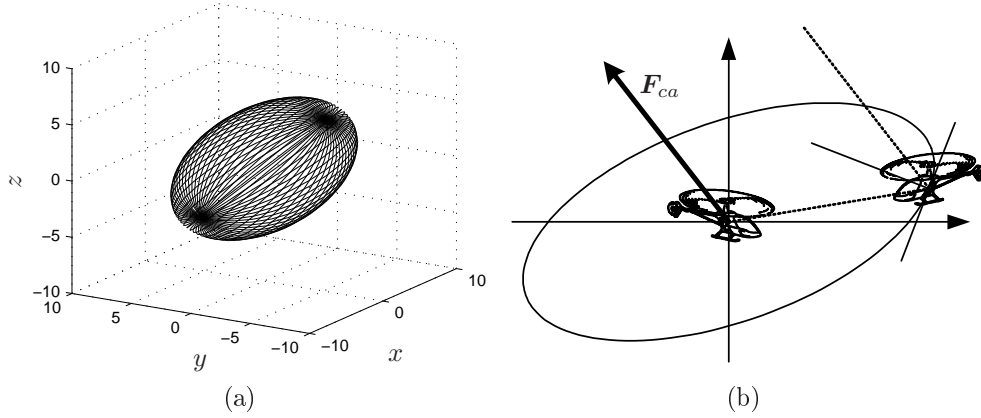


Figure 6.3: Ellipsoid using for collision and obstacle avoidance  
 Figure (a) shows the rotated ellipsoid, figure (b) the angle of incidence and the angle of reflection.

additional field component, pointing away from the invading vehicle or obstacle, comes up. To ensure the collision avoidance the additional component becomes infinity in the center of the sphere. For vehicle  $i$ , whose safety sphere is invaded by vehicle  $j$ , it is defined by

$$\mathbf{F}_{ca} = \begin{cases} \left( \frac{K_{ca}}{\|\mathbf{p}_i^n - \mathbf{p}_j^n\|} - \frac{K_{ca}}{r_{sav}} \right) \frac{\mathbf{p}_i^n - \mathbf{p}_j^n}{\|\mathbf{p}_i^n - \mathbf{p}_j^n\|} & \text{for } \|\mathbf{p}_i^n - \mathbf{p}_j^n\| < r_{sav} \\ 0 & \text{otherwise} \end{cases} \quad (6.8)$$

The term  $K_{ca}/r_{sav}$  is granting a continuous potential field what results in a continuous trajectory for each vehicle. Again,  $K_{ca}$  is a gain which needs to be tuned. If the vehicle is able to detect obstacles and to measure the shortest distance to these obstacles, equation (6.8) can be expanded on every detected object and avoid collisions. Modeling obstacles as a set of points, compared to the knots in a grid, each point can be treated like a vehicle and equation (6.8) needs only small adjustments. The gain  $K_{ca}$  is to replace by the obstacle gain  $K_{oa}$  and the vehicles  $\mathbf{p}_j^n$  by the dots, which represent the obstacle.

To increase the performance,  $r_{sav}$  could be chosen dynamically, depending on the vehicle's velocity.

#### 6.1.4 Potential field

Summing all components gives the field's magnitude and direction of the potential field for vehicle  $i$  at its current position.

$$\mathbf{F}_i^{tot} = \mathbf{F}_{vl} + \mathbf{F}_{ij}^{tot} + \mathbf{F}_{ca} + \mathbf{F}_{oa}. \quad (6.9)$$

The field is continuous and singularity free except places of other vehicles or obstacles where the field goes to infinity. It is reasonable to define a maximum

amplitude for the force vector while keeping its direction:

$$\mathbf{F}_i^{tot} = \begin{cases} \mathbf{F}_{vl} + \mathbf{F}_{ij}^{tot} + \mathbf{F}_{ca} & \text{for } \|\mathbf{F}_{vl} + \mathbf{F}_{ij}^{tot} + \mathbf{F}_{ca}\| < F_{\max} \\ F_{\max} \frac{\mathbf{F}_{vl} + \mathbf{F}_{ij}^{tot} + \mathbf{F}_{ca}}{\|\mathbf{F}_{vl} + \mathbf{F}_{ij}^{tot} + \mathbf{F}_{ca}\|} & \text{otherwise} \end{cases}. \quad (6.10)$$

$F_{\max}$  will be the upper limit of the field's magnitude and therefore a limitation for the vehicle's speed due to the fact that a larger field magnitude result in a larger distance between the actual vehicle's position and the reference. To use the whole speed bandwidth,  $F_{\max}$  must be chosen dynamically. This can be realized by adding the amount of the vehicle's NED velocity  $\|\dot{\mathbf{p}}^n\|$  to  $F_{\max}$ . As long as the vehicle is accelerating, the distance to the vehicle's reference position increases. This keeps the vehicle accelerating until the maximal velocity is reached:

$$F_{max}^* = F_{\max} + K_v \|\dot{\mathbf{p}}^n\|. \quad (6.11)$$

Figure 6.4 is showing a computed potential field for a specific vehicle interacting with two other vehicles. On figure 6.4(e) can a local minimum in the field's magnitude be noticed. This is because of the opposing virtual leader and collision avoidance force. Due to noise, the vehicles will not be caught in this minimum because it is not a stable minimum as the field's minimum at the desired position.

The position reference trajectory for vehicle  $i$ , which is used by the controller to calculate the helicopter's control inputs, is given by

$$\mathbf{p}_{i,r}^n = \mathbf{p}_i^n + \mathbf{F}_i^{tot}, \quad (6.12)$$

while the calculation of the remaining reference values is presented in section 4.2.

## 6.2 Formations

Every formation has its own advantages and disadvantages and so, the chosen formation is depending on the mission. The different formations consist of the absolute positions of the single vehicles. That's why, they are represented by a set of place vectors. The formations can be orientated in the space very simple by rotating the single place vectors with the transformation matrix given in equation (2.13) by choosing  $\Theta$ . Be aware that the rotation should be done in general around the formations center of gravity. The rotation for the  $i$ -th vehicle is given by

$$\hat{\mathbf{p}}_i^n = \mathbf{R}_b^n(\Theta) (\mathbf{p}_i^n - \mathbf{p}_{cm}^n) + \mathbf{p}_{cm}^n, \quad (6.13)$$

while  $\mathbf{p}_{cm}^n$  is given in equation (6.1).

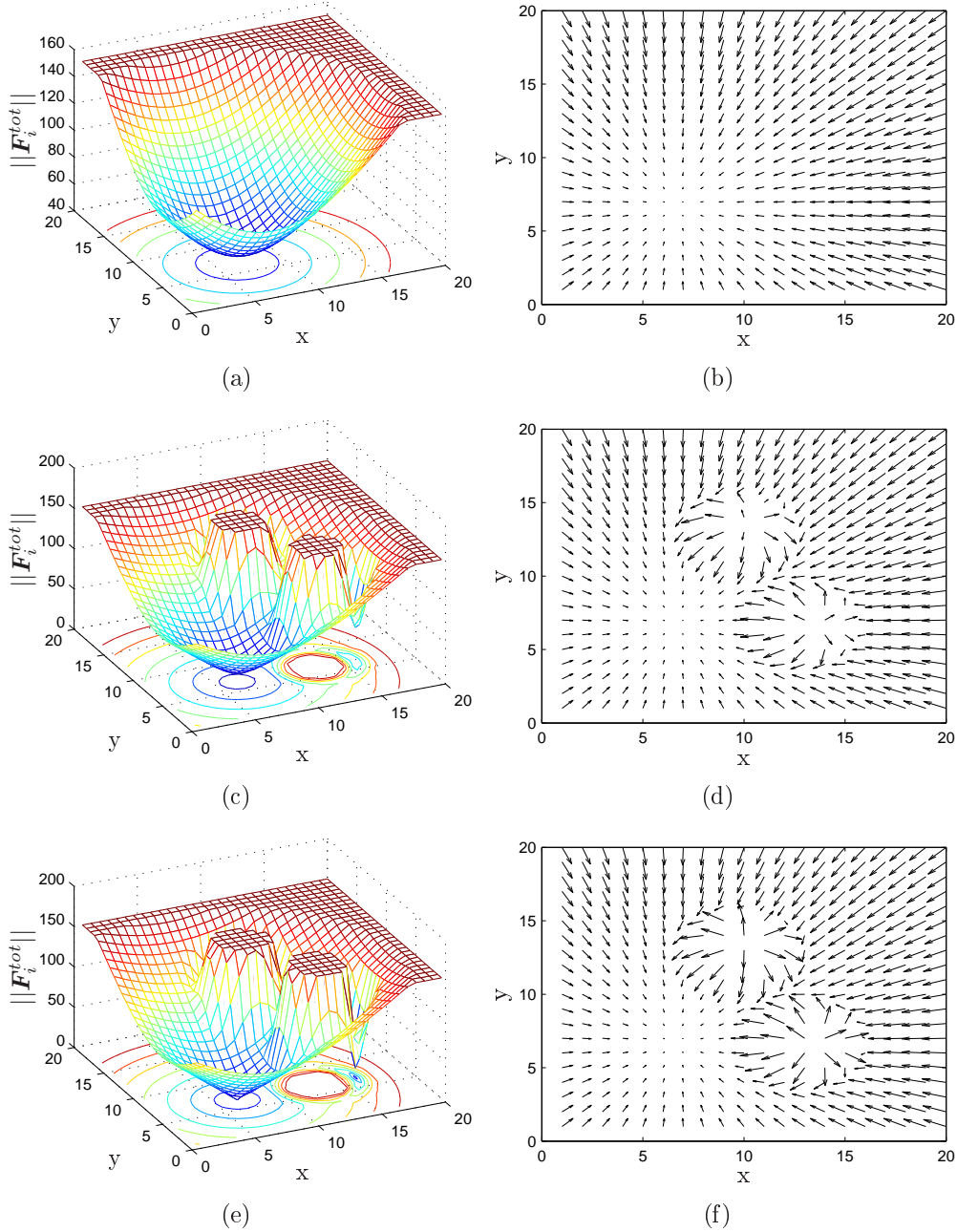


Figure 6.4: Potential field

The figures are showing the potential field of a desired formation of three vehicles for one specific vehicle in the plane. The safety radius is  $r_{\text{sav}} = 4$ . Figures (a)-(f) are showing the potential field in several heights, regarding to the other vehicles: (a) and (b) in  $h = \pm 5$ , (c) and (d)  $h = \pm 1$  and (e) and (f) on the same level as the other two vehicles. Pictures (a), (c), (e) are showing the fields magnitude while (b), (d), (f) are showing the field direction.

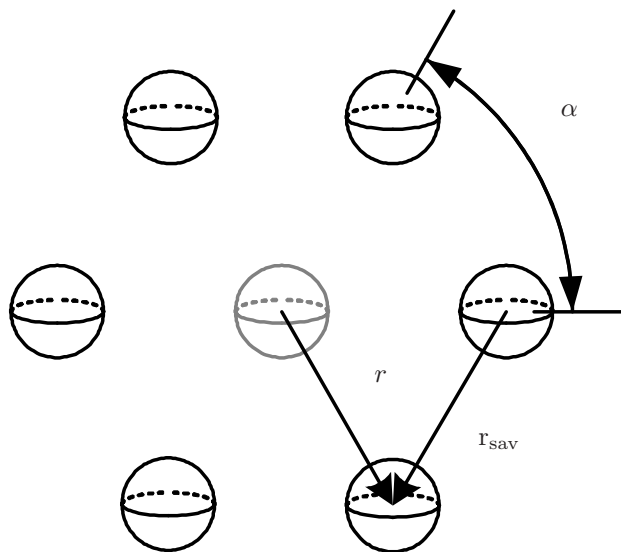


Figure 6.5: Circular formation  
Virtual leader (gray) in the center.

### 6.2.1 Circular formation

The classical *guard* position is to place the vehicles in a circle around a specific point, the position of the virtual leader  $\mathbf{p}_{vl}$ . The place vector of the  $i$ -th vehicle could be calculated by

$$\mathbf{p}_i^n = \mathbf{p}_{vl}^n + r \begin{bmatrix} \cos(2\pi i/N) \\ \sin(2\pi i/N) \\ 0 \end{bmatrix}. \quad (6.14)$$

$N$  represents the total number of vehicles in the formation while the circles radius  $r$  is depending on  $r_{sav}$ . For a circular formation the minimal distance between two vehicles is given by the chord between the positions of two neighbor vehicles. Setting the chord to  $r_{sav}$ , it is possible to calculate the circle's radius  $r$ :

$$r = \frac{r_{sav}}{2 \sin(\alpha/2)}. \quad (6.15)$$

While the angle  $\alpha$  between the vehicles is simply given by

$$\alpha = \frac{2\pi}{N}. \quad (6.16)$$

The formation is visualized in figure 6.5.

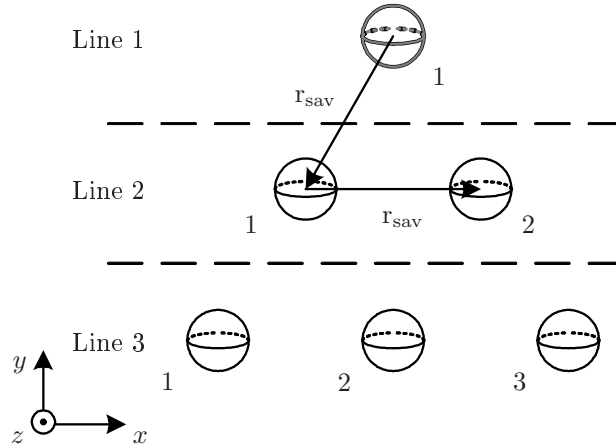


Figure 6.6: Triangular formation  
Virtual leader (gray) in the front.

### 6.2.2 Triangular formation

For moving the group from one point to another, the arrow or triangular formation is very effective. To calculate the row in which the  $i$ -th vehicle is placed, the Gauss formula of the summation of numbers is used:

$$i = \frac{1}{2}(l^* + 1)l^* = \sum_{a=1}^{l^*} a. \quad (6.17)$$

Rearranging this formula leads to the  $i$ -th vehicle's line in the triangle formation:

$$l^*(i) = -0.5 + \sqrt{0.25 + 2i}. \quad (6.18)$$

Because there are only exact lines, the solution  $l^*(i)$  needs to be rounded up to the next integer. What leads to  $l(i)$ , the line of vehicle  $i$ . The last vehicle  $j$  of a line  $k$  could be calculated by:

$$j(k) = (k + 1) \frac{k}{2}. \quad (6.19)$$

While the current position (first, second, ...) of vehicle  $i$  in a line is calculated by:

$$m(i) = i - j(l(i) - 1) + 1. \quad (6.20)$$

The distance between the vehicles in the formation is set by the normal flight distance  $r_{sav}$ . Using Pythagoras, the distance between two lines is given by

$$r_l = \sqrt{r_{sav}^2 - (r_{sav}/2)^2} = r_{sav} \sqrt{3/4}. \quad (6.21)$$

With these variables it is possible to calculate the place vector of vehicle  $i$  in a triangular formation:

$$\mathbf{p}_i^n = \mathbf{p}_{vl}^n + r_{sav} \begin{bmatrix} -(l(i) - 1)/2 + m(i) \\ -\sqrt{3/4}(l(i) - 1) \\ 0 \end{bmatrix}. \quad (6.22)$$

The position of the first vehicle is simply given by the position of the virtual leader. Figure 6.6 visualizes the formations structure.

### 6.2.3 Line formation

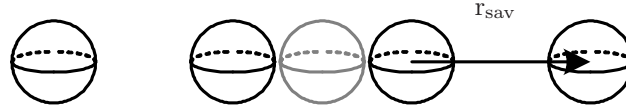


Figure 6.7: Line formation  
Virtual leader (gray) in the center of gravity.

A line formation with the virtual leader in the center of gravity of the line could be realized by:

$$\mathbf{p}_i^n = \mathbf{p}_{vl}^n + r_{sav} \begin{bmatrix} i - (N + 1)/2 \\ 0 \\ 0 \end{bmatrix} \quad (6.23)$$

and can be seen in figure 6.7.

## 6.3 Simulation results

### 6.3.1 Point mass

To verify the presented formation flight solution, the algorithm is used together with the model and controller presented in chapter 5. Before this, the approach was tested on point masses controlled by linear controllers. This was done because of short simulation time and due to the fact that the derived formation flight solution is independent of the underlying vehicle dynamics. Using the point masses, even formations with six vehicles could be simulated. Equation (3.3) is used for the representation of the point masses with  $\boldsymbol{\tau}$  as control input. To control the position,  $\mathbf{f}_o^b$  is set to

$$\mathbf{f}_o^b = K_1 \mathbf{R}_n^b(\boldsymbol{\Theta}) \dot{\mathbf{e}}^n - K_2 \mathbf{v}_o^b \quad \text{with} \quad (6.24)$$

$$\mathbf{e}^n = \mathbf{p}_{ref}^n - \mathbf{p}^n. \quad (6.25)$$

$K_1$  is set to 6 and  $K_2$  to 10. For attitude control

$$\mathbf{m}_o^b = K_3 \mathbf{e}_\Theta - K_4 \dot{\mathbf{e}}_\Theta \text{ with} \quad (6.26)$$

$$\mathbf{e}_\Theta = \Theta_{ref} - \Theta \quad (6.27)$$

is used. While  $K_3$  is set to  $-1$  and  $K_4$  to 3.

Figure 6.8 shows a simple formation change where the group adopts a triangular formation out of a circle formation. Figure 6.10 shows the result of a difficult maneuver and a successful collision avoidance. Six point masses start in a triangle formation and are advised to adopt a formation where the triangle is rotated around  $180^\circ$  (cp. figure 6.9). The difficulty of this exercise is that the direct way to the new formation leads all vehicles through the triangles' center. Therefore, a well working collision avoidance is needed. The parameter which are used for the presented simulations are printed in table A.3.

### 6.3.2 Simplified model

Due to simulation speed issues, the simulations performed with the simplified model are reduced to groups of three. Figure 6.11 shows an in flight formation change. A group of three helicopters changes from line to triangle formation. Figure 6.12 shows a well working collision avoidance with the simplified model. Three vehicles start from circle position and are advised to adopt an other circle formation, rotated around  $180^\circ$ . This causes the vehicles to fly directly through the circle's center what would end in collisions. An appropriate mission for groups of small scale helicopter UAVs are power line inspections, e.g. in the Scandinavian countries. In figure 6.13, a group of three helicopters is heading toward a power line.

As in figure 6.4, in front of the obstacle is a zero force area which the vehicles passed. Due to noisy flight behavior of the helicopters, the vehicles do not stay in this zero potential area and enter a trajectory which guides them to their desired destinations. This holds only if the zero potential area is limited to a point or a line. If a vehicle fly, for example, toward a wall this zero potential area will be a plane in front of the wall. The vehicle will be caught in this stable local minimum. An separate strategy must be developed to detect and fly around these obstacle, taking the virtual leader force into account. The parameter which are used for the presented simulations are printed in table A.4. Nevertheless, above shown situations should be avoided previously.

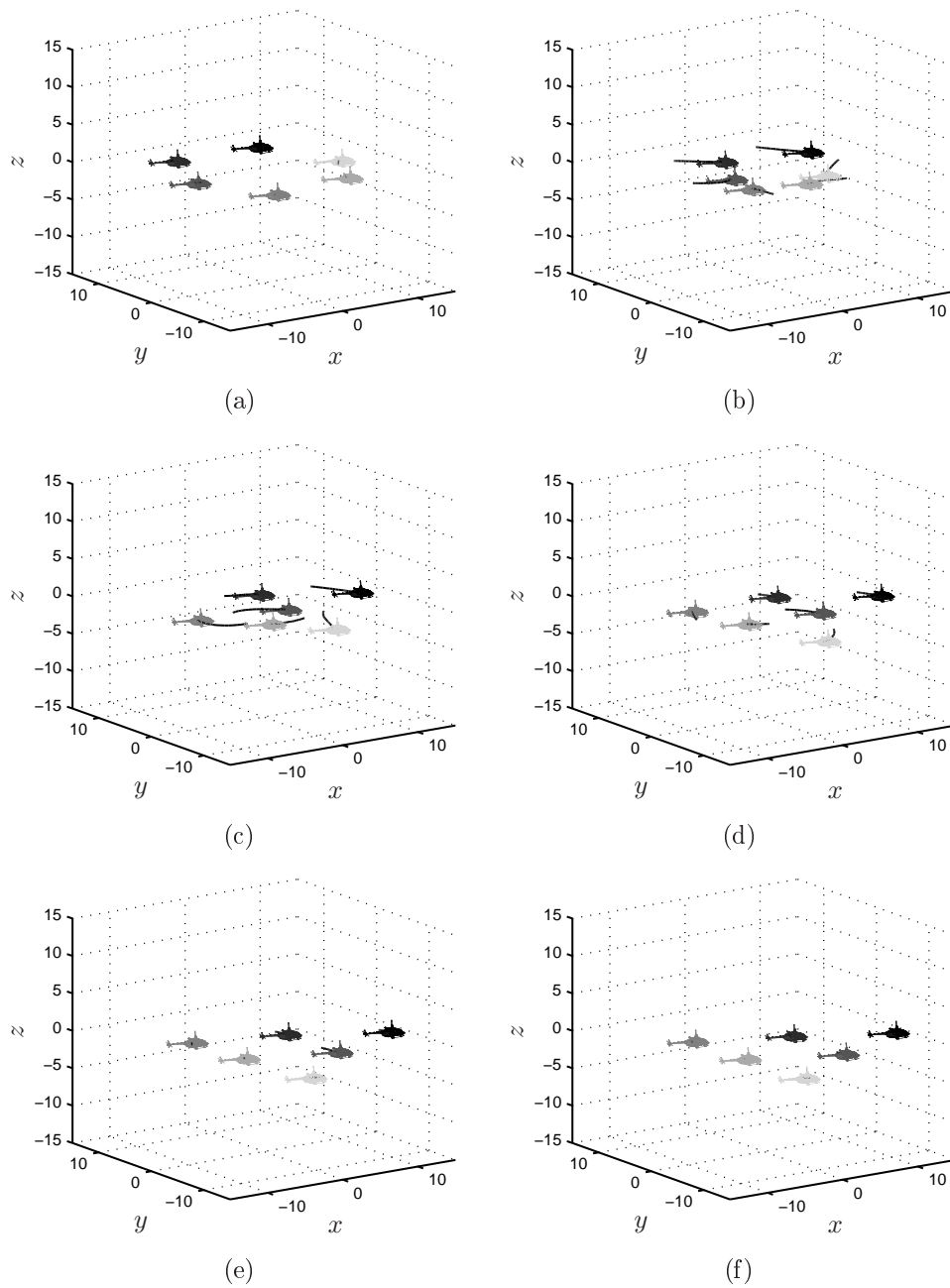


Figure 6.8: Point masses changing from circle to triangle formation.

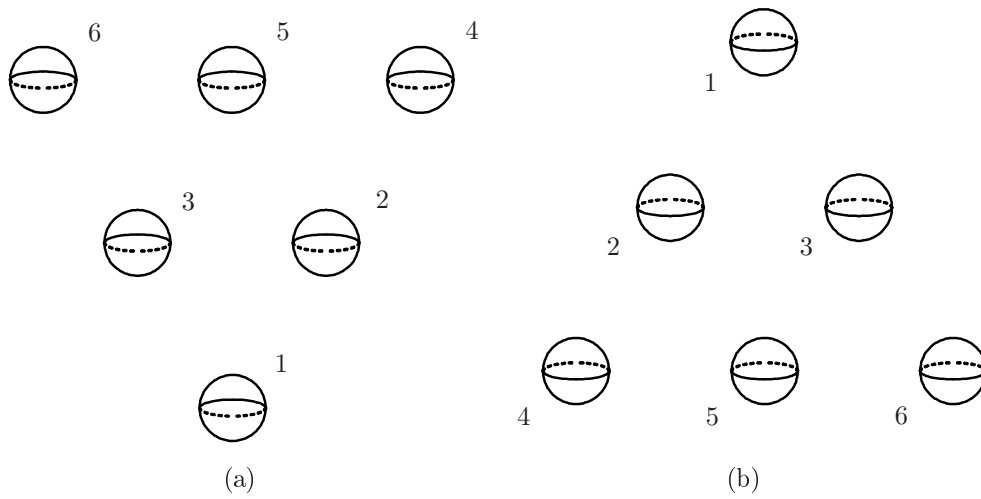


Figure 6.9: Scheme of exchanging places  
(a) Start formation, (b) End formation

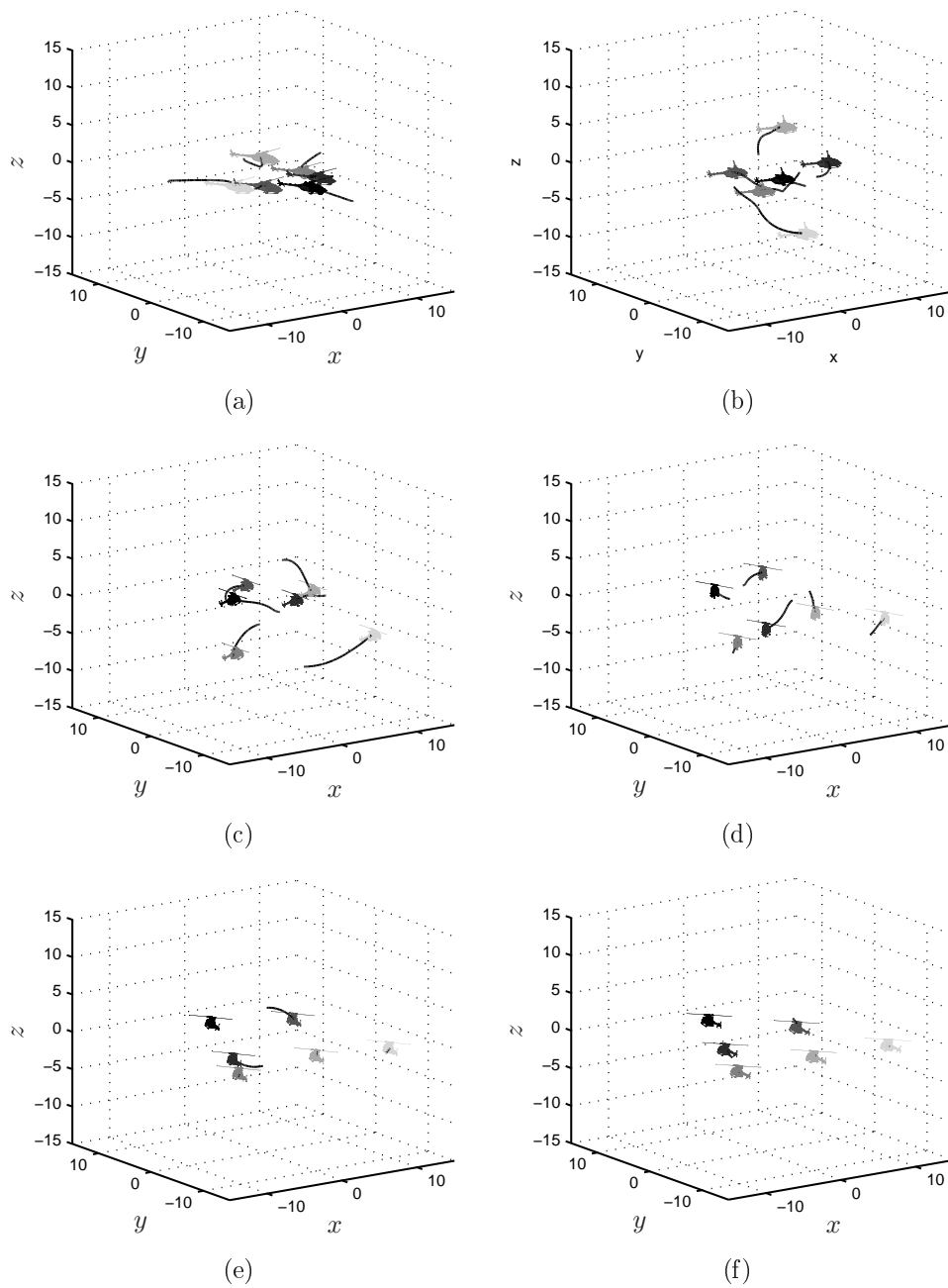


Figure 6.10: Simulation results of exchanging places.  
Point masses changing places corresponding to figure 6.9.

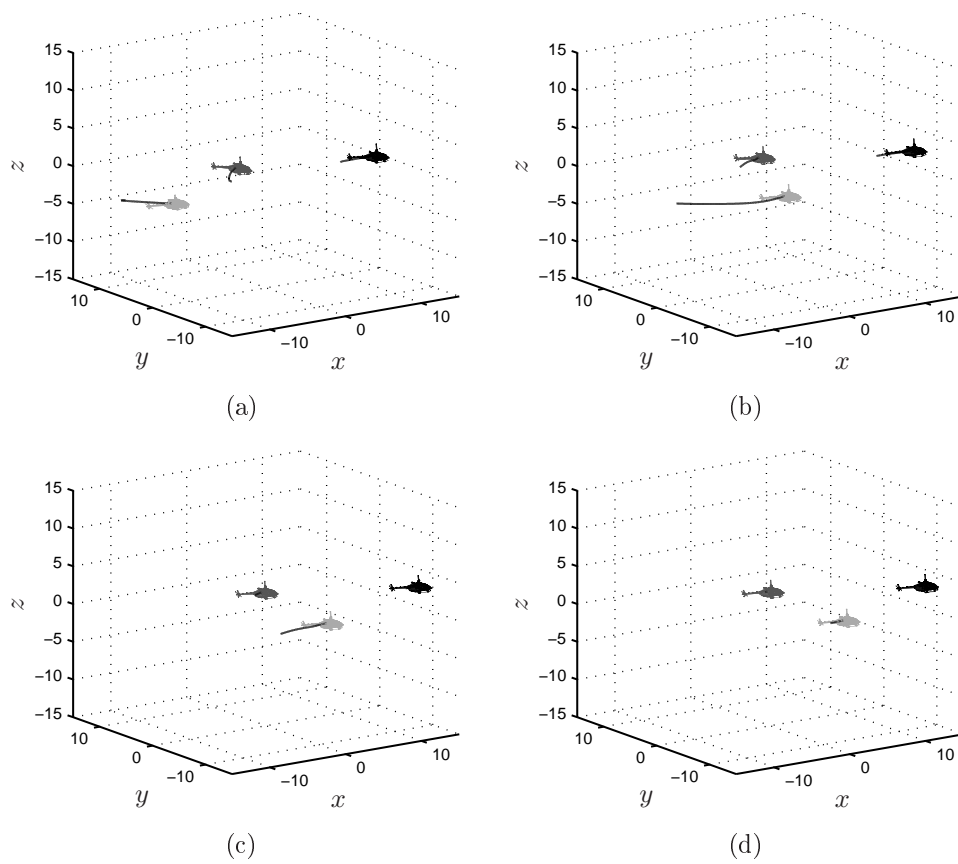


Figure 6.11: Formation flight with the simplified model  
The group changes from line to triangular formation.

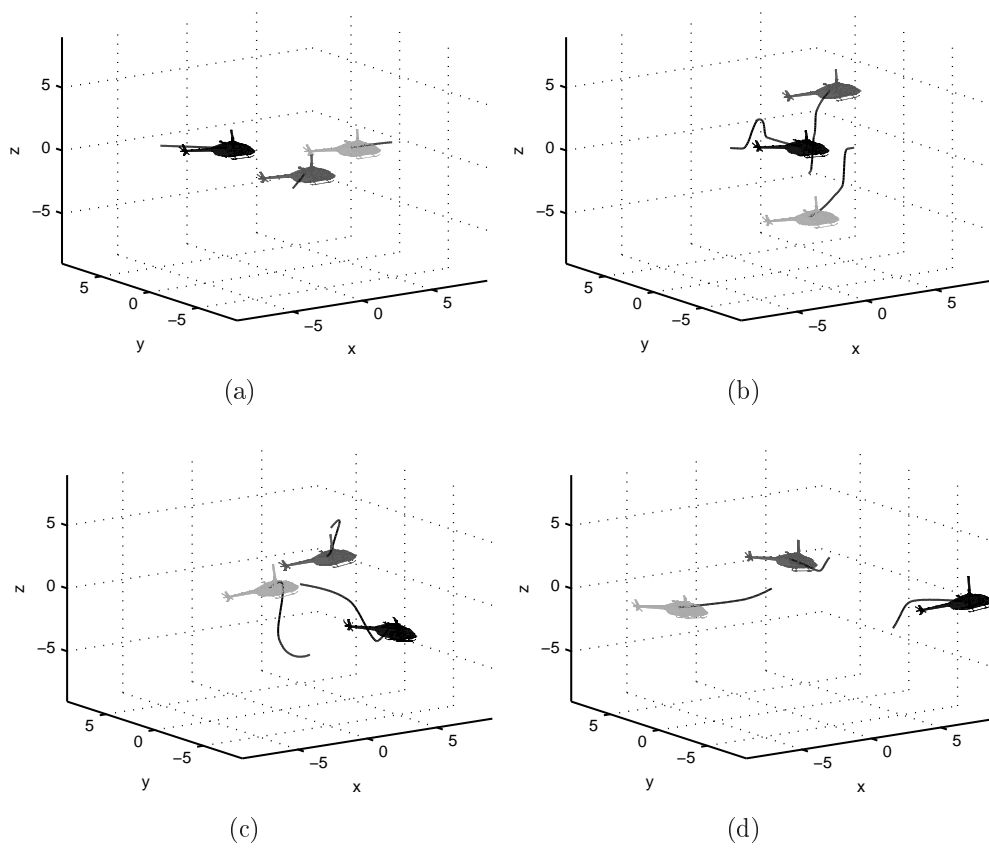


Figure 6.12: Collision avoidance with the simplified model

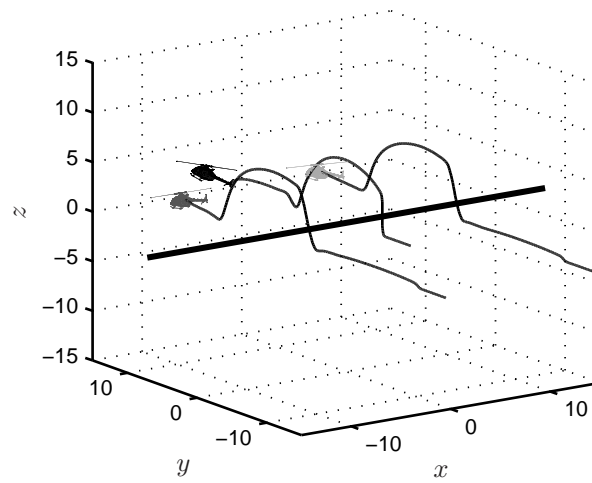


Figure 6.13: Obstacle avoidance  
A group of UAVs is heading toward a power line.

# Chapter 7

## Future work

Unmanned aerial vehicles, helicopter control and formation flight are very interesting topics which will get even more important in the future. Therefore it is necessary to continue the research in these fields.

**Thrust calculation** Due to the fact that the iterative calculation of the thrust is a big disadvantage for helicopter simulation it is advisable to search for a closed expression. This would lead to faster simulations and would also support the development of nonlinear control and the accordant proofs.

**Helicopter model** The presented small scale helicopter model does not include ground effects which is necessary to simulate vertical take-off and landing. Therefore it could be very interesting to model this important part of a flight.

**Nonlinear helicopter control** As shown, several approaches exist for nonlinear helicopter control but just a few are proved through simulations with complete helicopter models. A working flight controller is absolutely necessary for an UAV and the key to this technology. Therefore, the research should be continued while controller based neuronal networks seem to be most promising.

**Verifying of formation control** To verify the presented formation control, it should be use it with other UAVs. Especially with the presented full model of the small-scale helicopter.

**Obstacle avoidance** As shown in chapter 6, the presented obstacle avoidance using potential fields is under special circumstances not able to lead the vehicle around an obstacle. To provide this feature an intelligence is necessary which recognizes obstacle as complete objects and finds an optimal trajectory

around the obstacle, for example, taking the virtual leader component into account.

In addition, research for secure obstacle and vehicle recognition is necessary. Information about all vehicles in the swarm must be provided and strategies concerning lost of information should be found.

**Disturbances** The presented formation flight solution is not simulated with disturbances like communication failure or wind. Nevertheless, these disturbances will occur in a real flight and their influence should be analyzed.

# Bibliography

- J. Adamy. *Fuzzy Logik, Neuronale Netze und Evolutionäre Algorithmen*. Shaker Verlag, September 2005. In German.
- D. Angeli, Y. Chitour, and L. Marconi. New results on robust stabilization via saturated feedback. In *Proceedings of the 42nd IEEE Conference on Decision and Control*, December 2003.
- S. Årdal. Automatic landing of helicopter on wave-excited ship deck. Master's thesis, Norwegian University of Science and Technology, 2002.
- M. R. Aurstad. Modelling av dynamikken til et modellhelikopter. Master's thesis, Norwegian University of Science and Technology, Mai 2002. In Norwegian.
- A. Bogdanov and E. Wan. Sdre control with nonlinear feedforward compensation for a small unmanned helicopter. 2003.
- A. Bogdanov, E. Wan, and G. Harvey. Sdre flight control for x-cell and r-max autonomous helicopters. In *43rd IEEE Conference on Decision and Control*, pages 1196 – 1203, December 2004.
- F. Borrelli, D. Subramanian, A. U. Raghunathan, and L. T. Biegler. Milp and nlp techniques for centralized trajectory planning of multiple unmanned air vehicles. In *Proceedings of the American Control Conference*, June 2006.
- Y. Q. Chen and Z. Wang. Formation control: a review and a new consideration. In *IEEE/RSJ International Conference on Intelligent Robots and Systems*, pages 3181– 3186, August 2005.
- L. C. J. C. J. Dawkins. Unmanned combat aerial vehicles: Examining the political, moral, and social implications. Master's thesis, School of Advanced Air and Space Studies, 2005.
- K. D. Do. Formation control of mobile agents using local potential functions. In *Proceedings of the American Control Conference*, June 2006.

- G. Elkaim and R. Kelbley. A lightweight formation control methodology for a swarm of non-holonomic vehicles. In *Aerospace Conference*, March 2006.
- E. B. Erdem. *Analysis and Real-Time Implementation of State-Dependent Riccati Equation Controlled Systems*. PhD thesis, University of Illinois, 2001.
- T. I. Fossen. *Marine Control Systems - Guidance, Navigation, and Control of Ships, Rigs and Underwater Vehicles*. Marine Cybernetics, November 2002.
- D. Galzi and Y. Shtessel. Uav formations control using high order sliding modes. In *Proceedings of the American Control Conference*, pages 4249–4255, 2006.
- V. Gavrillets. *Autonomous Aerobatic Maneuvering of Miniature Helicopters*. PhD thesis, Massachusetts Institute of Technology, May 2003.
- V. Gavrillets, B. Mettler, and E. Feuron. Nonlinear model for a small-sized acrobatic helicopter. In *AIAA Guidance, Navigation and Control Conference*, number AIAA 2001-4333. AIAA, August 2001.
- A. Gonzalez, R. Mahtani, M. Bejar, and A. Ollero. Control and stability analysis of an autonomous helicopter. In *Proceedings of the World Automation Congress*, volume 15, pages 399–404, July 2004.
- H. Gulam and S. W. Lee. Uninhabited combat aerial vehicles and the law of armed conflict. *Australian Army Journal*, 3(2):1–14, 2006.
- K. Han, A. M. Garcia, I. M. Leo, M. M. del Campo, C. Muhammad, and L. Ortiz-Valles. Unmanned aerial vehicle (uav) cargo system. In *Proceedings of the System and Information Engineering Design Symposium*, pages 121–130, 2004.
- R. K. Heffley and M. A. Mnich. Minimum-complexity helicopter simulation math model. Technical Report NAS2-11665, NASA, April 1988.
- S. Herwitz, S. Dunagan, D. Sullivan, R. Higgins, L. Johnson, J. Zheng, R. Slye, J. Brass, J. Leung, B. Gallmeyer, and M. Aoyagi. Solar-powered uav mission for agricultural decision support. In *Proceedings of the IEEE International Geoscience and Remote Sensing Symposium*, volume 3, pages 1692–1694, July 2003.
- A. Isidori, L. Marconi, and A. Serrani. Robust nonlinear motion control of a helicopter. In *Proceedings of the 40th IEEE Conference on Decision and Control*. IEEE, December 2001.
- E. N. Johnson and S. Kannan. Adaptive flight control for an autonomous unmanned helicopter. In *AIAA Guidance, Navigation and Control Conference*, number AIAA-2002-4439, Monterey, CA, aug 2002.

- I. I. Kaminer, O. A. Yakimenko, V. N. Dobrokhodov, and M. I. Lizarrag. Cooperative control of small uavs for naval applications. In *43rd IEEE Conference on Decisions and Control*. IEEE, December 2004.
- K. Kondak, C. Deeg, G. Hommel, M. Musial, and V. Remuß. Mechanical model and control of an autonomous small size helicopter with a stiff main rotor. In *Proceedings of IEEE/RSJ International Conference on Intelligent Robot Systems*, pages 2469–2414. IEEE, October 2004.
- L. Marconi and R. Naldi. Robust nonlinear control of a miniature helicopter for aerobatic maneuvers. In *Proceedings 32th Rotorcraft Forum*, September 2006.
- B. Mettler, M. Tischler, and T. Kanade. System identification of a model-scale helicopter. Technical Report CMU-RI-TR-00-03, Robotics Institute, Carnegie Mellon Univesity, Pittsburgh, PA, January 2000.
- Munn. More about balloons. *Scientific American*, 4(26):205, March 1849.
- C. Munziger. Development of a real-time flight simulator for an experimental model helicopter. Master’s thesis, Georgia Institute of Technology, December 1998.
- G. D. Padfield. *Helicopter Flight Dynamics: The Theory and Application of Flying Qualities and Simulation Modelling*. Backwell Science, 1996.
- T. Paul, T. R. Krogstad, and J. T. Gravdahl. Uav formation flight using 3d potential field. March 2007.
- R. Q. Prouty and H. C. C. Jr. Helicopter control systems: A history. *Journal of Guidance, Control, and Dynamics*, 26(1):12–18, January-February 2003.
- A. Restas. Wildfire management supported by uav based air reconnaissance: Experiments and results at the szendro fire department, hungary. In *First International Workshop on Fire Management*, April 2006.
- Z. Sarris. Survey of uav applications in civil markets (june 2001). In *9th Mediterranean Conference in Control and Automation*, June 2001.
- J. M. Sullivan. Evolution or revolution? the rise of uavs. *IEEE Technology and Society Magazine*, Fall 2006:43–49, 2006.
- C. M. Vélez and A. Agudelo. Control and parameter estimation of a mini-helicopter robot using rapid prototyping tools. *WSEAS Trans. on Systems*, 5:2250–2256, 2006.

# Appendix A

## Data

### A.1 UAV model

Parameter	Description
$A_{\delta_{lon}}^{nom} = 4.2 \text{ rad/rad}$	long. cyclic to flap gain at nominal rpm
$a_{mr} = 5.5 \text{ rad}^{-1}$	m.r. blade Lift curve slope
$a_{tr} = 5.0 \text{ rad}^{-1}$	t.r. blade lift curve slope
$B_{\delta_{lat}}^{nom} = 4.2 \text{ rad/rad}$	lateral cyclic to flap gain at nominal rpm
$C_{D_0}^{mr} = 0.024$	m.r. blade zero lift drag coefficient
$C_{D_0}^{tr} = 0.024$	t.r. blade zero lift drag coefficient
$C_{L_\alpha}^{vf} = 2.0 \text{ rad}^{-1}$	vertical fin lift curve slopw
$C_{L_\alpha}^{ht} = 3.0 \text{ rad}^{-1}$	horizontal tail lift curve slope
$C_{T_{max}}^{mr} = 0.0055$	m.r. max thrust coefficient
$C_{T_{max}}^{tr} = 0.0055$	t.r. max thrust coefficient
$c_{mr} = 0.058 \text{ m}$	m.r. chord
$c_{tr} = 0.029 \text{ m}$	t.r. chord
$f_j = 0.6$	convergence rate coefficient
$f_q^s = 9.0 \text{ Hz}$	pitching resonance frequency of suspension system
$f_r^s = 9.0 \text{ Hz}$	yawing resonance frequency of suspension system
$f_s^p = 12.5 \text{ Hz}$	rolling resonance frequency of suspension system
$g = 9.80665 \text{ m/s}^2$	acceleration due to gravity at sea level
$h_{mr} = 0.235 \text{ m}$	m.r. hub height above center of gravity
$h_{tr} = 0.08 \text{ m}$	t.r. height above center of gravity
$I_{xx} = 0.18 \text{ kg m}^2$	rolling moment of inertia
$I_{yy} = 0.34 \text{ kg m}^2$	pitching moment of inertia
$I_{zz} = 0.28 \text{ kg m}^2$	yawing moment of inertia
$I_{\beta_{mr}} = 0.038 \text{ kg m}^2$	m.r. blade flipping inertia
$K_i = 0.02 \text{ 1/rad}$	inegral governor gain
$K_p = 0.01 \text{ sec/rad}$	proportionl governor gain

Parameter	Description
$K_\beta = 54 \text{ Nm/rad}$	hub torsional stiffness
$K_\mu = 0.2$	scaling of flap response to speed variation
$l_{ht} = 0.71 \text{ m}$	stabilizer location behind center of gravity
$l_{tr} = 0.91 \text{ m}$	t.r. hub location behind center of gravity
$m = 8.2 \text{ kg}$	helicopter mass
$n_{es} = 9.0$	gear ratio of engine shaft to m.r.
$n_{tr} = 4.66$	gear ratio of t.r. to m.r.
$P_{eng}^{idle} = 0.0 \text{ W}$	engine idle power
$P_{eng}^{max} = 2000.0 \text{ W}$	engine maximum power
$R_{mr} = 0.775 \text{ m}$	m.r. radius
$R_{tr} = 0.13 \text{ m}$	t.r. radius
$S_{ht} = 0.01 \text{ m}^2$	horizontal fin area
$S_{vf} = 0.012 \text{ m}^2$	effective vertical fin area
$S_x^{fus} = 0.1 \text{ m}^2$	frontal fuselage drag area
$S_y^{fus} = 0.22 \text{ m}^2$	side fuselage drag area
$S_z^{fus} = 0.15 \text{ m}^2$	vertical fuselage drag area
$T_{mr}^{max} = 2.5 \text{ mg}$	maximum rotor thrust
$V_{imr} = 4.2 \text{ m/s}$	m.r. induced velocity
$\gamma_{fb} = 0.8$	stabilizer bar Lock number
$\delta_r^{trim} = 0.1 \text{ rad}$	t.r. pitch trim coefficient
$\epsilon_{vf}^{tr} = 0.2$	fraction of vert. fin area exposed to t.r. induced vel.
$\eta_w = 0.9$	coefficient of non-ideal wake contraction
$\mu_z^{tr}$	normal t.r. inflow components
$\mu_{tr}$	in-plane t.r. inflow components
$\xi^s = 0.05$	damping ratio of the suspension system material
$\rho = 1.293 \text{ kg/m}^3$	density of air at standart temperature and pressure
$\tau_e \approx 0.1 \text{ sec}$	rotor time constant for flapping motion
$\Omega_{nom} = 167 \text{ rad/sec}$	nominal m.r. speed

Table A.1: Parameter of the helicopter model

## A.2 Simplified model and corresponding controller

Parameter	Description
$c = 1.6 \cdot 10^{-4}$	Constant of helicopter model
$c_M^{Q,T} = 52$	Constant of helicopter model
$d = 1.2 \cdot 10^{-3}$	Constant of helicopter model
$k_1 = 0.8$	Gain of vertical controller

Parameter	Description
$k_2 = 100$	Gain of vertical controller
$k_3 = 4.5/\Omega_{nom}^2 = 1.6135 \cdot 10^{-4}$	Gain of engine controller
$k_4 = 1/\Omega_{nom}^2 = 3.5856 \cdot 10^{-5}$	Gain of engine controller
$K_1 = 0.002$	Gain of nested saturation controller
$K_2 = 0.4$	Gain of nested saturation controller
$K_3 = 0.5$	Gain of nested saturation controller
$K_D = 0.6$	Gain of lon./lat. controller
$K_{TM} = 5.8 \cdot 10^{-2}$	Constant of helicopter model
$K_{TT} = 1 \cdot 10^{-2}$	Constant of helicopter model
$K_P = 48.4$	Gain of lon./lat. controller
$K_\psi = 0.8$	Gain of lon./lat. controller
$\lambda_1 = 160$	Gain of nested saturation controller
$\lambda_2 = 8$	Gain of nested saturation controller
$\lambda_3 = 0.4$	Gain of nested saturation controller

Table A.2: Parameter of the simplified UAV

### A.3 Formation flight

Parameter	Description
$F_{max} = 15$	Maximum offset, added to the current vehicles position
$F_{min} = 1$	Minimum distance when a position is reached
$r_{sav} = 1$	Safety radius
$K_{vl} = 1$	Virtual leader gain
$K_{iv} = 0.1$	Inter vehicle gain
$K_{ca} = 150$	collision avoidance gain

Table A.3: Parameter of six point mass formation solution

---

Parameter	Description
$F_{max} = 15$	Maximum offset, added to the current vehicles position
$F_{min} = 2$	Minimum distance when a position is reached
$r_{sav} = 11$	Safety radius
$K_{vl} = 1$	Virtual leader gain
$K_{iv} = 0.1$	Inter vehicle gain
$K_{ca} = 165$	collision avoidance gain

Table A.4: Parameter of three helicopter formation solution

# Appendix B

## SDC parameter

**$X_{fus}$ -force**

$$X_{fus}^u = -0.5\rho S_x^{\text{fus}} V_\infty(\mathbf{x}) \quad (\text{B.1})$$

$$\Delta X_{fus} = 0.5\rho S_x^{\text{fus}} V_\infty(\mathbf{x}) u_w \quad (\text{B.2})$$

**$Y_{mr}$ -force**

$$Y_{mr}^p = -\Delta T_{mr}(\mathbf{x}, \mathbf{x}_w, \delta_{col}^0) \tau_e \quad (\text{B.3})$$

$$Y_{mr}^v = \Delta T_{mr}(\mathbf{x}, \mathbf{x}_w, \delta_{col}^0) \frac{\partial b_1}{\partial \mu_v} \frac{1}{\Omega_{mr} R_{mr}} \quad (\text{B.4})$$

$$Y_{mr}^{\delta_{col}} = \frac{\partial T_{mr}(\mathbf{x}, \mathbf{x}_w, \delta_{col}^0)}{\partial \delta_{col}} b_1(\mathbf{x}, \mathbf{x}_w, 0) \quad (\text{B.5})$$

$$Y_{mr}^{\delta_{lat}} = \Delta T_{mr}(\mathbf{x}, \mathbf{x}_w, \delta_{col}^0) A_{\delta_{lat}}^{\text{nom}} \quad (\text{B.6})$$

$$\begin{aligned} \Delta Y_{mr} = & - \left( \Delta T_{mr}(\mathbf{x}, \mathbf{x}_w, \delta_{col}^0) + \frac{\partial T_{mr}(\mathbf{x}, \mathbf{x}_w, \delta_{col}^0)}{\partial \delta_{col}} \delta_{col} + O^2 \right) \\ & \cdot \frac{\partial b_1}{\partial \mu_v} \frac{v_w}{\Omega_{mr} R_{mr}} + \left( \frac{\partial T_{mr}(\mathbf{x}, \mathbf{x}_w, \delta_{col}^0)}{\partial \delta_{col}} \delta_{col} + O^2 \right) B_{\delta_{lat}}^{\text{nom}} \delta_{lat} \end{aligned} \quad (\text{B.7})$$

**$Y_{fus}$ -force**

$$Y_{fus}^v = -0.5\rho S_y^{\text{fus}} V_\infty(\mathbf{x}) \quad (\text{B.8})$$

$$\Delta Y_{fus} = 0.5\rho S_y^{\text{fus}} V_\infty(\mathbf{x}) v_w \quad (\text{B.9})$$

**$Y_{tr}$ -force**

$$Y_{tr}^{\delta_r} = -\frac{\partial T_{tr}(\mathbf{x}, \mathbf{x}_w, \delta_r^0)}{\partial \delta_r} \quad (\text{B.10})$$

$$\Delta Y_{tr} = -(\Delta T_{tr}(\mathbf{x}, \mathbf{x}_w, \delta_r^0) + O^2) \quad (\text{B.11})$$

 **$Y_{vf}$ -force**

$$Y_{vf}^v = -0.5\rho S_{vf} (C_{L\alpha}^{vf} V_\infty^{tr}(\mathbf{x}) + |v_{vf}(\mathbf{x})|) \quad (\text{B.12})$$

$$Y_{vf}^r = 0.5\rho S_{vf} (C_{L\alpha}^{vf} V_\infty^{tr}(\mathbf{x}) + |v_{vf}(\mathbf{x})|) l_{tr} \quad (\text{B.13})$$

$$\Delta Y_{vf} = -0.5\rho S_{vf} (C_{L\alpha}^{vf} V_\infty^{tr}(\mathbf{x}) + |v_{vf}(\mathbf{x})|) (-v_w) - \epsilon_{vf}^{tr} V_{itr} \quad (\text{B.14})$$

 **$Z_{mr}$ -force**

$$Z_{mr}^{\delta_{col}} = -\frac{\partial T_{mr}(\mathbf{x}, \mathbf{x}_w, \delta_{col}^0)}{\partial \delta_{col}} \quad (\text{B.15})$$

$$\Delta Z_{mr} = -(\Delta T_{mr}(\mathbf{x}, \mathbf{x}_w, \delta_{col}^0) + O^2) \quad (\text{B.16})$$

 **$Z_{fus}$ -force**

$$Z_{fus}^w = -0.5\rho S_z^{\text{fus}} V_\infty(\mathbf{x}) \quad (\text{B.17})$$

$$\Delta Z_{fus} = 0.5\rho S_y^{\text{fus}} V_\infty(\mathbf{x})(w_w - V_{imr}) \quad (\text{B.18})$$

 **$Z_{ht}$ -force**

$$Z_{ht}^w = 0.5\rho S_{ht} \{C_{L\alpha}^{ht} |(u - u_w)| + |w_{ht}(\mathbf{x}, \mathbf{x}_w)|\} \quad (\text{B.19})$$

$$Z_{ht}^q = 0.5\rho S_{ht} \{C_{L\alpha}^{ht} |(u - u_w)| + |w_{ht}(\mathbf{x}, \mathbf{x}_w)|\} l_{ht} \quad (\text{B.20})$$

$$\Delta Z_{ht} = 0.5\rho S_{ht} \{C_{L\alpha}^{ht} |(u - u_w)| + |w_{ht}(\mathbf{x}, \mathbf{x}_w)|\} (w_w - K_\lambda V_{imr}) \quad (\text{B.21})$$

**$L_{mr}$ -moment**

$$L_{mr}^p = - (K_\beta + \Delta T_{mr}(\mathbf{x}, \mathbf{x}_w, \delta_{col}^0) h_{mr}) \tau_e \quad (\text{B.22})$$

$$= -L_{mr\beta}^* \tau_e \quad (\text{B.23})$$

$$L_{mr}^v = (K_\beta + \Delta T_{mr}(\mathbf{x}, \mathbf{x}_w, \delta_{col}^0) h_{mr}) \frac{\partial b_1}{\partial \mu_v} \frac{1}{\Omega_{mr} R_{mr}} \quad (\text{B.24})$$

$$= L_{mr\beta}^* \frac{\partial b_1}{\partial \mu_v} \frac{1}{\Omega_{mr} R_{mr}} \quad (\text{B.25})$$

$$L_{mr}^{\delta_{col}} = \frac{\partial T_{mr}(\mathbf{x}, \mathbf{x}_w, \delta_{col}^0)}{\partial \delta_{col}} h_{mr} b_1(\mathbf{x}, \mathbf{x}_w, 0) \quad (\text{B.26})$$

$$(\text{B.27})$$

$$L_{mr}^{\delta_{lat}} = (K_\beta + \Delta T_{mr}(\mathbf{x}, \mathbf{x}_w, \delta_{col}^0) h_{mr}) B_{\delta_{lat}}^{\text{nom}} \quad (\text{B.28})$$

$$= L_{mr\beta}^* B_{\delta_{lat}}^{\text{nom}} \quad (\text{B.29})$$

$$\begin{aligned} \Delta L_{mr} = & - (K_\beta + \{ \Delta T_{mr}(\mathbf{x}, \mathbf{x}_w, \delta_{col}^0) + O^2 \} h_{mr}) \frac{\partial b_1}{\partial \mu_v} \frac{v_w}{\Omega_{mr} R_{mr}} \\ & + \left( \frac{\partial T_{mr}(\mathbf{x}, \mathbf{x}_w, \delta_{col}^0)}{\partial \delta_{col}} \delta_{col} + O^2 \right) B_{\delta_{lat}}^{\text{nom}} \delta_{lat} \end{aligned} \quad (\text{B.30})$$

 **$L_{vf}$ -moment**

$$L_{vf}^v = Y_{vf}^v h_{tr} \quad (\text{B.31})$$

$$L_{vf}^r = Y_{vf}^r h_{tr} \quad (\text{B.32})$$

$$\Delta L_{vf} = \Delta Y_{vf} h_{tr} \quad (\text{B.33})$$

 **$L_{tr}$ -moment**

$$L_{tr}^{\delta_r} = Y_{tr}^{\delta_r} h_{tr} \quad (\text{B.34})$$

$$\Delta L_{tr} = \Delta Y_{tr} h_{tr} \quad (\text{B.35})$$

**$M_{mr}$ -moment**

$$M_{mr}^q = - \left( K_\beta + \left\{ T_{mr}(\mathbf{x}, \mathbf{x}_w, \delta_{col}^0) - \frac{\partial T_{mr}(\mathbf{x}, \mathbf{x}_w, \delta_{col}^0)}{\partial \delta_{col}} \delta_{col}^0 \right\} h_{mr} \right) \cdot \tau_e \quad (\text{B.36})$$

$$= - (K_\beta + \Delta T_{mr}(\mathbf{x}, \mathbf{x}_w, \delta_{col}^0) h_{mr}) \tau_e \quad (\text{B.37})$$

$$= -L_{mr\beta}^* \tau_e \quad (\text{B.38})$$

$$M_{mr}^u = (K_\beta + \Delta T_{mr}(\mathbf{x}, \mathbf{x}_w, \delta_{col}^0) h_{mr}) \frac{\partial a_1}{\partial \mu} \frac{1}{\Omega_{mr} R_{mr}} \quad (\text{B.39})$$

$$= L_{mr\beta}^* \frac{\partial a_1}{\partial \mu} \frac{1}{\Omega_{mr} R_{mr}} \quad (\text{B.40})$$

$$M_{mr}^w = (K_\beta + \Delta T_{mr}(\mathbf{x}, \mathbf{x}_w, \delta_{col}^0) h_{mr}) \frac{\partial a_1}{\partial \mu_z} \frac{1}{\Omega_{mr} R_{mr}} \quad (\text{B.41})$$

$$= L_{mr\beta}^* \frac{\partial a_1}{\partial \mu_z} \frac{1}{\Omega_{mr} R_{mr}} \quad (\text{B.42})$$

$$M_{mr}^{\delta_{col}} = \frac{\partial T_{mr}(\mathbf{x}, \mathbf{x}_w, \delta_{col}^0)}{\partial \delta_{col}} h_{mr} a_1(\mathbf{x}, \mathbf{x}_w, 0) \quad (\text{B.43})$$

$$(\text{B.44})$$

$$M_{mr}^{\delta_{lon}} = (K_\beta + \Delta T_{mr}(\mathbf{x}, \mathbf{x}_w, \delta_{col}^0) h_{mr}) A_{\delta_{lon}}^{\text{nom}} \quad (\text{B.45})$$

$$= L_{mr\beta}^* A_{\delta_{lon}}^{\text{nom}} \quad (\text{B.46})$$

$$\begin{aligned} \Delta M_{mr} &= - (K_\beta + \{ \Delta T_{mr}(\mathbf{x}, \mathbf{x}_w, \delta_{col}^0) + O^2 \} h_{mr}) \\ &\quad \cdot \left( \frac{\partial a_1}{\partial \mu} \frac{u_w}{\Omega_{mr} R_{mr}} + \frac{\partial a_1}{\partial \mu_z} \frac{w_w}{\Omega_{mr} R_{mr}} \right) \\ &\quad + \left( \frac{\partial T_{mr}(\mathbf{x}, \mathbf{x}_w, \delta_{col}^0)}{\partial \delta_{col}} \delta_{col} + O^2 \right) A_{\delta_{lon}}^{\text{nom}} \delta_{lon} \end{aligned} \quad (\text{B.47})$$

 **$M_{ht}$ -moment**

$$M_{ht}^w = Z_{ht}^w l_{ht} \quad (\text{B.48})$$

$$M_{ht}^q = Z_{ht}^q l_{ht} \quad (\text{B.49})$$

$$\Delta M_{ht} = \Delta Z_{ht} l_{ht} \quad (\text{B.50})$$

**$Q_e$ -moment**

$$\Delta Q_e = \frac{P_e^{\max}}{\Omega_{mr}} \delta_t \quad (\text{B.51})$$

 **$N_{vf}$ -moment**

$$N_{vf}^v = -Y_{vf}^v l_{tr} \quad (\text{B.52})$$

$$N_{vf}^r = -Y_{vf}^r l_{tr} \quad (\text{B.53})$$

$$\Delta N_{vf} = -\Delta Y_{vf} h_{lr} \quad (\text{B.54})$$

 **$N_{tr}$ -moment**

$$N_{tr}^{\delta r} = -Y_{tr}^{\delta r} l_{tr} \quad (\text{B.55})$$

$$\Delta N_{tr} = -\Delta Y_{tr} l_{tr} \quad (\text{B.56})$$

# Appendix C

Submitted paper to the 2008  
American Control Conference

# UAV Formation Flight using 3D Potential Field

Tobias Paul\* Thomas R. Krogstad† Jan Tommy Gravdahl†

\* Department of Electrical Engineering and Information Technology, Technical University of Darmstadt, Germany  
email: tobias.paul@stud.tu-darmstadt.de

† Department of Engineering Cybernetics, Norwegian University of Science and Technology, Trondheim, Norway  
email: {thomas.krogstad, tommy.gravdahl}@itk.ntnu.no

**Abstract**—This paper presents a solution for formation flight and formation reconfiguration of UAVs. The solution is based on a virtual leader approach, combined with an extended local potential field. It is verified, using a simplified helicopter model, simulated in MATLAB<sup>TM</sup>/Simulink<sup>TM</sup>. As necessary for helicopters, the potential field approach is realized in 3D including obstacle and collision avoidance.

## I. INTRODUCTION

UAV technology is a rapidly evolving research area and came into the focus of the scientific community during the last years. Beside the abilities to be built in small size, light weight and operating autonomously, UAVs can also be replaced at low cost. These qualities make UAVs also interesting for industrial and military purposes. Possible UAV missions are autonomous building inspection or search and rescue missions using video and infra red sensors. This equipment enables the vehicle to search and localize humans in water, on land, and even through dust. UAVs have been used for mapping of hot spots during forest fires [1]. Even agricultural and crop (coffee, etc.) monitoring has already be done [2]. The wide field of military applications is easy to imagine. A main argument for the use of UAVs in combat (UCAV) is to preserve pilots from high risk or long endurance missions. Applications are, among others, surveillance and reconnaissance, radio jamming, artillery acquisition, and target simulation.

Formations of UAVs can distribute the equipment, necessary for a specific mission, to all vehicles in the swarm and offer a huge increase of performance and robustness compared to a single operating vehicle. The two main approaches for formation control are potential field and leader-follower approaches. Combinations of those two approaches are often used to build and move formations because they are very effective, robust and easy to handle [3], [4].

As UAVs, helicopters are of special interest. They are able to perform vertical take-offs and landings (VTOL) and to hover. With these abilities they are able to operate from a ship, undeveloped, or urban areas. Modeling a helicopter is challenging because of the different fly modes. Nevertheless, with [5] and [6] one can find at least two nonlinear models for full scale helicopters. For UAVs are especially small scale helicopter interesting. They have a very high thrust to weight ratio and can perform extreme maneuvers. Furthermore, a small scale helicopter UAV could be used inside a building. Mathematical models for small scale helicopter are presented by [7], [8] and [9], who derived a complete and very detailed

model of a modified *X-Cell 60 hobby helicopter*.

Control of a helicopter is challenging because of coupling and the different fly modes. A classical control approach is based on a cascade approach, controlling the attitude in the inner and the lateral and longitudinal movement in the outer loop [10]. Other approaches are based on solving the state dependent Riccati equation [11] or neural networks [12].

This paper presents a virtual leader formation approach combined with an extended version of the potential field solution presented in [4] and [3]. The approach is applied to a formation of helicopter UAVs presented in [10], providing obstacle and collision avoidance. The algorithm provides maximum speed in the sense of the vehicles speed. To the authors knowledge, this approach has not previously been applied on helicopter UAVs. However, a two dimensional approach for marine vehicles is presented in [3] while [4] presents a solution for tricycles. Other formation flight approaches, focusing on fixed wing aircrafts, can be found in [13]–[15], or [16].

## II. MODEL

The helicopter is modeled as a rigid body. The north-east-down (NED) inertial frame with position  $\mathbf{p}^n$  and attitude  $\Theta$  (Euler angles) and a body fixed coordinate frame with body fixed velocities  $\mathbf{v}_b^o$  and body fixed angular velocities  $\omega_{nb}^b$  are used.

$$\begin{array}{l} \text{Body frame:} \\ \text{NED frame:} \end{array} \quad \begin{array}{l} \boldsymbol{\nu} \left\{ \begin{array}{l} \mathbf{v}_b^o \\ \omega_{nb}^b \end{array} \right. \left\{ \begin{array}{l} u \\ v \\ w \\ p \\ q \\ r \end{array} \right. \\ \boldsymbol{\eta} \left\{ \begin{array}{l} \mathbf{p}^n \\ \Theta \end{array} \right. \left\{ \begin{array}{l} x \\ y \\ z \\ \phi \\ \theta \\ \psi \end{array} \right. \end{array}$$

$\boldsymbol{\nu}$  and  $\boldsymbol{\eta}$  are, together with the main rotor speed  $\Omega_{mr}$  and the blade flapping angles  $a_1$  and  $b_1$  the states  $\mathbf{x}$  of the helicopter:

$$\mathbf{x} = [ \boldsymbol{\nu}^T \quad \boldsymbol{\eta}^T \quad a_1 \quad b_1 \quad \Omega_{mr} ]^T. \quad (1)$$

The kinematic equation for a six degree of freedom vehicle is given by [17]

$$\dot{\boldsymbol{\eta}} = \begin{bmatrix} \mathbf{R}_b^n(\boldsymbol{\Theta}) & \mathbf{0}_{3 \times 3} \\ \mathbf{0}_{3 \times 3} & \mathbf{T}_{\boldsymbol{\Theta}}(\boldsymbol{\Theta}) \end{bmatrix} \boldsymbol{\nu}, \quad (2)$$

using the rotation matrix

$$\mathbf{R}_b^n(\boldsymbol{\Theta}) = \begin{bmatrix} c_\psi c_\theta & c_\psi s_\theta s_\phi - s_\psi c_\phi & s_\psi s_\phi + c_\psi c_\phi s_\theta \\ s_\psi c_\theta & c_\psi c_\phi + s_\phi s_\theta s_\psi & s_\theta s_\psi c_\phi - c_\psi s_\phi \\ -s_\theta & c_\theta s_\phi & c_\theta c_\phi \end{bmatrix}, \quad (3)$$

and the kinematic transformation matrix

$$\mathbf{T}_{\boldsymbol{\Theta}}(\boldsymbol{\Theta}) = \begin{bmatrix} 1 & s_\phi t_\theta & c_\phi t_\theta \\ 0 & c_\phi & -s_\phi \\ 0 & s_\phi/c_\theta & c_\phi/c_\theta \end{bmatrix}, \quad (4)$$

with  $s. \equiv \sin(\cdot)$ ,  $c. \equiv \cos(\cdot)$ , and  $t. \equiv \tan(\cdot)$ .

To control the lift and flight direction of a helicopter, it is possible to rotate the main rotor blades. One gets a similar effect, as using the flaps and ailerons by a fixed-wing aircraft. It is possible to rotate all blades at the same time (collective) or induce an angle depending on the position of the blade. Doing this, the blade angle performs a sinusoidal movement (cyclic) during one round. The collective setting is used to control the altitude while the cyclic setting controls the attitude and so the flight in a specific direction.

The control inputs of the presented model are equal to those a pilot uses:

$$\mathbf{u} = [\delta_{col} \quad \delta_{lon} \quad \delta_{lat} \quad \delta_r \quad \delta_t]^T. \quad (5)$$

$\delta_{col}$  is the collective control input for the collective pitch of the main rotor blades given in rad as all angular in the article.  $\delta_{lon}$  and  $\delta_{lat}$  are the cyclic control inputs giving the explicit pitch in longitudinal ( $u$ ) and lateral ( $v$ ) direction.  $\delta_r$  is the collective pitch for the tail rotor, where no cyclic pitch is necessary. Finally  $\delta_t$  is the engine control input to keep the rotor speed constant and varies between 0 and 1.

The components responsible for the helicopter's flight characteristics may be seen in Fig. 1.

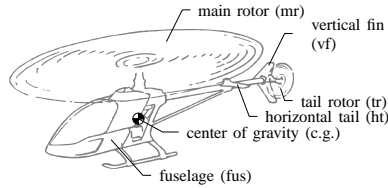


Fig. 1. Helicopter components

#### A. Rigid body dynamics

The equations of motion will be presented following [17]:

$$\mathbf{M}_{RB} \dot{\boldsymbol{\nu}} + \mathbf{C}_{RB}(\boldsymbol{\nu}) \boldsymbol{\nu} = \boldsymbol{\tau}(\mathbf{u}). \quad (6)$$

Here,  $\mathbf{M}_{RB}$  is the system inertia matrix,  $\mathbf{C}_{RB}(\boldsymbol{\nu})$  the coriolis-centripetal matrix, and  $\boldsymbol{\tau}$  a vector of forces and moments

caused by aerodynamics, gravity and engine.

$\mathbf{M}_{RB}$  has a very simple form because the cross-axis moments of inertia can be neglected due to the fact that the origin of the body frame is placed in the helicopter's center of gravity while rotational symmetry is assumed. Doing so,  $\mathbf{M}_{RB}$  is given by:

$$\mathbf{M}_{RB} = \begin{bmatrix} m \mathbf{I}_{3 \times 3} & \mathbf{0}_{3 \times 3} \\ \mathbf{0}_{3 \times 3} & \mathbf{I}_0 \end{bmatrix}. \quad (7)$$

Here,  $\mathbf{I}_{3 \times 3}$  is a unity matrix,  $\mathbf{I}_0$  the system inertia matrix and  $m$  the mass of the helicopter.  $\mathbf{C}_{RB}$  can be realized in different ways. In [17] Kirchoff's equations were used to derive an explicit expression. While

$$\mathbf{M}_{RB} = \mathbf{M}_{RB}^T = \begin{bmatrix} \mathbf{M}_{11} & \mathbf{0}_{3 \times 3} \\ \mathbf{0}_{3 \times 3} & \mathbf{M}_{22} \end{bmatrix} \quad (8)$$

holds,  $\mathbf{C}_{RB}$  can be build up from the elements of  $\mathbf{M}_{RB}$ :

$$\mathbf{C}_{RB}(\boldsymbol{\nu}) = \begin{bmatrix} \mathbf{0}_{3 \times 3} & -S(\mathbf{M}_{11} \boldsymbol{\nu}_1) \\ -S(\mathbf{M}_{11} \boldsymbol{\nu}_1) & -S(\mathbf{M}_{22} \boldsymbol{\nu}_2) \end{bmatrix} \quad (9)$$

using the vector cross product operator  $S(\cdot)$ , defined as

$$\boldsymbol{\lambda} \times \mathbf{a} := S(\boldsymbol{\lambda}) \mathbf{a}, \quad (10)$$

where  $\boldsymbol{\lambda}, \mathbf{a} \in \mathbb{R}^3$  and  $S(\cdot)$  is defined as

$$S(\boldsymbol{\lambda}) = -S(\boldsymbol{\lambda})^T = \begin{bmatrix} 0 & -\lambda_3 & \lambda_2 \\ \lambda_3 & 0 & -\lambda_1 \\ -\lambda_2 & \lambda_1 & 0 \end{bmatrix}. \quad (11)$$

#### B. Forces and moments

A complex model of a small scale helicopter is presented in [9] including all parameter values. The modeled forces and moments  $\boldsymbol{\tau} = [\mathbf{f}_o^b \quad \mathbf{m}_o^b]^T$  of the small-scale helicopter are

$$\mathbf{f}_o^b = \begin{bmatrix} X_{mr} + X_{fus} \\ Y_{mr} + Y_{fus} + Y_{tr} + Y_{vf} \\ Z_{mr} + Z_{fus} + Z_{ht} \end{bmatrix} + \mathbf{f}_g^b, \quad (12)$$

$$\mathbf{m}_o^b = \begin{bmatrix} L_{mr} + L_{vf} + L_{tr} \\ M_{mr} + M_{ht} \\ -Q_e + N_{vf} + N_{tr} \end{bmatrix}. \quad (13)$$

The used indexes can be found in Fig. 1.  $\mathbf{f}_g^b$  is the force caused by gravity decomposed in the body frame:

$$\mathbf{f}_g^b = \mathbf{R}_b^n(\boldsymbol{\Theta})^T \begin{bmatrix} 0 \\ 0 \\ mg \end{bmatrix}. \quad (14)$$

The main rotor forces dominate the vertical, pitch and roll dynamics, while the tail rotor dominates the yaw dynamic. The main rotor forces and moments are caused by the thrust  $T_{mr}$  which depends on the inflow. The inflow depends on the thrust. Because of that, an iterative approach is necessary. Almost all components are depending on the main rotor down wash. Consequently, the equations are coupled. Control is also complicated because of coupling between the control inputs. Because of those issues, the full model of the small-scale helicopter is difficult to control and to simulate.

As our formation control approach is independent of the

underlying dynamics, we choose to instead use a simplified model, presented by [10], for the simulation. Using this model, the forces in the equations of motion change to:

$$\mathbf{f}_o^b = \begin{bmatrix} 0 \\ 0 \\ Z_{mr} \end{bmatrix} + \mathbf{f}_g^b, \quad (15)$$

$$\mathbf{m}_o^b = \begin{bmatrix} L_{mr} \\ M_{mr} \\ N_{mr} \end{bmatrix} + \begin{bmatrix} Y_{mr}h_{mr} + Y_{tr}h_{mr} \\ -X_{mr}h_{mr} \\ -Y_{tr}h_{tr} \end{bmatrix}. \quad (16)$$

The forces and moments in (15) and (16) are modeled in [10] as follows:

$$X_{mr} = -T_{mr}\delta_{lon}, \quad (17)$$

$$Y_{mr} = -T_{mr}\delta_{lat}, \quad (18)$$

$$Z_{mr} = -T_{mr}, \quad (19)$$

$$Y_{tr} = -T_{tr}, \quad (20)$$

$$L_{mr} = c_M^{Q,T} \delta_{lat} - \frac{P_{max}\delta_t}{\Omega_{mr}} \delta_{lon}, \quad (21)$$

$$M_{mr} = c_M^{Q,T} \delta_{lon} + \frac{P_{max}\delta_t}{\Omega_{mr}} \delta_{lat}, \quad \text{and} \quad (22)$$

$$N_{mr} = -\frac{P_{max}\delta_t}{\Omega_{mr}}. \quad (23)$$

The thrusts  $T_{mr}$  and  $T_{tr}$  are linearized in [10]:

$$T_{mr} = K_{TM} \Omega_{mr}^2 \delta_{col} \quad \text{and} \quad (24)$$

$$T_{tr} = K_{TT} \Omega_{mr}^2 \delta_r. \quad (25)$$

The engine dynamic is given by

$$\dot{\Omega}_{mr} = \frac{1}{I_{rot}} (Q_e - Q_{mr}). \quad (26)$$

The engine torque  $Q_e$  is modeled by

$$Q_e = \frac{P_e^{max}\delta_t}{\Omega_{mr}}. \quad (27)$$

The torque  $Q_{mr}$ , caused by the aerodynamic resistance of the rotor, is modeled as

$$Q_{mr} = (c + d\delta_{col}^2) \Omega_{mr}^2. \quad (28)$$

The values of the constants are given in [10]. Fuselage, vertical fin and horizontal tail are not modeled. The main rotor force in  $u$  direction is neglected due to the fact that the longitudinal and lateral movement of a helicopter is dominated by the vehicle attitude. It is assumed that  $Y_{mr} + Y_{tr} = 0$ .

The controller used with the model is based on a vertical controller and a cascade controller. The cascade controller controls the attitude in the inner loop and finally the longitudinal and lateral movement in the outer loop. All necessary parameter are included in [10].

### III. FORMATION CONTROL

The approach presented in the following generates trajectories depending on the interaction of the swarm, the desired position and formation. It is a combination of virtual leader and potential field approach. A movement of the virtual leader

results in a deflection from the desired position and causes the affected vehicles to correct their positions. To control the movement of single vehicles, a potential field is used. Taking the distributed positions and distances into account one can derive a place dependent potential field for each vehicle. This field is finally used for obstacle and collision avoidance. A specific position can be assigned to a specific vehicle in the formation. We give an overview on vehicle's system in Fig. 2. The advantage of the approach, we present in the following, compared to other approaches is the application of a potential field formation control in three dimensions. In addition, a continuous field and thus a continuous trajectory for each vehicle is guaranteed, while providing obstacle and collision avoidance. The algorithm creates a vector which we use to guide the single vehicles. Finally, it provides maximum vehicle speed.

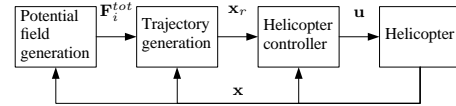


Fig. 2. Vehicle block diagram

The potential field of each vehicle depends on the virtual leader, the other vehicles of the swarm, and on possible collisions, or obstacles.

#### A. Virtual leader

The virtual leader is the anchor of each formation and controls the formation movement. Depending on the underlying control system its trajectory can either be given as waypoints or as continuous trajectory.

The virtual leader's part of the local time dependent potential field is:

$$\mathbf{F}_{vl} = K_{vl} (\mathbf{p}_{vl}^n - \mathbf{p}_i^n - [\mathbf{p}_{vl}^n - \mathbf{p}_{i_0}^n]) \quad (29)$$

$$= K_{vl} (\mathbf{d}_i - \mathbf{d}_{i_0}) \quad (30)$$

$K_{vl}$  is the virtual leader gain which needs to be tuned. The meaning of the variables is explained by Fig. 3.

#### B. Inter vehicle influence

The influence of the other vehicles to the potential field is expressed by:

$$\mathbf{F}_{ij} = K_{ij} (\mathbf{p}_j^n - \mathbf{p}_i^n - [\mathbf{p}_{j_0}^n - \mathbf{p}_{i_0}^n]) \quad (31)$$

$$= K_{ij} (\mathbf{d}_{ij} - \mathbf{d}_{ij_0}) \quad (32)$$

Similar to equations (29) and (30),  $\mathbf{r}_j$  is the position vector for vehicle  $j$  and  $\mathbf{p}_{j_0}^n$  is the position vector pointing to vehicle  $j$ 's place in the formation.  $K_{ij}$  is the inter vehicle gain which needs to be tuned. This leads for vehicle  $i$  to the total amount of

$$\mathbf{F}_{ij}^{tot} = \sum_{j=1}^N \mathbf{F}_{ij}(i, j). \quad (33)$$

The ratio of  $K_{vl}$  and  $K_{ij}$  decides if the vehicles fly primary to the next waypoint or adopt primary their new formation.

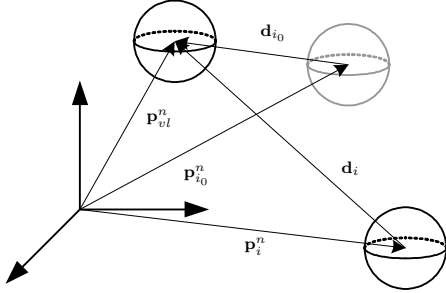


Fig. 3. Vector definitions for formation flight;  $\mathbf{p}_{vl}^n$ : position vector of virtual leader;  $\mathbf{p}_i^n$ : current position vector of vehicle  $i$ ;  $\mathbf{p}_{i0}^n$ : position vector of vehicle  $i$ 's place in the formation

### C. Collision and obstacle avoidance

To avoid collision between the vehicles or obstacles a safety space around each vehicle is defined. This space is also used to build up formations. Because of simplicity this area is defined as a sphere with positive radius  $r_{sav}$ . Other shapes like ellipsoids or even more complex, are also possible, to cover the shape of the vehicle in a better way if necessary. Tests have been performed, using an ellipsoid space. By adding a small pitch angle to the ellipsoid, the vehicle should be supported in going up or down while avoiding a collision. This should be realized using the surface of the sphere as a reflection surface like a mirror. Fig. 4 clarifies the idea. Nevertheless, using the

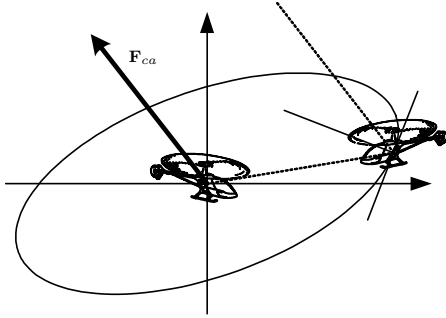


Fig. 4. Ellipsoid used for collision and obstacle avoidance

simplified model, the additional calculation costs do not justify the advantage in compare to the sphere. If something enters this sphere an additional field component, pointing away from the invading vehicle or obstacle comes up. To ensure collision avoidance the additional component converges to infinity in the center of the sphere. The additional field component for vehicle  $i$  whose safety sphere is invaded by vehicle  $j$  is defined by

$$\mathbf{F}_{ca}^{ij} = \begin{cases} \left( \frac{K_{ca}}{\|\mathbf{d}_{ji}\| + \epsilon} - \frac{K_{ca}}{r_{sav}} \right) \frac{\mathbf{d}_{ji}}{\|\mathbf{d}_{ji}\|} & \text{for } \|\mathbf{d}_{ji}\| < r_{sav} \\ 0 & \text{otherwise} \end{cases} \quad (34)$$

with  $0 < \epsilon \ll 1$  to avoid singularities and using the vector 2-norm. The vector 2-norm  $\|\cdot\|_2$  of a vector  $\mathbf{x} \in \mathbb{R}^n$  is defined as

$$\|\mathbf{x}\|_2 := \sqrt{x_1^2 + x_2^2 + \dots + x_n^2}. \quad (35)$$

In the rest of this work, if not specified, the expression  $\|\cdot\|$  refers to the 2-norm. Furthermore  $\mathbf{d}_{ji} = \mathbf{p}_i^n - \mathbf{p}_j^n$ . The term  $K_{ca}/r_{sav}$  is granting a continuous potential field. Again,  $K_{ca}$  is a gain which needs to be tuned. The total amount of the collision avoidance term is given by:

$$\mathbf{F}_{ca}^{tot} = \sum_{j=1}^N \mathbf{F}_{ca}^{ij} \text{ for } i \neq j. \quad (36)$$

Equation (34) can be expanded on every object. Modeling obstacles as a set of points, compared to the knots in a grid, each point can be treated like the vehicles of the swarm. Equation (34) and (36) change to

$$\mathbf{F}_{oa}^{ik} = \begin{cases} \left( \frac{K_{oa}}{\|\mathbf{d}_{ji}\|} - \frac{K_{oa}}{r_{sav}} \right) \frac{\mathbf{d}_{ki}}{\|\mathbf{d}_{ki}\|} & \text{for } \|\mathbf{d}_{ki}\| < r_{sav} \\ 0 & \text{otherwise} \end{cases} \quad (37)$$

$$\mathbf{F}_{oa}^{tot} = \sum_{j=1}^M \mathbf{F}_{oa}^{ik} \text{ for } i \neq j. \quad (38)$$

Here,  $\mathbf{d}_{ji}$  represents one of the  $M$  place vectors which model a detected obstacle. The distance between the place vectors should not be larger than  $r_{sav}/2$  to provide a complete obstacle recognition for the avoidance. To increase the performance,  $r_{sav}$  can be chosen dynamically, depending on the vehicle's velocity:

$$r_{sav} = r_{sav}^{\min} + K_{sav} \|\dot{\mathbf{p}}^n\|. \quad (39)$$

### D. Potential field

Summation of field components gives magnitude and direction of the potential field for vehicle  $i$  at its current position.

$$\mathbf{F}_i^{tot*} = \mathbf{F}_{vl} + \mathbf{F}_{ij}^{tot} + \mathbf{F}_{ca}^{tot} + \mathbf{F}_{oa}^{tot} \quad (40)$$

The field is continuous and singularity free. It is reasonable to define a maximum amplitude for the force vector while keeping its direction:

$$\mathbf{F}_i^{tot} = \begin{cases} \mathbf{F}_i^{tot*} & \text{for } \|\mathbf{F}_i^{tot*}\| < F_{\max} \\ F_{\max} \frac{\mathbf{F}_i^{tot*}}{\|\mathbf{F}_i^{tot*}\|} & \text{otherwise} \end{cases} \quad (41)$$

$F_{\max}$  will be the upper limit of the field's strength and therefore a limitation for the vehicle's speed. To use the whole speed bandwidth,  $F_{\max}$  must be chosen dynamically. This can be realized by adding the amount of the vehicle's NED velocity  $\|\dot{\mathbf{p}}^n\|$  to  $F_{\max}$ . As long as the vehicle is accelerating, the distance to the vehicle's reference position will also increase. This keeps the vehicle accelerating until the maximal velocity is reached.

$$F_{\max}^* = F_{\max} + K_v \|\dot{\mathbf{p}}^n\| \quad (42)$$

Fig. 5 is showing a computed potential field for a specific vehicle interacting with two other vehicles.

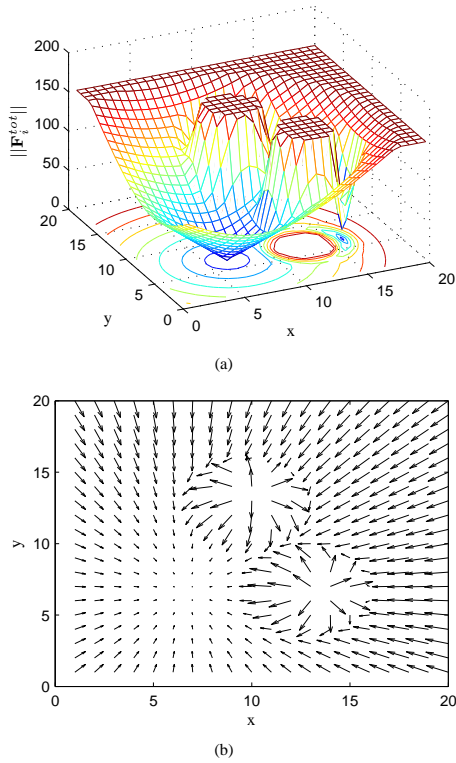


Fig. 5. (a) Potential field magnitude (b) Potential field direction

Following [10], the output of the trajectory generation in Fig. 2, which is used by the controller to calculate the helicopter's control inputs, is given by

$$\mathbf{p}_{i,r}^n = \mathbf{p}_i^n + \mathbf{F}_i^{tot}. \quad (43)$$

The attitude reference is then calculated by

$$\mathbf{a}_r^n = \ddot{\mathbf{p}}_{i,r}^n - \begin{bmatrix} 0 \\ 0 \\ g \end{bmatrix}, \quad (44)$$

$$\mathbf{n} = \begin{bmatrix} n_x \\ n_y \\ n_z \end{bmatrix} = \frac{\mathbf{a}_r^n}{\|\mathbf{a}_r^n\|}, \quad (45)$$

$$\theta_r = \text{atan2}(-s_{\psi_r} n_y + c_{\psi_r} n_x, n_z), \text{ and} \quad (46)$$

$$\phi_r = \text{atan2}(-c_{\theta_r} s_{\phi_r} n_x + c_{\theta_r} c_{\psi_r} n_y, -n_z). \quad (47)$$

$g$  is the gravity constant and  $\psi_r$  part of the formation description. We calculate  $\nu_r$  using equation (2).

On Fig. 5 can a local minimum in the field's magnitude be noticed. This is because of the opposing virtual leader and collision avoidance force. Due to noise, the vehicles will not be caught in this minimum because it is not a stable minimum as the the desired position.

### E. Stability

It is advisable to limit the virtual leader influence, due to the fact that a waypoint can be far away from the actual position, equation (29) respectively (30) can become large because of a large  $\mathbf{d}_i$ . This would result in a domination of the virtual leader part in the potential field and could constrict an effective collision or obstacle avoidance.

Stability of the overall formation system is guaranteed if the generated trajectories are feasible for the underlying control system. Therefore the gains need to be tuned. We give starting assumption in the following:

$$K_{ij} = K_{vl}/N, \quad (48)$$

$$K_{ca} = 10 K_{vl} \tau_{sav}, \quad (49)$$

where  $N$  is the number of vehicles in the group. Due to the fact, that the controller in Fig. 2 normally takes the reference velocity into account,  $\mathbf{F}_i^{tot}$  should be chosen as the distance, the vehicle needs to perform a stop from full speed.

Using the distances  $\mathbf{d}_{i_0}$  and  $\mathbf{d}_{i_{j_0}}$  in (30) and (32) increases the robustness of the algorithm. These distances need to be submitted to the vehicles once while following the virtual leader. A continuous calculation and update of the position of each vehicle in the formation, while the formation is moving, is not necessary.

## IV. SIMULATION RESULTS

Fig. 6 shows an in flight formation change. A group of three helicopters changes from line to triangle formation.

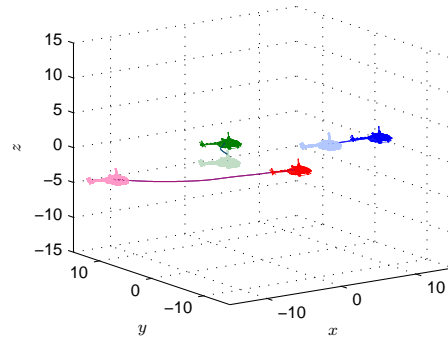


Fig. 6. Formation reconfiguration

Fig. 7 shows a well working collision avoidance with the simplified helicopter model. Three vehicles start from circle position and are advised to adopt an other circle formation, rotated around 180°. This causes the vehicles to fly directly through the circle's center what would result in collisions if the collision avoidance term would not be present.

An appropriate mission for groups of small scale helicopter UAVs are power line inspections, e.g. in the Scandinavian countries. In Fig. 8, a group of three helicopters is heading toward a power line.

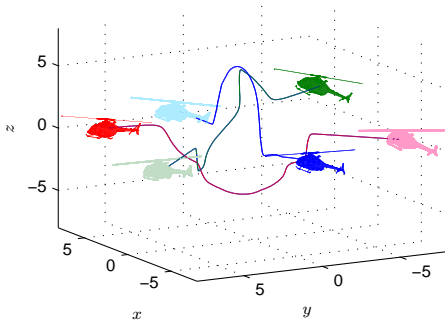


Fig. 7. Collision avoidance

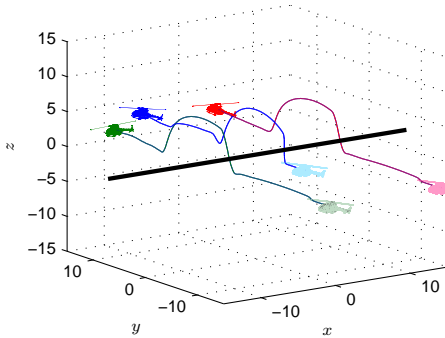


Fig. 8. Obstacle avoidance

As in Fig. 5, in front of the obstacle is a zero force area which the vehicles passed. The parameter which are used for the presented simulations are printed in table I.

Parameter	Description
$F_{max} = 15$	Maximum field strength
$r_{sav} = 11$	Safety radius
$K_{vl} = 1$	Virtual leader gain
$K_{iv} = 0.1$	Inter vehicle gain
$K_{ca} = 165$	collision avoidance gain

TABLE I  
POTENTIAL FIELD PARAMETER

## V. CONCLUSION

In this paper, we have presented a solution for collision and obstacle free formation flight and reconfiguration of groups of autonomous helicopters. The solution is based on potential fields using a virtual leader and taking the vehicle's velocities into account. The solution is universal applicable using the vehicle's auto pilot. The formation flight solution works very well with the presented simplified helicopter model. Future work should concentrate on validation with the complete model and other vertical take-off and landing (VTOL) UAVs.

## REFERENCES

- [1] A. Restas, "Wildfire management supported by uav based air reconnaissance: Experiments and results at the szendro fire department, hungary," in *First International Workshop on Fire Management*, April 2006.
- [2] S. Herwitz, S. Dunagan, D. Sullivan, R. Higgins, L. Johnson, J. Zheng, R. Slye, J. Brass, J. Leung, B. Gallmeyer, and M. Aoyagi, "Solar-powered uav mission for agricultural decision support," in *Proceedings of the IEEE International Geoscience and Remote Sensing Symposium*, vol. 3, July 2003, pp. 1692–1694.
- [3] K. D. Do, "Formation control of mobile agents using local potential functions," in *Proceedings of the American Control Conference*, June 2006.
- [4] G. Elkaim and R. Kelbley, "A lightweight formation control methodology for a swarm of non-holonomic vehicles," in *Aerospace Conference*, March 2006.
- [5] G. D. Padfield, *Helicopter Flight Dynamics: The Theory and Application of Flying Qualities and Simulation Modelling*. Backwell Science, 1996.
- [6] R. K. Heffley and M. A. Mnich, "Minimum-complexity helicopter simulation math model," NASA, Tech. Rep. NAS2-11665, April 1988.
- [7] C. Munziger, "Development of a real-time flight simulator for an experimental model helicopter," Master's thesis, Georgia Institute of Technology, December 1998.
- [8] S. Årdal, "Automatic landing of helicopter on wave-excited ship deck," Master's thesis, Norwegian University of Science and Technology, 2002.
- [9] V. Gavrillets, B. Mettler, and E. Feuron, "Nonlinear model for a small-sized acrobatic helicopter," in *AIAA Guidance, Navigation and Control Conference*, no. AIAA 2001-4333. AIAA, August 2001.
- [10] L. Marconi and R. Naldi, "Robust nonlinear control of a miniature helicopter for acrobatic maneuvers," in *Proceedings 32th Rotorcraft Forum*, September 2006.
- [11] A. Bogdanov, E. Wan, and G. Harvey, "Sdre flight control for x-cell and r-max autonomous helicopters," in *43rd IEEE Conference on Decision and Control*, December 2004, pp. 1196 – 1203.
- [12] E. N. Johnson and S. Kannan, "Adaptive flight control for an autonomous unmanned helicopter," in *AIAA Guidance, Navigation and Control Conference*, no. AIAA-2002-4439, Monterey, CA, aug 2002.
- [13] F. Xie, X. Zhang, R. Fierro, and M. Motter, "Autopilot-based nonlinear uav formation controller with extremum-seeking," in *Proceeding of the 44th IEEE Conference on Decision and Control*, 2005.
- [14] L. Vig and J. A. Adams, "Multi-robot coalition formation," *IEEE Transactions on Robotics*, vol. 22, no. 4, pp. 637–649, August 2006.
- [15] D. V. Dimarogonas and K. J. Kyriakopoulos, "Formation control and collision avoidance for multi-agent systems and a connection between formation infeasibility and flocking behavior," in *Proceedings of the 44th IEEE Conference on Decision and Control*, 2005.
- [16] D. Galzi and Y. Shtessel, "Uav formations control using high order sliding modes," in *Proceedings of the American Control Conference*, 2006, pp. 4249–4255.
- [17] T. I. Fossen, *Marine Control Systems - Guidance, Navigation, and Control of Ships, Rigs and Underwater Vehicles*. Marine Cybernetics, November 2002.